Spring 2021

Thermomechanical simulation and process optimization for hot rolling of steel

Shouvik Ganguly

Department: Mechanical and Aerospace Engineering

THERMOMECHANICAL SIMULATION AND PROCESS OPTIMIZATION FOR HOT ROLLING OF STEEL

by

SHOUVIK GANGULY

A DISSERTATION

Presented to the Graduate Faculty of the

MISSOURI UNIVERSITY OF SCIENCE AND TECHNOLOGY

In Partial Fulfillment of the Requirements for the Degree

DOCTOR OF PHILOSOPHY

in

MECHANICAL ENGINEERING

2021

Approved by:

K. Chandrashekhara, Advisor
Ronald. J. O'Malley
Lokeswarappa. R. Dharani
Ashok Midha
Steven Corns

PUBLICATION DISSERTATION OPTION

This dissertation consists of the following four articles, formatted in the style used by the Missouri University of Science and Technology:

Paper I, found on pages 8–45, has been published in Journal Steel Research International in 2020.

Paper II, found on pages 46–71, has been published in the Journal of Manufacturing Processes in 2021

Paper III, found on pages 72–87, has been published in the proceedings of the Iron and Steel Technology Conference 2020

Paper IV, found on pages 88–116, is intened for submission to the Journal of Manufacturing Processes.

ABSTRACT

Hot rolling is a manufacturing process that involves large material deformation, complicated geometries, contact conditions and non-uniform temperature gradients. Steel industries are motivated to prevent hot rolled steel products to be defect free and with desired shape and size. In order to simulate the process accurately, it is essential that the material model for steel accounts for the viscoplasticity and changes in properties that occur in steel at elevated temperatures as grain growth and recrystallization.

The healing of existing voids during hot rolling was investigated using finite element simulations. Voids are highly undesirable as they not only degrade the product quality but also serve to initiate cracks and fissures. During rolling most of the voids are expected to close due to deformation of the rolled material at high temperature. The influence of various rolling parameters on void closure were predicted using simulations.

During multi-pass hot rolling of steel microstructural changes occur due recrystallization and temperature. Elevated temperatures result in grain coarsening, while recrystallization triggers grain refinement. The parameters governing the static recrystallization kinetics were determined using the double hit compression test. Various steel grades were characterized to determine the change in grain size at elevated temperature. The effect of grain size on the flow stress was also found using a set of experiments. These findings helped to create a new plasticity model based on the classical Johnson-Cook model that included the influence of grain size on the flow stress and static softening due to recrystallization.

ACKNOWLEDGMENTS

Firstly, I wish to thank my supervisor, Dr. K. Chandrashekhara, for his assistance, encouragement and guidance during my journey through the Ph.D. Dr. Chandrashekhara has provided an excellent research environment and supporting team that was extremely helpful in pursuing this research.

I would like to thank my committee members, Dr. O'Malley, Dr. Dharani, Dr. Midha, and Dr. Corns for providing encouragement and council during my studies.

I would also like to acknowledge our composite research team members who have helped me during my tenure as a research student, including Dr. X. Wang, Dr. A. Abutunis, Dr. S. Anandan, Mr. F. Okanmisope, Mr. M. Rangapuram and Mr. S. K. Dasari. A special thanks to PSMRC research mentors Dr S. Lekakh and Dr. M. Buchely for their guidance and support in the area of steel rolling and experimentation.

Finally, I would also like to thank my family members and my wife for their continuous support during my Ph.D work.

TABLE OF CONTENTS

Page

PUBLICATION DISSERTATION OPTION iii

ABSTRACT iv

ACKNOWLEDGMENTS v

LIST OF ILLUSTRATIONS x

LIST OF TABLES xiv

SECTION

1. INTRODUCTION 1

2. LITERATURE REVIEW 3

3. SCOPE AND OBJECTIVES 6

PAPER

I. MODELING AND SIMULATION OF VOID CLOSURE DURING STECKEL MILL ROLLING FOR STEEL PLATE 8

ABSTRACT 8

1. INTRODUCTION 9

2. MATERIALS AND METHODS 13

2.1. MATERIAL CHARACTERIZATION AND MATERIAL MODEL 13

2.2. FINITE ELEMENT MODEL 16

2.3. ROLLING PROCESS PARAMETERS 21

3. RESULT AND DISCUSSION 27

3.1. MULTI-PASS ROLLING AND VOID CLOSURE 29

3.2. EFFECT OF VOID LOCATION ON VOID CLOSURE 31

3.3. EFFECT OF TEMPERATURE ON VOID CLOSURE 33

3.4. DEPTH OF PLATE REDUCTION AND RATE OF VOID CLOSURE 34

3.5. EFFECT OF RECRYSTALLIZATION 38

4. CONCLUSION 40

ACKNOWLEDGEMENTS 42

REFERENCES 42

II. MODELING AND SIMULATION OF MASS FLOW DURING HOT ROLLING LOW CARBON STEEL I-BEAM 46

ABSTRACT 46

1. INTRODUCTION 47

2. MATERIALS AND METHODS 51

2.1. HOT TENSILE TESTS 51

2.2. MATERIAL MODELING 53

2.3. FINITE ELEMENT MODELING 53

3. RESULTS AND DISCUSSION 56

3.1. TENSILE TESTS AND MATERIAL MODEL 56

3.2. SIMULATION RESULTS OF BREAKDOWN MILL 58

3.3. EFFECT OF ROLLING GAP ON FINAL BEAM PROFILE 61

3.4. EFFECT OF AS CAST BLANK DISTORTION ON FINAL BEAM PROFILE 63

4. CONCLUSION 67

ACKNOWLEDGEMENTS 68

REFERENCES 68

III. A MODIFIED JOHNSON-COOK MODEL INCORPORATING THE EFFECT OF GRAIN SIZE ON FLOW STRESS 72

ABSTRACT 72

1. INTRODUCTION 72

2. EXPERIMENTAL PROCEDURE 74

2.1. JC STRENGTH MODEL 74

2.2. GRAIN GROWTH MODEL 75

2.3. MEASUREMENT OF FLOW STRESS 75

2.4. FINITE ELEMENT MODEL 77

3. RESULTS AND DISCUSSION 79

3.1. JC STRENGTH PARAMETERS 79

3.2. GRAIN SIZE EVOLUTION 79

3.3. FLOW STRESS EVALUATION 81

3.4. NUMERICAL ANALYSIS 83

4. CONCLUSIONS 85

ACKNOWLEDGEMENTS 85

REFERENCES 86

IV. MODELING OF STATIC RECRYSTALLIZATION KINETICS OF HIGH STRENGTH STEEL DURING MULTI-PASS HOT ROLLING 88

ABSTRACT 88

1. INTRODUCTION 89

2. EXPERIMENTAL PROCEDURE 91

2.1. JC STRENGTH MODEL 91

2.2. STATIC RECRYSTALLIZATION 92

2.3. DETERMINATION OF FRACTION OF RECRYSTALLIZATION 93

2.4. MODELING THE KINETICS OF STATIC RECRYSTALLIZATION 94

3. FINITE ELEMENT MODEL 99

4. RESULTS AND DISCUSSION 101

4.1. EVOLUTION OF STATIC RECRYSTALLIZATION AND SOFTENING 101

4.2. EFFECT OF PASS REDUCTION ON STATIC RECRYSTALLIZATION 103

4.3. INFLUENCE OF TEMPERATURE ON RECRYSTALLIZATION 109

4.4. INFLUENCE OF ROLLING SPEED ON RECRYSTALLIZATION 112

5. CONCLUSIONS 113

ACKNOWLEDGEMENTS 114

REFERENCES 115

SECTION

4. CONCLUSIONS 117

BIBLIOGRAPHY 119

VITA 121

LIST OF ILLUSTRATIONS

PAPER I Page

Figure 1. Example of experimental stress-strain curves for the studied steel plate. 14

Figure 2. Full scale modeling of reversible Steckel mill plate hot rolling..... 16

Figure 3. Symmetry model of rolled slab about the vertical plane with void at the center..... 19

Figure 4. Mesh along the vertical plane of symmetry and around the void..... 19

Figure 5. Change in shape of void due to rolling showing the parameters to calculate the constriction ratio. 21

Figure 6. Schematic view of the void location in the slab. 22

Figure 7. Schematic of flow curve for material showing loading, unloading and reloading paths 25

Figure 8. a) Compression test on bar sample b) Effect of strain recovery on the stress-strain for accumulated and non-accumulated model 27

Figure 9. Effect of varying element size around void on mesh constriction 28

Figure 10. Shape change of void during simulation 29

Figure 11. Variation of a) normal plastic strain b) stress and c) temperature along the slab thickness during simulation..... 30

Figure 12. Constriction ratio of voids located at varying distances from the centerline for seven pass rolling 31

Figure 13. Variation of normal strains along the plate thickness at the side and centerline during the third pass rolling 32

Figure 14. Variation of equivalent plastic strain along midplane from centerline to sides at the end of seven pass rolling schedule 32

Figure 15. Constriction ratio of void at different rolling temperatures for void with 25 mm initial diameter for seven pass rolling..... 33

Figure 16. Constriction ratio of voids of varying sizes..... 35

Figure 17. Lower cumulative pass reduction sufficient to close 25 mm diameter void ... 36

Figure 18. Variation of normal plastic strain along the thickness at 1100 °C 37

Figure 19. Variation of the normal stress along the thickness of the plate 37

Figure 20. Effect of accumulated versus non-accumulated strain during a) seven pass rolling and b) five pass rolling on void closure. 39

PAPER II

Figure 1. Schematic view of testing samples utilized in the study 52

Figure 2. Schematic of I-beam production 55

Figure 3. Mesh of I-beam hot rolling process 56

Figure 4. Experimental engineering and true stress-strain curves from hot tensile tests.. 57

Figure 5. Deformation process and plastic strain of the beam blank from passes P1 to P3 59

Figure 6. The deformation process form passes P4 to P7 59

Figure 7. The I-beam shape and plastic strain for passes P8 and P11 60

Figure 8. Simulated accumulated strain during hot rolling and changes in beam shape after 13 passes in the breakdown mill 61

Figure 9. Comparison of I-beam shapes of simulation and experimental results 62

Figure 10. (a) Actual deformed shape of I-beam flange after rolling in industrial set up and (b) simulation results for maximum, designed and minimum gaps 63

Figure 11. Flange surface distortion observed in as cast I beam (left) and used in model (right) 64

Figure 12. Comparison of accumulated plastic strain and simulated hot rolled I beam geometry for ideal shape of cast blank with cast blank having surface distortion 65

Figure 13. Simulation results of coupled effect of surface distortion and rolling gap on accumulated strain for designed gap and minimum gap 66

PAPER III

Figure 1. (a) Steps during grain size measurement, and (b) metallographic observation of the prior austenitic grain size in A572 steel grade, after austenitization at 1100 ºC per 600 s 76

Figure 2. Compression test 77

Figure 3. Boundary conditions applied to finite element model of rectangular sample used to simulate compression and relaxation 78

Figure 4. Grain growth parameter plot for (a) A572 steel and (b) A690 steel 80

Figure 5. Stress strain curves after compression tests at 1100 ºC and 1s-1 81

Figure 6. The maximum flow stress with varying grain size for the studied steel grades 82

Figure 7. Comparison of varying steel grades 83

PAPER IV

Figure 1. Experimental stress-strain curves for hot tensile tests for strain rate 1 and varying temperatures 91

Figure 2. Steps during double hit test using the Gleeble machine 93

Figure 3. Stress-strain curves obtained from double hit compression test at a strain rate of 5 /s, pre-strain of 0.4, and interpass time of 5s for temperatures of a) 1100 ºC and b) 1000 ºC 94

Figure 4. Experimentally obtained fraction of static recrystallization at 1100 °C and strain rate 5 /s 95

Figure 5. Experimentally obtained fraction of static recrystallization at 1000 °C and strain rate 5 /s 95

Figure 6. Variation of half time with a) strain b) strain rate 97

Figure 7. Comparison between the traditional and modified model for strain 0.1 at 1000 ºC and strain rate 5 /s 98

Figure 8. Finite element model of the rectangular slab and rollers used to simulate the hot rolling process 100

Figure 9. Fraction of static recrystallization after a) 10 s b) 15 s c) 20 s, and d) 25 s 102

Figure 10. Plastic strain after a) 10 s b) 15 s c) 20 s and d) 25 s 103

Figure 11. Variation of degree of static recrystallization during the first three rolling passes at 1000 °C 104

Figure 12. Static softening for different rolling passes for classical JC model and modified JC model 104

Figure 13. Simulation results for degree of recrystallization for a) pass 1, b) pass 2, and c) pass 3 105

Figure 14. Simulation results for static softening during a) pass 1, b) pass 2, and c) pass 3 106

Figure 15. Increase in static recrystallization with time for a) pass 1, b) pass 2, and c) pass 3 107

Figure 16. Increase in static softening with time for a) pass 1, b) pass 2, c) pass 3 108

Figure 17. Variation of degree of static recrystallization during first rolling pass for different temperatures 109

Figure 18. Simulation results for static recrystallization for a) 900 °C, b) 1000 °C, and c) 1100 °C 110

Figure 19. Static softening during the first rolling pass 111

Figure 20. Simulation results of static softening at different temperatures a) 900 °C, b) 1000 °C, and c) 1100 °C 112

Figure 21. Variation of degree of static recrystallization for varying rolling speeds 113

LIST OF TABLES

PAPER I Page

Table 1. Johnson-Cook JC parameters for studied steel 15

Table 2. Studied rolling schedules of slab rolling..... 17

Table 3. Thermal and mechanical properties used in simulation..... 20

Table 4. Varying distances for void considered for rolling simulations..... 23

Table 5. Different sizes of elements used around the void 28

Table 6. Variation of plastic strain for different rolling temperatures during third pass rolling..... 34

Table 7. Comparison of strain during the third pass for both models..... 40

Table 8. Effect of different parameters on void closure 40

PAPER II

Table 1. Calibrated JC model parameters for the studied steel..... 58

Table 2. Measurements of the flange depression after hot rolling 63

Table 3. Effect of dent in the flange depression (mm) after hot rolling 65

Table 4. Coupled effect of dent and rolling gap in the flange depression (mm) after hot rolling..... 66

PAPER III

Table 1. Calibrated Johnson-Cook parameters for studied steel grades 79

Table 2. Grain growth parameters for the studied steel grades..... 80

Table 3. Modified JC model grain size parameter..... 82

Table 4. Comparison of stress relaxation for varying steel grades 84

PAPER IV

Table 1. Static recrystallization kinetic parameters determined 96

Table 2. Calibrated Johnson-Cook parameters for studied steel grades 99

SECTION

1. INTRODUCTION

Rolling is one of the main manufacturing processes for large products. Hot rolling is conducted at elevated temperatures, usually above the austenite recrystallization temperature for steel. It allows the advantage of being able to produce bulk products within a short time and at low costs. A modern hot strip mill can produce more than 6 million tons of steel per annum [1]. However, hot rolling is a complex thermo-mechanical process wherein non-uniform state of stress and strain develop along the rolled material due to rolling pressure, tool contact, non-uniform temperature distribution and changing mechanical properties of steel. The mechanical properties of the steel are dictated by the thermo-mechanical conditions, steel chemistry and microstructural changes.

In the past, many researchers have used analytical equations to describe the hot rolling process. However, the large deformation, friction due to contact and non linear boundary conditions make it extremely challenging to develop a comprehensive analytical relation for the process.

In addition, it is also necessary to correctly represent the viscoplastic behavior of the steel undergoing large deformation. Numerical models are best suited to adequately describe the non linear material behavior of steel as well as the complex hot rolling process.

Although there is a wide range of empirical as well as phenomenological models available in literature there is a dearth of microstructural based elastic-plastic models.

Most of the microstructural based models are empirical that depend on large number of physical parameters that cannot be easily converted in a numerical form. Furthermore, such models are developed at a microscale level and hence not practically implementable for large scale realistic rolling operation.

In this dissertation, the goal has been to develop a microstructural based material model for steel, that takes into account the affect of temperature and recrystallization on grain size. Further the model considers the influence of grain size on the work hardening response of the material. Using this novel model a non-linear finite element analysis (FEA) is conducted of the industrial hot rolling process to predict the final product geometry, plastic strain and stress condition. The model also predicted possibility of defects or crack initiation, as well as possibility of void closure after hot rolling.

2. LITERATURE REVIEW

At room temperature steels exhibit elastic response until yield stress is reached and thereafter show plastic behavior. However, at elevated temperatures steels exhibit visco-plastic behavior. There is a marked decrease in yield strength and stiffness of the metal at elevated temperatures and an increase in ductility. This behavior is due to the ease in movement of dislocations by slip at elevated temperatures. Tensile tests are the best methodology to characterize the stress-strain behavior of steels [2]. These tests need to be conducted at a range of temperatures and strain rate inorder to accurately record the change in strain hardening and visco-pastic behavior with temperature change and varying rates of deformation.

Various empirical as well as physical models have been proposed in literature. Physical models depend on variables that represent the physical state of the material and are cumbersome to obtain. Zerilli–Armstrong (ZA) model [3] is a physical model based on dislocation mechanism. Empirical models have a closed mathematical form and generally use a smaller number of parameters that depend on simpler tests. The Johnson-Cook model [4] is an empirical model that considers the effect of strain hardening, strain rate as well as temperature on the visco-plastic behavior of metals. The Johnson-Cook model offers several advantages over other empirical models as Shida [5] and the Ludwig models [6].

In addition to strain hardening the visco-plastic behavior of metals at elevated temperatures is also governed by grain size coarsening and grain refinement due to recrystallization. Steels experience recrystallization when deformed at temperatures above the austenizing temperature [7]. On undergoing deformation during rolling at high

temperatures the steel beam first undergoes dynamic recrystallization wherein new grains are formed at the grain boundaries. Thereafter when the beam leaves the rollers the process of grain nucleation continues, and this is known as static recrystallization. It is generally assumed that static recrystallization has a more profound effect than dynamic recrystallization for hot rolling process [8]. The physical properties of the steel are highly affected and the material softens due to loss of residual strain accumulated during rolling [9]. The avrami model is commonly used to describe the evolution of fraction of recrystallization with time [10]. The static recrystallization half time is predicted using Sellar's model [7]. The effect of static softening has also been predicted using FEA by Jung et al. [11].

Recrystallization is often followed by temperature driven grain coarsening. The Sellars model has shown that at elevated temperatures the grain size of austenite, the holding time and the heating temperature can be related as [12].

$$d_g = d_0 + atexp(\frac{-Q_{gg}}{RT}) \quad (1)$$

where d_g is the austenitic grain size at time t, d_0 is the initial grain size, Q_{gg} is the austenitic grain growth energy, T is the absolute temperature and a is constant.
For grains of small size the dislocations that pile up at the grain boundaries serve as a deterrent for slip to occur. Hence the stress has to be increased inorder to force dislocations to move. This phenomenon is known as grain size hardening. Contrarily, if the grain size is large it is easier for dislocations to move and hence the material softens. The Hall-Petch equation [13] relates the mechanical property of steel to the grain size at

room temperature. The value of yield strength typically increases with the reciprocal root of the grain size.

$$\sigma_y = \sigma_0 + K_y d^{0.5} \quad (2)$$

where σ_y is the yield strength for grains of size d, σ_0 is the initial grain size. Similar relationships have been considered for predicting cleavage fracture stress and also strength at elevated temperatures.

The hot rolling process generally consists of a reheating furnace, roughing mill, finishing mill, and finally accelerated cooling. Although strip rolling is one of the most commonly rolled products, structural shape rolling of I-beam, H-beam, U-beam channels and railroads are also widely used. For complex shape rolling the effect of localized deformation and non-uniform temperature gradient are critical on final product quality [14]. The presence of pre-existing imperfections and defects can also have critical influence on creation of cracks and fissures. Finite element method is the best tool that can predict the rolled profile of such beams and also possibility of damage. Takashima and Hiruta [14] conducted FEA on U shaped channel and found that the strain gradient along the cross-section influenced the formation of bulge along the flange. Studies have also shown that loss of heat during rolling has an impact on rolling torque [15].

Finally, FEA has been importantly used to predict possibility of cracks developing in the rolled beam. Residual stress has been found to play a big role that influenced the fatigue behavior of rolled beams [16]. Pre-existing defects also have strong impact on the probability of developing cracks and surface fissures during hot rolling. The Johnson-Cook damage model [17] is an extremely powerful tool that helps determine final hot rolled product quality.

3. SCOPE AND OBJECTIVES

The dissertation consists of four papers corresponding to the following problems.

The first paper is titled "Modeling and Simulation of Void Closure during Steckel Mill Rolling of Steel Plate". In this paper the rate of void closure in steel plates during hot rolling was investigated. A comprehensive viscoplastic material model for steel was developed based on the Johnson-Cook equation. Influence of various rolling parameters as pass reduction, rolling temperature, and recrystallization on void closure was analyzed using FEA.

The second paper is titled "Modeling and Simulation of Mass Flow during Hot Rolling Low Carbon Steel I-Beam". In this paper the influence of rolling gap on the creation of defect on the beam surface was examined using FEA. A depression was observed to form during industrial multi-pass breakdown mill rolling of I-beam on the middle of the flange. In addition, the effect of a pre-existing distortion on the beam surface on the shape of the depression was also predicted using simulations.

The third paper is titled "A Modified Johnson-Cook Model Incorporating the Effect of Grain Size on Flow Stress" . In this paper the influence of grain size changes on the flow stress of various steel grades was studied. The classical Johnson-Cook equation that relates flow stress with plastic strain, strain rate and temperature was modified to include the additional effect of grain size. Experiments were conducted to measure the influence of temperature on grain size of steel. Additional experiments were conducted to measure the effect of grain size on flow stress. An explicit subroutine was developed to include the modified Johnson-Cook model and implemented into a finite element model.

The fourth paper is titled “Modeling of static recrystallization kinetics of high strength steel during multi-pass hot rolling”. In this work the extent of static recrystallization occurring in steel beam during multi-pass rolling was determined. Double hit test experiments were conducted to determine the fraction of static recrystallization at elevated temperatures. Parameters relevant to static recrystallization kinetics were determined as per the avrami equation. The model was coded in an explicit subroutine and implemented into a three dimensional finite element model for hot rolling. The static softening process was also simulated.

PAPER

I. MODELING AND SIMULATION OF VOID CLOSURE DURING STECKEL MILL ROLLING FOR STEEL PLATE

S. Ganguly[1], X. Wang[1], K. Chandrashekhara1[1], M. F. Buchely[2], S. Lekakh[2], and R. J. O'Malley[2]

1. Department of Mechanical and Aerospace Engineering
2. Department of Materials Science and Engineering
Missouri University of Science and Technology, Rolla, MO 65409
D. Bai and Y. Wang
SSAB Americas, Muscatine, IA 52761

ABSTRACT

Internal void defects as shrinkage porosity, gas bubble and thermo-mechanical cracks are usually formed during steel casting processes. These defects have critical impact on the quality and service life of hot rolled products. Study of the possibility of self-healing of existing internal defects during hot rolling process has been of interest to industry and researchers. Prediction of void closure is extremely useful in relation to better product design and manufacturing process optimization. In this work, a three-dimensional finite element model of the slab hot rolling process was developed to simulate and analyze the healing of internal voids in hot rolled steel plate. The material model for the steel plate was developed based on Johnson-Cook constitutive relation to accurately represent its viscoplastic behavior at high temperatures as well as account for strain rate sensitivity. The study evaluated the thermal and mechanical response of low carbon steel slabs having pre-existing voids during multi pass strands reverse hot rolling process. Through thickness plastic strains within the slab are found to influence void

closure. Results show that variation in void size and locations also affect the healing possibilities. Finally, the effect of thermal history and thermo-mechanical stresses on void closure was studied.

1. INTRODUCTION

Hot rolling is an important deformation process in steel manufacturing. In hot rolling, the rolls are subjected to cyclic thermal and mechanical loadings to reduce the thickness of the part. Among the various forms of rolling, flat rolling has been conventionally used [1]. A complicated state of stress and strain occurs in the steel product due to rolling pressure, tool contact, and non-uniform temperature distribution [2]. Final product quality is highly dependent on the thermal-mechanical deformation and mass flow behavior during hot rolling.

The Steckel mill employs a type of hot rolling process wherein the plate goes back and forth between one pair of rolls [3]. This process is also known as reverse rolling. In this process, a coiler is placed at the entry and exit of the mill to feed and pull the steel material. Each pass contributes a small deformation of the plate. Finite element method (FEM) provides an effective and economical way to predict the final product quality and shape during rolling [4] eliminating the need for cumbersome experimental process.

The rolling process involves large deformation and non-linear boundary conditions that are impossible to solve using analytical equations. Hence numerical analysis is the preferred means to predict mass flow and stresses during hot rolling. FEM, meshless methods, finite difference and finite volume methods are some of the most

suitable numerical analysis tool that are used in obtaining solutions to the differential equations of thermal and mechanical equilibrium involved in complex manufacturing processes. Hanoglu and Sarler [5] used the meshless method based on radial basis function collocation method to solve hot rolling thermo-mechanical problem considering elastic material properties. The meshless solution was also extended to consider elastic and ideal plastic material properties of hot rolled steel[6][7]. The solutions obtained were compared with FEM and were found to be highly accurate.

Many researchers have developed finite element models to study the plastic strains and mass flow during hot rolling process. Cao et al [8] used FEM to analyze roll wear and flatness control during hot strip rolling. Kim and Im [9] provided a finite element simulation of non-isothermal hot rolling analysis, showing temperature gradients during the rolling process. Duan and Sheppard [10] used FEM to simulate thermo-mechanical properties of an aluminum alloy during hot rolling processes. Galantucci and Tricarico [11] studied the effect of heat loss along strip roll interface on temperature gradient using FEM. Montmitonnet [12] used one-dimensional, two-dimensional as well as three-dimensional finite element models to simulate strip rolling. Kim et al [13] developed a finite element model to analyze the roll-strip interface during hot rolling. Li et al [14] studied the effect of bending force during hot rolling on strip profile and roll gap profile. Ding et al [15] developed finite element numerical simulation for microstructure evolution during hot rolling of a Mg-alloy, and showed temperature had a more significant effect on recrystallization than roll speed. Wang et al [16] developed a finite element model to simulate strip temperature during hot strip rolling. Benasciuttiet al [17] provided a finite element model to predict product thermal stresses during hot

rolling. Additionally, Nalawade et al [18] studied multi-pass hot rolling of micro-alloyed 38MnVS6 steel.

In order, to simulate the hot rolling process, it is essential to develop a robust material model for the steel. Various material models have been developed to describe mass flow behavior during hot rolling process in FEM. The Johnson-Cook model [19] is one of the most widely used phenomenological constitutive models considering effects of strain hardening, strain rate hardening and temperature softening. Another widely used model, the Zerilli-Armstrong model [20], is based on dislocation mechanisms including models for body centered cubic and face centered cubic structures. Wang et al [21] used a combined Johnson-Cook and Zerilli-Armstrong material model to simulate hot rolling processes for steel. The Shida model [22] provides an empirical constitutive model considering the effects of carbon content, strain, strain rate and temperature on plain carbon steels. Montmitonnet et al [23] developed an anisotropic viscoelastic material model for material undergoing hot rolling. Chen et al [24] used the Shida model to study void closure of a hot radial forging process.

It has been noted by previous researchers that the plastic strains vary not only along the thickness of the slab but also across the width during rolling [25]. Similarly, stresses also vary along the thickness and the width of the slab. It is critical for the numerical model to be able to predict the correct gradient of stress and strain along the cross-section of material being rolled.

Temperature has a tremendous impact on the mass flow behavior and microstructure of slab material. The effect of temperature has to be taken into consideration to adjust the rolling torques and loads in order to ensure desired final

product quality [26]. During rolling, thermal stresses are generated due to non-uniform temperature gradients in the slab, whereas mechanical stresses are a product of rolling pressure [17]. These combined stresses play a crucial role in determining the residual stresses and mass flow within the slab material. The overall intention of hot rolling is not only to obtain the desired thickness of material but also the right microstructure.

The presence of cracks or voids in a steel product is highly undesirable with reference to final product quality as they affect the service life of the material. Saby et al [27] evaluated the effect of voids of varying geometries and orientation on closure using finite element analysis of hot rolling. Nalawade et al [28] studied the effect of temperature, rolling torque and void volume fraction on void closure during hot rolling. Faini et al [29] also studied void closure using hot rolling simulations for steel material and obtained a correlation with percentage reduction, cooling time and location of void. It is observed that high temperatures, compressive stresses and diffusion help in crack healing and induce closure [30]. It has also been noted that reduction of material per pass has an important influence on depth penetration and hence void closure [31].

Finally, hot rolling involves temperatures at which dynamic and static recrystallization occurs within the rolled material. The recrystallized material exhibits a regenerated microstructure and complete strain recovery on unloading. In the absence of recrystallization, the material recovers only the elastic strain on unloading. Thereafter on reloading the material yields at a new yield point, higher than the previous one. Hence if recrystallization is accounted for during simulation, it is expected to dynamically influence the mass flow [32]. As a result, it is expected that void healing is also affected due to recrystallization. However, there is a lack of study to correlate the effect of

temperature profile and microstructural evolution within the rolled material and void closure.

The overall objective of the current work is to simulate the complete steel reverse hot rolling process. A three-dimensional nonlinear finite element model was built to simulate plate hot rolling. The effects of void size, location and temperature on void healing were analyzed by the numerical model. Voids were assumed to be cylindrical with its axis aligned along the width of the slab. The relation between plastic strains and void constriction during hot rolling was also analyzed. Furthermore, the effect of recrystallization dependent strain recovery on void healing was compared. The present work intends to determine the critical conditions that influence void closure within a slab undergoing hot rolling process.

2. MATERIALS AND METHODS

2.1. MATERIAL CHARACTERIZATION AND MATERIAL MODEL

Gleeble thermal simulator has been commonly used to obtain compression experiment data used to model the constitutive relationship between flow stress, true strain, strain rate and temperature.

Sun et al [33] have described the methodology in detail. In this paper, hot compression tests were conducted on a medium carbon steel using the Gleeble system at different temperatures (900°C, 1000°C, 1100°C, and 1200°C) and strain rates (1s-1, 10s-1 and 20s-1) to obtain the stress-strain curves for the hot rolled material. Stress-strain curves are shown in Figure 1.

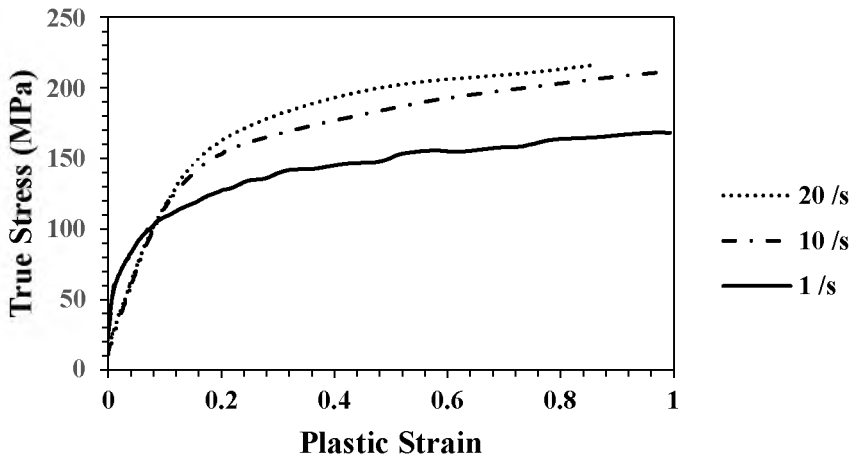

a)

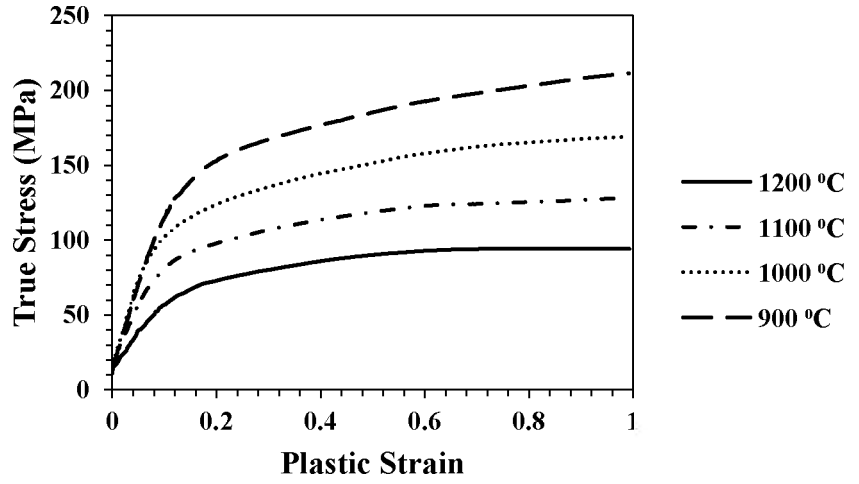

b)

Figure 1. Example of experimental stress-strain curves for the studied steel plate. Flow stress: a) at different strain rates at 900 °C and b) at different temperatures and at strain rate of 10 /s [34].

In this study, the Johnson-Cook (JC) strength model is presented in the following equation:

$$\sigma = (A + B\varepsilon^{n})(1 + C \ln \dot{\varepsilon}^{*})(1 - T^{*m}) \quad (1)$$

where: σ is equivalent flow stress, ε is equivalent plastic strain, $\dot{\varepsilon}^*$ is dimensionless strain rate given by $\dot{\varepsilon}^* = \dot{\varepsilon}/\dot{\varepsilon}_0$, $\dot{\varepsilon}$ is strain rate and $\dot{\varepsilon}_0$ is reference strain rate, T^* is homologous temperature given by:

$$\mathrm{T}^* = \frac{T - T_r}{T_m - T_r} \tag{2}$$

where: $T$is the material temperature,T_r is a reference temperature and T_m is metal melting temperature, A, B, C, m and n are material parameters.

The constants A, B and n describe the strain hardening effect, C describes the strain rate effect, and m describes the thermal softening effect of the material. JC material parameters were calibrated using the experimental compression data by a non-linear regression method. The sum of squares error between experimental data and prediction of JC equation was minimized, as follows:

$$\min f(x) = min \sum_{i=1}^{N} (\sigma_i^{exp} - \sigma_i^{JC}(X))^2, \text{ with } X = [A, B, n, C, m] \tag{3}$$

where: N is number of experimental data points, σ_i^{exp} is experimental stress value at data point i, and $\sigma_i^{JC}(X)$ is Johnson-Cook model prediction based on constant set Xat data point i. Using the previous approach, the JC material parameters were determined for the studied material, and they are shown in Table 1 for a reference strain rate of magnitude 1 and reference temperature 1000 °C for the studied steel material.

Table 1. Johnson-Cook JC parameters for studied steel

A (MPa)	**B (MPa)**	**C**	**n**	**m**	**T_{ref} (°C)**	**$\dot{\varepsilon}_{ref}$**
20	155	0.136	0.340	0.912	1000	1

2.2. FINITE ELEMENT MODEL

Two separate rolling schedules of the reverse rolling process, for the studied steel plate is shown in Table 2. Three-dimensional nonlinear finite element model for reversible plate hot rolling process was developed using commercial code Abaqus 6.16 [35].

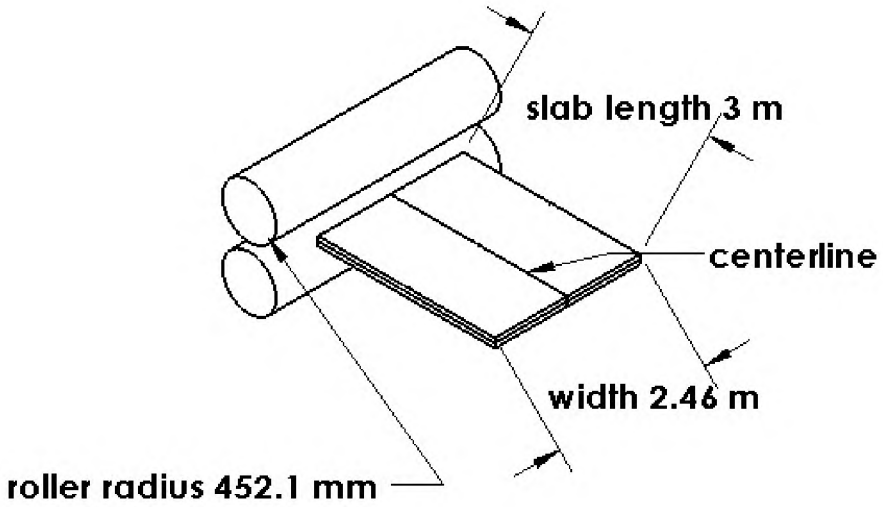

a)

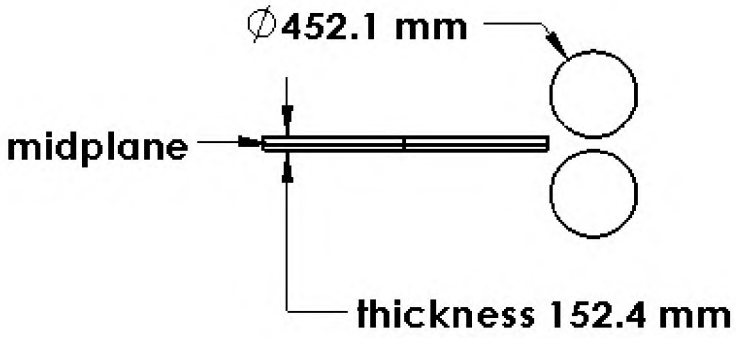

b)

Figure 2. Full scale modeling of reversible Steckel mill plate hot rolling: a) isometric view of rolls and b) side view of rolls and slab.

A single pair of rolls was used to deform the steel plate having rectangular cross-section 97 in × 6 in (2460 mm × 152.4 mm) as shown in Figure 2. The plate was moved back and forth between the rolls according to the schedule in Table 2, until the final shape was obtained in order to simulate the reversible rolling process of Steckel mill. The gap between the rolls decreases for each new rolling pass, and the final thickness of the slab was 3.088 in (78.43 mm) at the end of the rolling process.

Table 2. Studied rolling schedules of slab rolling

	Thickness Reduction%		
	Schedule 1 Seven Pass Rolling	**Schedule 2 Five Pass Rolling**	**Roll velocity (m/s)**
1	5.97	11.58	1.799
2	5.78	11.95	2.04
3	13.41	14.53	2.56
4	14.49	12.65	2.106
5	10.62	11.39	2.98
6	6.57	-	2.53
7	6.05	-	1.51
Total Reduction	50	50	

A series of three-dimensional finite element analysis using the non-linear material model (Eq 1,2) were conducted to simulate plate hot rolling with varying process parameters. Formulation of three-dimensional dynamic analysis is expressed as follows:

$$[M^e]\{\ddot{\Delta}^e\} + [K^e]\{\Delta^e\} = \{F^e\} + \{F^t\} \quad (4)$$

where: [Me] and [Ke] are mass matrix and stiffness matrix respectively, {Fe} is the loading vector, {Ft} is the thermal loading, $[\ddot{\Delta}^e]$ and $[\Delta^e]$ are the acceleration and displacement vectors.

The mechanical model was coupled to a thermal model using the following heat transfer formulation:

$$[C_T]\{\dot{\theta}\} + [K_T]\{\theta\} = \{Q\} \tag{5}$$

where: [CT] is the heat capacitance matrix, [KT] is the conductivity matrix, {Q} is total heat flow, Θ is the temperature. The conductivity of the material is obtained from Table 3 and assumed to be uniform along all directions. Q consists of the sum of heat generated due to surface loads Qs, internal heat generation rate Qi and heat flux across boundaries Qb.

$$Q_s = \mu p S(v_r - v) \tag{6}$$

where: μ is the coefficient of friction, p is the contact pressure, S is the contact area, and $v_r - v$ is the roll plate relative speed.

$$Q_b = h(T - T_{atm}) + \sigma_{st} . e . (T - T_{atm})^4 \tag{7}$$

where: h is the coefficient of convection, T is the slab temperature, Tatm is the ambient temperature, σst is Stefan-Boltzman constant, e is the emissivity coefficient provided in Table 3.

$$Q_i = \eta \frac{\partial}{\partial t} \int \sigma d\varepsilon \tag{8}$$

where: η is the Taylor-Quinney parameter that gives the ration of deformation turning into heat, σ is the effective stress and ε is the effective strain [6]. Using equation 5 the temperature at each node in the finite element model is calculated.

The geometrical void was modeled as a cylindrical hole, cut in the center of the slab. The initial diameter of the hole was varied from 10 to 25 mm, and its initial length was kept constant at 40 mm. The cylindrical hole was located along the midplane with its

longitudinal axis along the width direction of the slab as schematically shown in Figure 3. The symmetry model was used for conducting the simulations in order to save computational time and cost. The void interface was modelled as a free geometric surface.

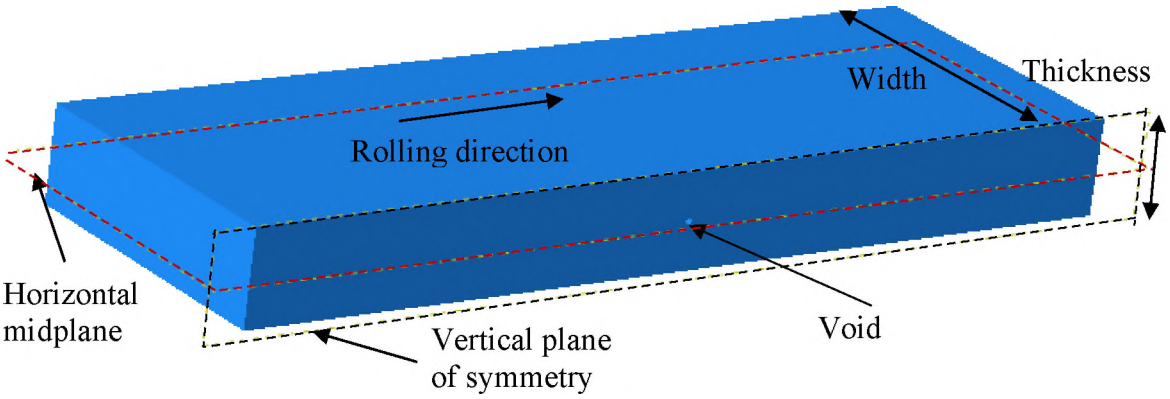

Figure 3. Symmetry model of rolled slab about the vertical plane with void at the center.

The refinement of the mesh along the void in comparison to the bulk of the slab is shown in Figure 4 as high stress concentration is expected around the hole.

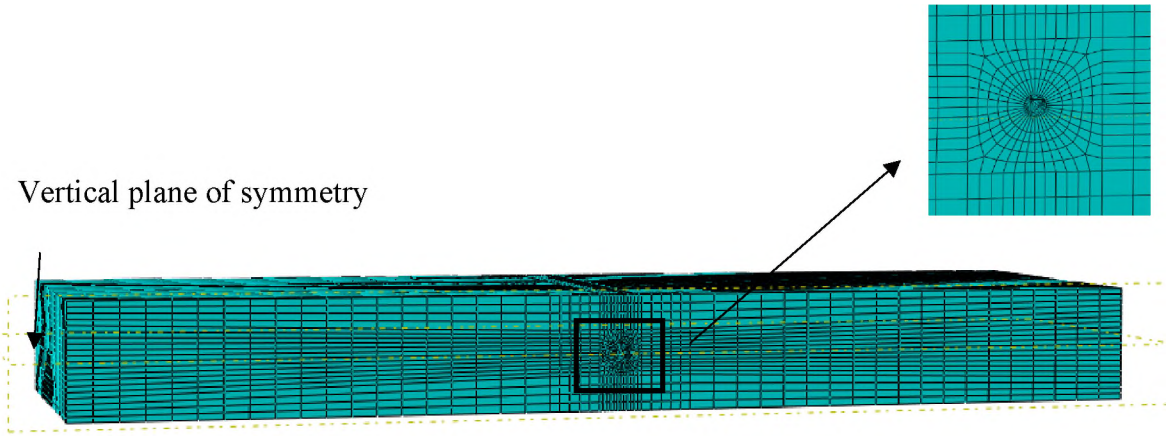

Figure 4. Mesh along the vertical plane of symmetry and around the void.

The bulk of the slab was meshed with eight node thermally coupled hexahedral elements (C3D8RT), while the rolls were modeled as rigid and meshed with the same element type. The slab was meshed with a total of 56800 elements, while the rolls had 7650 elements. A velocity in the range of 91.13 m/min – 178.91 m/min varying for each rolling step was applied to the rolls. The velocity of the slab was adjusted to match the rolling speed. The slab was initially held at 1200^{o}C and then allowed to experience heat loss to the surrounding (room temperature) under the effect of convection and radiation. The rolls were kept at a constant temperature of 150 ^{o}C. The coefficient of friction between the rolls and slab was set as 0.3 and governed by coulomb friction law [36] . The heat transfer coefficient and thermal conductivity are obtained from literature [37][38]. Other physical and thermal properties related to the slab and the rolls used in the simulation are listed in Table 3.

Table 3. Thermal and mechanical properties used in simulation

Property	**Value**
Density	7450 kg/m^3
Poisson's ratio	0.33
Young's modulus	100 MPa
Specific heat capacity	600 J/kg K
Coefficient of friction	0.3
Conductivity	50 W/m K
Heat transfer coefficient	100 W/(m^2 K)
Emissivity	0.9

2.3. ROLLING PROCESS PARAMETERS

The effect of void location and thermo-mechanical changes on void closure was studied. In addition, the effect of extent of reduction in plate thickness on void closure was analyzed. The extent of void closure was quantified using the constriction ratio. Figure 5 shows the sectioned view of the initial shape of a 25 mm diameter void prior to rolling and the shape of void after second pass. The constriction ratio was defined as the ratio of the final depth of void Df to the initial void diameter D0 (Figure 5). The constriction ratio has been considered as a void closure parameter in this paper, on similar lines as Qin et al [39].

$$\text{Constriction ratio} = (D_0 - D_f)/D_0 \quad (9)$$

The normal strain is expected to affect the mass flow in the thickness direction and hence considered to be the primary influencing factor for void constriction.

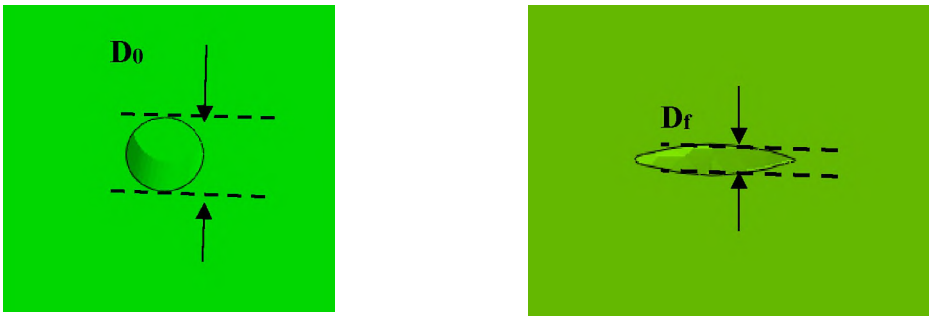

Figure 5. Change in shape of void due to rolling showing the parameters to calculate the constriction ratio a) initial shape of void before rolling b) final shape of void after second pass rolling.

The following parameters were studied with reference to void closure.

Void location: The state of material at the center is plane strain due to symmetric conditions and hence the transverse flow of the material is restricted. In contrast, plane stress conditions exist along the edges as material is free to flow along the sides. This causes a variation in flow stress along the width of the plate, with higher stresses at the central region than the edges. Additionally, normal or compressive strain is observed to be lower along the sides and higher at the central region. Prior studies by Chen et al [40] have determined using analytical methods that void closure is increased with higher compressive strains. Therefore, the constriction of voids was studied at different distances from the centerline along the width of the rolled slab. Figure 6 shows the position of the considered centerline.

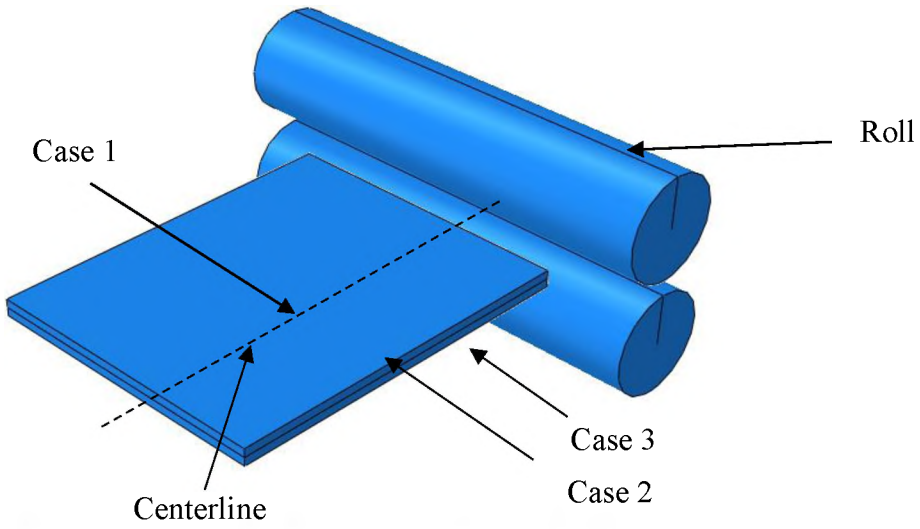

Figure 6. Schematic view of the void location in the slab.

Simulations were conducted for 25 mm diameter and 40 mm long voids located at the midplane of the rolled slab but at three different distances from the centerline. A

thermally sensitive elasto-plastic material model was used for the steel slab assuming no change in microstructure during the entire process. The different studied cases are shown in Table 4.

Table 4. Varying distances for void considered for rolling simulations

Case	Distance from the slab side
1	At centerline
2	At 40 mm from the side
3	Along side

Temperature: An increase in temperature is expected to result in an increase in mass flow and ductility of the material. Hence in order to verify the sensitivity of the model to temperature, four different temperature gradients were considered in this work. Hot rolling was conducted for plates having the same dimensions (25 mm void diameter and 40 mm length located at the center of the slab) with all rolling parameters kept same except for the slab temperature. The effect of increase in overall slab temperature on void closure was studied. The seven pass rolling schedule was conducted with the initial slab temperature kept uniformly at 1100ºC, 1200ºC and 1300ºC respectively. An increase in material temperature is observed to result in an increase in compressive (normal) strain as well as equivalent plastic strain. Experimental studies conducted by Kukuryk [41] have confirmed that an increase in equivalent plastic strain increases the void closure state during compression.

Depth of plate reduction: Hot rolling simulations were conducted under identical conditions for plates having holes of diameters 10mm, 15mm, 20 mm and 25 mm respectively along the mid plane. The complete rolling schedules (Table 2) were

simulated at an initial temperature of 1100 °C for the two rolling schedules shown in Table 2. The effect of varying thickness reduction of slab on void closure was analyzed. Previous studies by SSAB have suggested that heavy reduction per pass is more beneficial for void closure than low reduction per pass [31]. The deformation penetration has been predicted to be dependent on pass reduction and work roll diameter.

Strain recovery: During hot rolling, when the hot deformed metal experiences plastic strains greater than a critical strain, dynamic recrystallization occurs. Thereafter, when the material is not experiencing deformation, it undergoes static recrystallization. During this process, the microstructure evolution takes place due to recrystallization. The process of recrystallization involves nucleation of new grains that grow by usurping adjacent grain boundaries [42].

On full recrystallization, the complete material consists of new recrystallized grains. The rolling schedule considered in this work involves an inter-pass time that is enough to induce 100% static recrystallization. As a result of recrystallization, the metallurgical memory of the material is lost, and the strain is removed. Due to the strain relaxation the material shows plastic flow from the original yield point and hence no change in flow stress is expected. This should enable greater mass flow and void closure. This phenomenon is referred to as non-accumulated model and was incorporated in the simulation.

As an effect of removal of metallurgical memory at the end of each rolling pass, back stress is removed, and material is more ductile. Non-uniform material deformation in the strip during rolling also gives rise to residual stresses. In the absence of recrystallization (accumulated model), the material experiences an increase in the yield

strength. After each rolling pass, the material undergoes unloading of the elastic strain and is again reloaded during which it yields at a higher stress (shown by point 1 in Figure 7). This phenomenon leads to strengthening and increase in stress for the same plastic strain. The material with accumulated strain behaves similar to one with prestrain during multi-pass rolling. Madi et al [43] have shown that prestrained alloy steel experiences a loss of ductility. In comparison the non-accumulated model makes the material less rigid and more deformable as the material loses all its strain after each rolling pass.

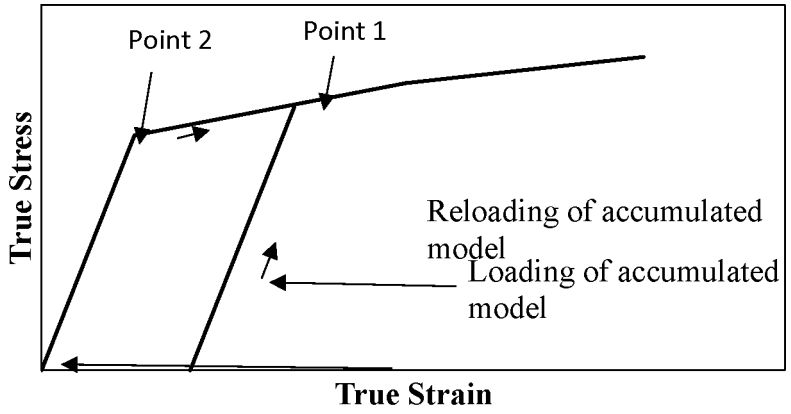

a)

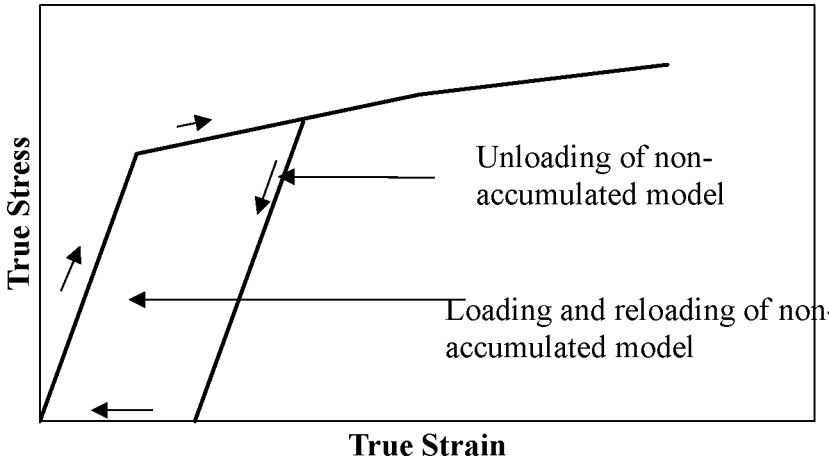

b)

Figure 7. Schematic of flow curve for material showing loading, unloading and reloading paths a) accumulated model b) non-accumulated model

On reloading, the material will yield at the original stress as shown by point 2 in Figure 7. Hence, greater ductility and higher geometric strains are achieved in the case of the non-accumulated strain case. This work studies the influence of non-accumulated strain model on strain and void closure. The difference in material properties for the two discrete states and their influence on void closure has been studied in this work.Although the material model used in this work does not include the grain growth dynamics, this loss of stresses and plastic strains has been incorporated in the non-accumulated strain model and compared with the accumulated strain model.

The non-accumulated model was verified using a simplistic compression test, prior to the rolling simulation. In this numerical test, a cylindrical piece of material 100 mm in length and 50 mm in diameter was compressed until 25% strain and then left to relax. The material models were simulated representing the accumulated model (non-recrystallized) and the non-accumulated (recrystallized) model. The non-accumulated model was calibrated to completely recover its plastic strain on unloading using a customized subroutine VUMAT available in commercial code Abaqus Finite element code Abaqus was used to perform the compression test in two steps (Figure 8a). In the first step, the cylindrical specimen is compressed till 25% strain at a temperature of 1200 ^{o}C. Thereafter in step 2, the specimen is released and allowed to unload while the temperature of the sample is maintained at 1200 ^{o}C. As soon as the step 2 begins the plastic strains are completely recovered and a major part of stresses in the material is released. The loading and unloading process of the non-accumulated model incorporating strain removal was compared with that of the accumulated model (Figure 8b). The stress-strain state of recrystallized material was compared with non-recrystallized material.

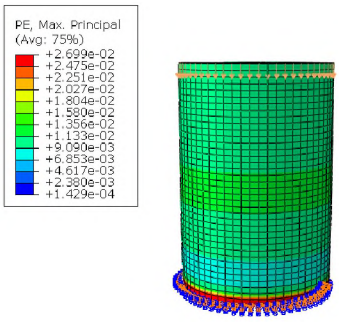

a)

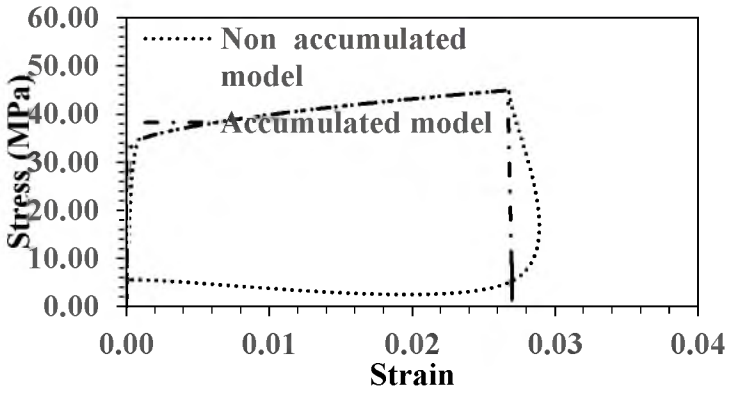

b)

Figure 8. a) Compression test on bar sample b) Effect of strain recovery on the stress-strain for accumulated and non-accumulated model

Discrete hot rolling simulations were conducted for slabs having 30 mm diameter voids for five and seven pass schedules using both the material models. The void constriction was compared for the two models.

3. RESULT AND DISCUSSION

The effect of plastic strain and temperature in the rolled slab on void constriction is discussed in this section. A fine mesh was considered adjoining the void for greater accuracy. The size of the elements were gradually reduced until mesh independence was obtained. Elements with sizes around the cylindrical void were tested for the simulation

as enumerated in Table 5. A coarse mesh consisted of 25 elements along the void circumference and 9 elements along the axis of the cylindrical void. Figure 9 shows the effect on mesh constriction during seven pass rolling for varying element sizes around the void. It was observed that using finer elements and smaller the mesh did not influence the void constriction.

Table 5. Different sizes of elements used around the void

Mesh	Number of axial elements	Number of circumferential elements
Coarse mesh	9	25
Finer mesh	15	40
Fine mesh	21	60

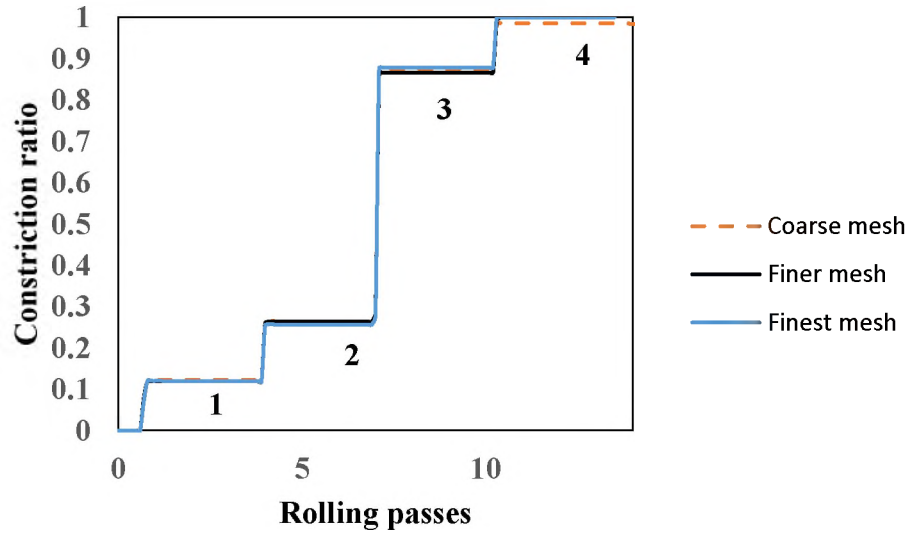

Figure 9. Effect of varying element size around void on mesh constriction

Subsections 3.1 to 3.4 present results of hot rolling simulation with accumulated strain. In accumulated strain models, the material model does not account for the strain

recovery due to recrystallization at the end of each rolling pass. Subsections 3.1 to 3.3 consider seven pass rolling, while subsection 3.4 compares effect of difference in plate reduction using seven pass versus five pass rolling. Finally, subsection 3.5 considers strain recovery during hot rolling and effect on void closure, assuming 100% recrystallization at the end of each rolling pass.

3.1. MULTI-PASS ROLLING AND VOID CLOSURE

For the seven pass rolling with centrally located void the constriction during each pass until void closure is shown in Figure 10.

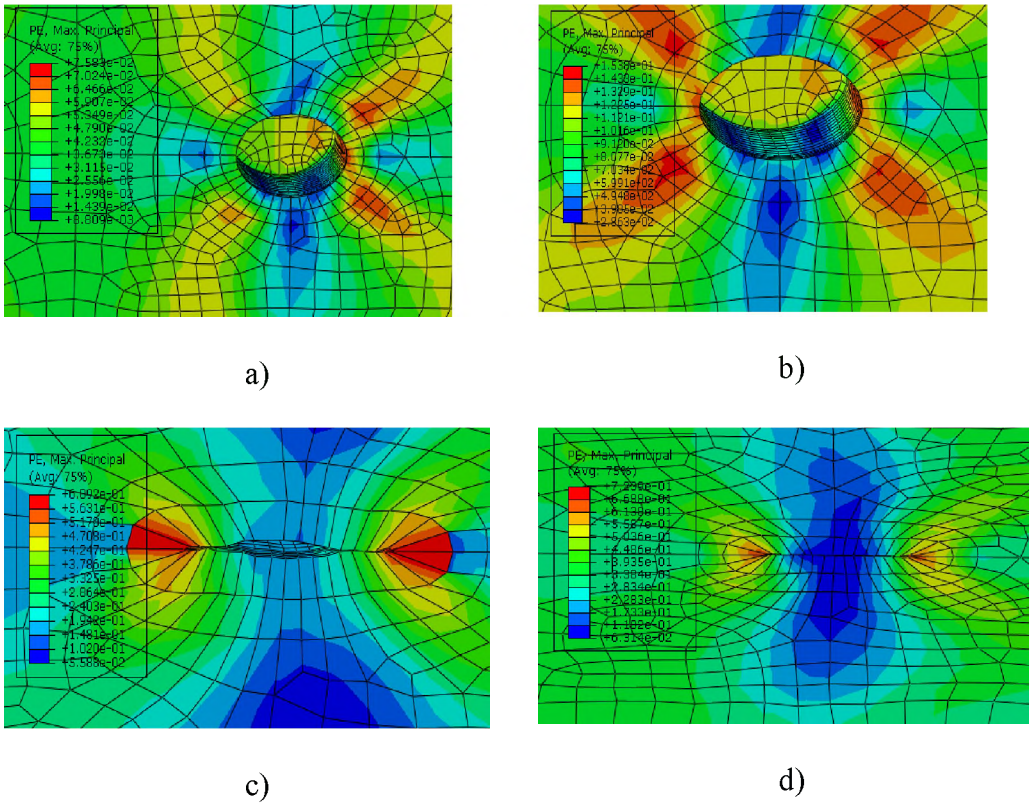

Figure 10. Shape change of void during simulation a) first pass b) second pass c) third pass d) fourth pass

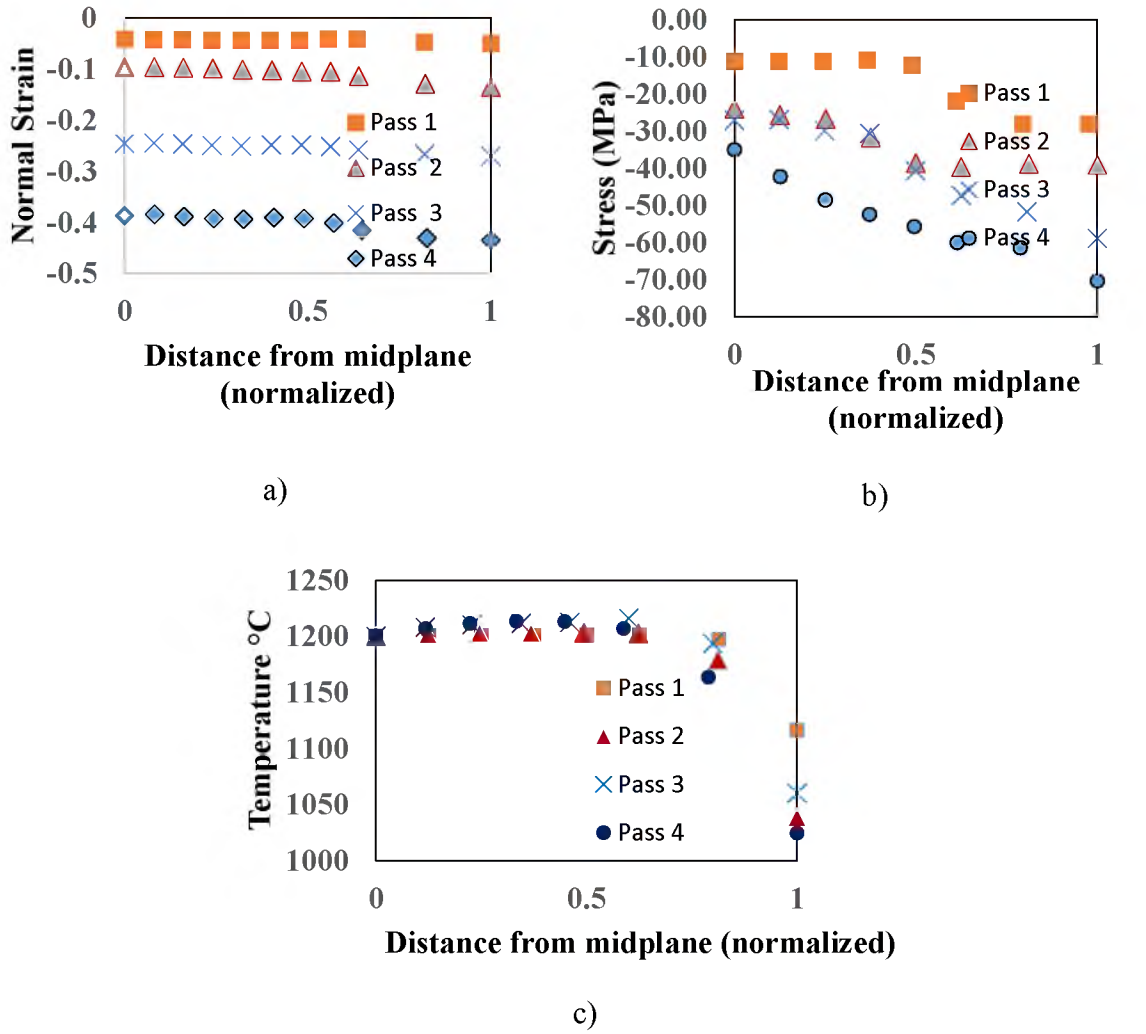

Figure 11. Variation of a) normal plastic strain b) stress and c) temperature along the slab thickness during simulation.

The variation of normal plastic strain, stresses and temperature during each rolling pass is compared in Figure 11. The normal strain increases for each rolling pass and is slightly higher at the surface in comparison to the center. Stress is also observed to increase for each rolling pass. The simulation results are considered for initial slab temperature at 1200 ℃. The surface of the slab shows lower temperature due to contact with the rolls that are at lower temperature.

3.2. EFFECT OF VOID LOCATION ON VOID CLOSURE

The void constriction was studied on simulating seven pass hot rolling. The effect of change in void position on void constriction is shown in Figure 12. The 25 mm diameter void at the center (Case 1) closes completely during the fourth pass, but the same void at the edge (Case 3) is found to close 90% at the end of seventh pass. Hence a void located along the edge of the slab does not close using the seven pass rolling schedule. A void located at a distance of 40 mm from the edge towards the centerline (Case 2) closes almost completely up to 99% at the end of seventh pass. This shows that 25 mm voids at this location could be closed using this schedule.

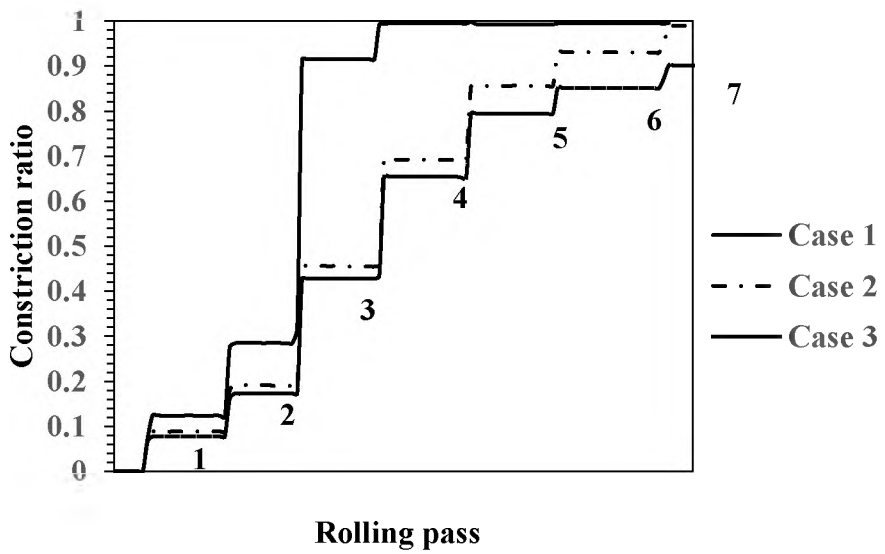

Figure 12. Constriction ratio of voids located at varying distances from the centerline for seven pass rolling

Hence a definite trend is observed for voids located away from the centerline towards the edge. For locations closer to the edge of the slab, greater deformation is needed to obtain closure. The normal strains at the centerline are compressive throughout

the slab, though decreasing from midplane towards the surface. The strains along the side surfaces are also compressive but lower at the midplane and increasing towards the side surfaces. Overall, the compressive strains at the midplane are lower at the sides in comparison to the centerline shown in Figure 13.

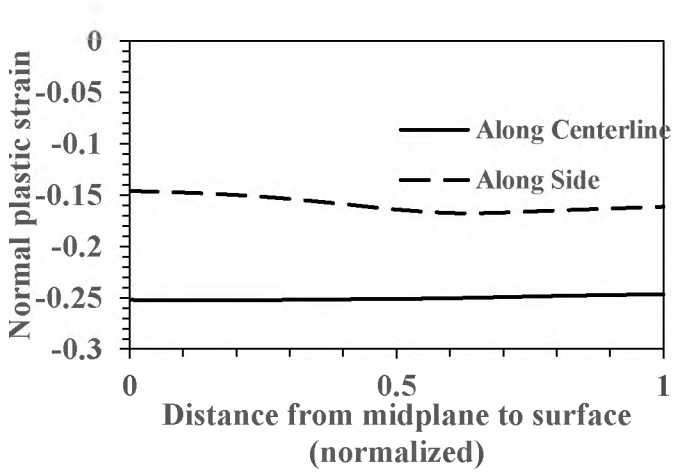

Figure 13. Variation of normal strains along the plate thickness at the side and centerline during the third pass rolling

The variation of equivalent plastic strains is plotted from the center towards the sides in Figure 14.

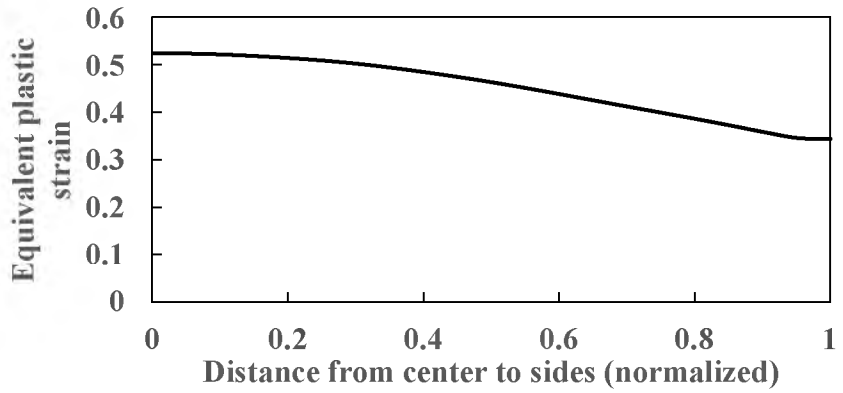

Figure 14. Variation of equivalent plastic strain along midplane from centerline to sides at the end of seven pass rolling schedule

It is evident that the strain is lower along the sides. Therefore, void closure is expected to be reduced at the sides and greater along the centerline as observed using seven pass hot rolling simulations as well.

3.3. EFFECT OF TEMPERATURE ON VOID CLOSURE

The effect of increase in slab temperature on void constriction was simulated using seven pass hot rolling schedule is shown in Figure 15.

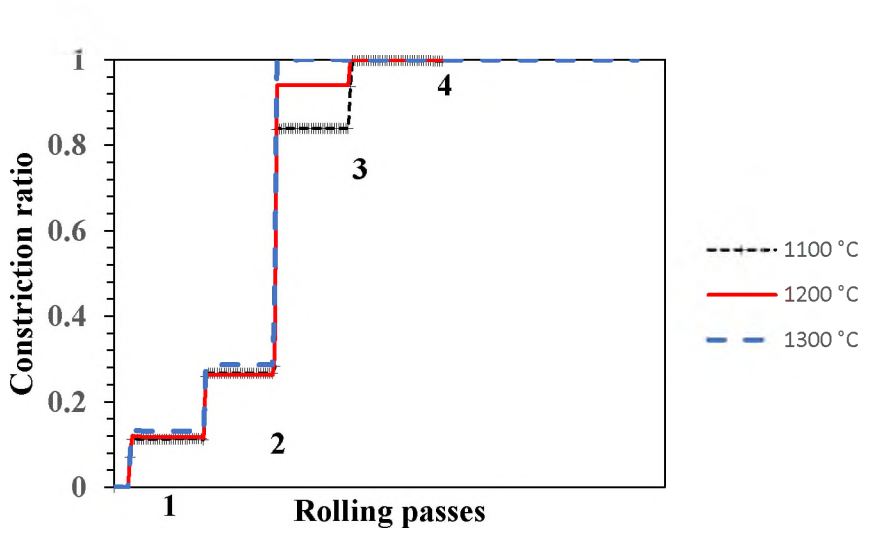

Figure 15. Constriction ratio of void at different rolling temperatures for void with 25 mm initial diameter for seven pass rolling

The 25 mm void closes after the third pass itself at 1300ºC, while it takes four passes to close the same void at 1200ºC and 1100ºC. The maximum thickness reduction is observed during the third pass and hence the strain profile along the thickness of the slab was studied at the end of the third pass rolling for the varying cases. Plastic strain, compressive in nature is observed to decrease along the thickness from the central region towards the surface. It is found that an increase in the overall temperature results in a

slight increase in the compressive plastic strain and major increase in equivalent plastic strain (Table 6). It is therefore expected that void closure is accelerated at higher temperatures.

Table 6. Variation of plastic strain for different rolling temperatures during third pass rolling

Temperature	Normal plastic strain at	Equivalent plastic
1300	0.27	0.45
1200	0.265	0.42
1100	0.25	0.3

3.4. DEPTH OF PLATE REDUCTION AND RATE OF VOID CLOSURE

The effect of plate thickness reduction on void closure was studied using the five and seven pass rolling schedules. The five pass rolling accomplishes the same overall thickness reduction as the seven pass rolling. The same reduction at the end of rolling schedule is obtained by utilizing higher reduction during each individual pass for the five pass rolling. The constriction of voids ranging from 10 mm – 25 mm is plotted in Figure 16 (a) for seven pass rolling. For each rolling pass the slab experiences reduction in thickness and accompanied by constriction of the void. It was found that for holes of 10 mm, 15 mm, 20 mm and 25 mm diameter, complete closure is obtained during the fourth pass of rolling. In comparison the five pass rolling achieves greater pass reduction after each pass and is found to increase the rate of void closure. All voids ranging from 10 mm – 25 mm are found to closewithin two pass rolling.

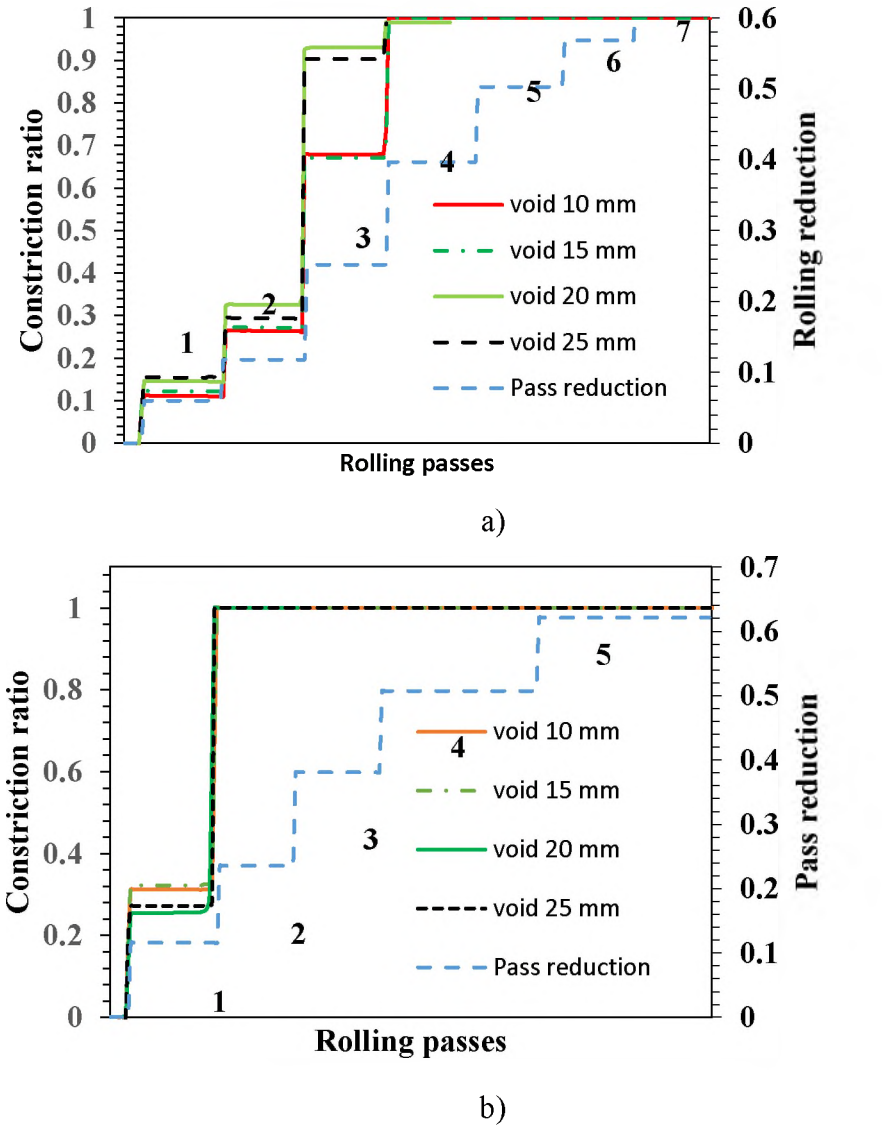

Figure 16. Constriction ratio of voids of varying sizes a) seven pass rolling b) five pass rolling

By the end of the third pass 71.25 % constriction is obtained for the 15 mm diameter void and 73.5% constriction for the 10 mm void. Whereas almost 84% reduction was obtained for 25 mm and 91 % for 20 mm void by the end of the third pass for seven pass rolling.

In comparison, voids of all sizes from 10 mm – 25 mm close within the second pass itself for five pass rolling (Figure 16 (b)).

Since the five pass rolling accomplishes the same final thickness reduction (50%) of the plate in fewer rolling passes, the reduction of thickness per pass is much greater. Hence it is noted that as the extent of plate thickness reduction is increased the rate of void closure also increases. This is in agreement with prior studies done that experimentally determine the change in void closure with heavier pass reductions [31].

In summary a void of diameter 25 mm closes if a cumulative 23.5% pass reduction is applied for five pass rolling. Whereas the same void closes within 39.6% pass reduction for seven pass rolling as shown in Figure 17.

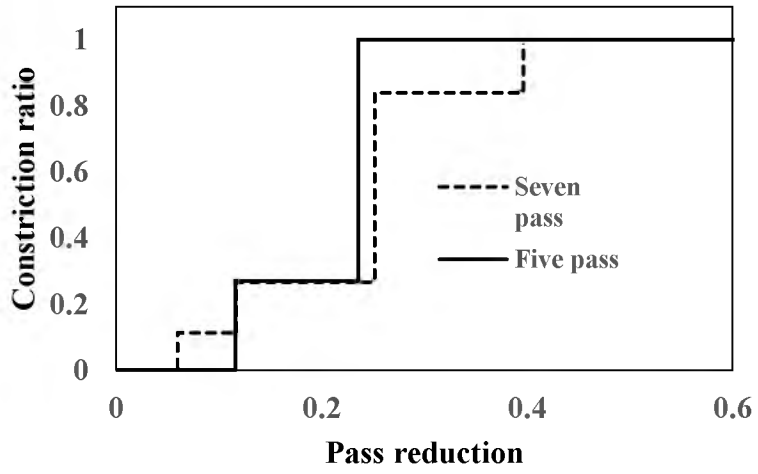

Figure 17. Lower cumulative pass reduction sufficient to close 25 mm diameter void

In order to analyze the influence of material properties on void closure, the stress and plastic strain gradients were determined along the thickness of the slab. Figure 18 shows the variation of normal plastic strains along the thickness of the slab during the

third pass rolling. The strain gradients obtained corresponds well with prior studies [25]. The normal plastic strain, compressive in nature is observed to decrease along the thickness from the midplane towards the surface. Similarly, the normal compressive stress is noted to also decrease from the midplane towards the surface.

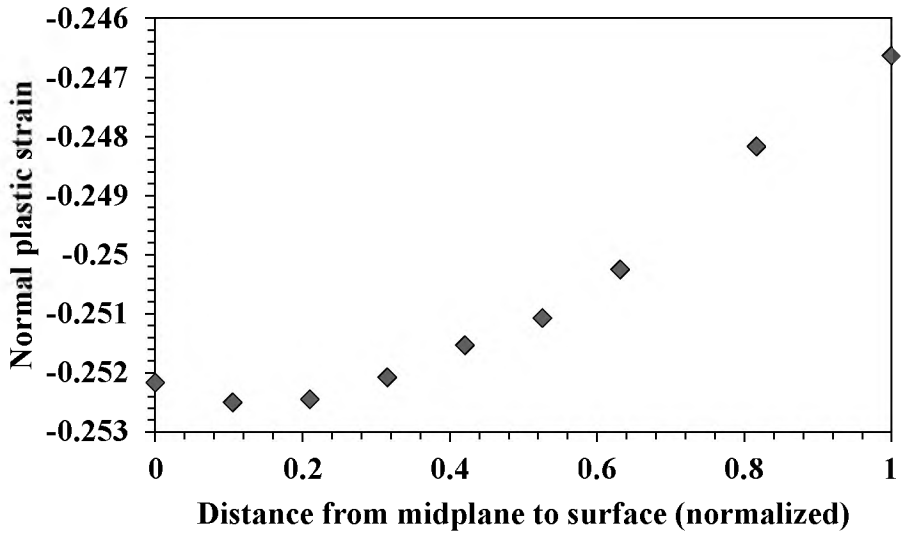

Figure 18. Variation of normal plastic strain along the thickness at 1100 °C

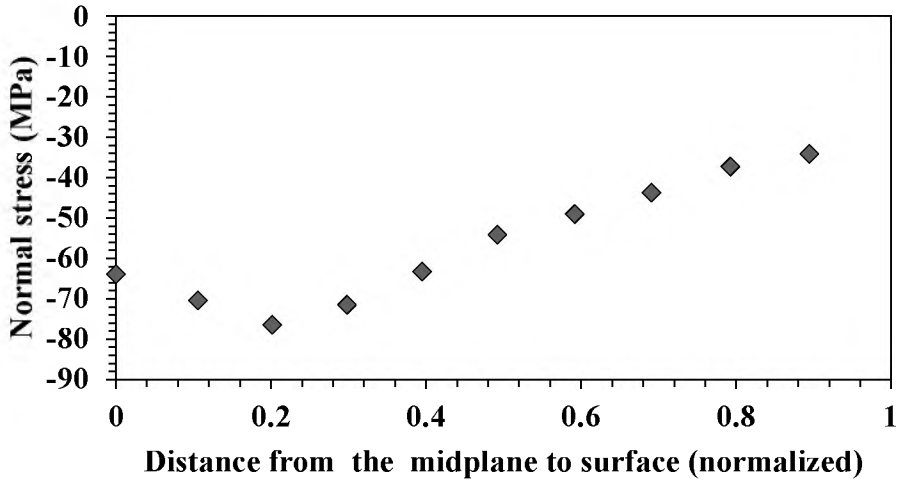

Figure 19. Variation of the normal stress along the thickness of the plate

The effect of normal strain is considered to be the primary influencing factor for void constriction in the thickness direction. Since the largest compressive strains are at the midplane the present work focuses on voids in this region and the critical void size is determined along this plane. The variation of the normal compressive stress along the thickness of the plate is shown in Figure 19. The stress is largest at the midplane and decreases towards the outer surface.

3.5. EFFECT OF RECRYSTALLIZATION

The influence of the accumulated and non-accumulated models on void closure was analyzed by conducting hot rolling simulation of slab with 30 mm diameter hole. Figure 20 a) shows the constriction of a 30 mm diameter void during the seven pass hot rolling process for both the accumulated and non-accumulated models. It was observed that in the case of non-accumulated model, the material shows faster void closure signifying the greater deformability of the material. The void closes during the fourth pass for non-accumulated strain model whereas the closure occurs during the fifth pass for the accumulated strain model. Similarly, for five pass rolling also void closure is accentuated for the non-accumulated model as shown in Figure 20 b).

During the rolling process, the slab experiences compressive stresses that are removed during the inter-pass period. Overall, the recrystallized material experiences greater mass flow and ductility at the center of the slab, and this is expected to influence the void closure to a greater extent in comparison to the non-recrystallized material. Strains along the midplane of the rolled slab are noted in Table 7 for the third rolling pass that has the highest thickness reduction.

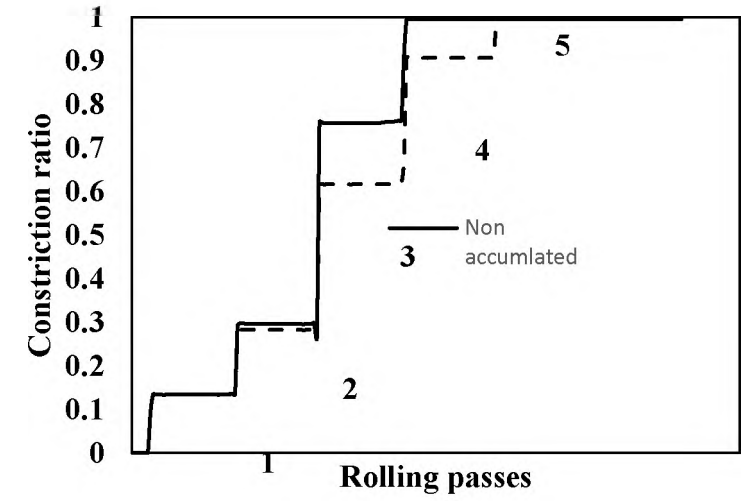

a)

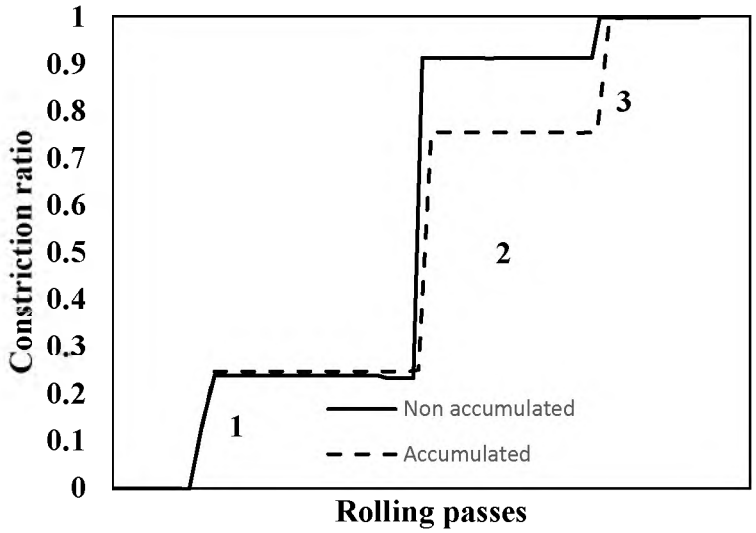

b)

Figure 20. Effect of accumulated versus non-accumulated strain during a) seven pass rolling and b) five pass rolling on void closure.

It was observed that the non-accumulated model showed higher normal strains in comparison to the accumulated model during each rolling pass. Hence, it is expected that void closure be higher for non-accumulated model as confirmed using hot rolling simulations.

Table 7. Comparison of strain during the third pass for both models

	Normal plastic strain
Accumulated strain model	0.25
Non-accumulated strain model	0.27

The Table 8 summarizes the influence of individual parameters on void healing. The effect of pass reduction was found to be the most paramount in influencing void closure.

Table 8. Effect of different parameters on void closure

Parameter	**Effect on void closure**
Pass reduction	High
Void location	Medium
Temperature	Low
Strain recovery	Medium

4. CONCLUSION

A thermally sensitive elasto-plastic material model was considered to study void closure during hot rolling process. The study evaluated the influence of critical rolling parameters as thickness reduction, slab temperature, recrystallization as well as location of void on plastic strains and void constriction using finite element simulations. Prior experimental studies have determined that increase in compressive strains as well as effective strains experienced within the material increase void closure. The present work

considered 6-inch thick slabs reversibly rolled to 50% reduction using five and seven pass rolling schedules. Voids 10mm, 15 mm, 20 mm and 25 mm in diameter closed after the fourth pass during the seven pass rolling employed in this study. In comparison, each of the voids closed after the second pass for the five pass rolling. Hence, larger pass reductions have bigger impact on void closure.

The closure is reduced near the slab sides. The 25 mm diameter void closes up to 90% when it is located along the edges of the slab. The extent of void closure increases progressively towards the interior of the slab, with voids located at a distance more than 40 mm from the sides close entirely. From the point of view of industrial rolling, it would be beneficial to scale off 40 mm of material from the sides to prevent presence of voids. The compressive strains are lower along the edges than the centerline. Hence, an increase in compressive strain enhances the void closure for plate hot rolling.

Simulations of slab rolling at different temperatures showed that compressive as well as equivalent plastic strain increases with increasing deformation temperature. This will increase the mass flow, resulting in an acceleration of void closure. Finally, the effect of slab rolling with recrystallization induced stress-strain relaxation during inter-pass was studied with reference to void closure. Effect of recrystallization or strain removal on slab rolling was found to increase the rate of void closure to a small extent. This is due to the greater ductility achieved as a result of lowering the yield criterion in comparison to accumulated strain model. The study was able to correlate that rolling process parameters that contributed to an increase in plastic strains within the material also resulted in an increase in void closure during hot rolling.

ACKNOWLEDGEMENTS

This work was supported by the Peaslee Steel Manufacturing Research Center at Missouri University of Science and Technology.

REFERENCES

[1] B. Moazeni and M. Salimi, "Investigations on formation of shape defects in square rolling of uniform thin flat sheet product," *Iron Steel Institute Japan Int.*, vol. 53, pp. 257–264, 2013.

[2] A. P. Voskamp and E. J. Mittemeijer, "State of residual stress induced by cyclic rolling contact loading," *Mater. Sci. Technol.*, vol. 13, pp. 430–438, 2014.

[3] L. E. Collins, F. Hamad, M. Kostic, and T. Lawrence, "Production of high strength line pipe steel by steckel mill rolling and spiral pipe forming," Frontier Pipe Research Unit, Regina Canada, 1999.

[4] H. B. Yang, L. J. Zhang, and Z. H. Hu, "The analysis of the stress and strain in skew rolling," *Adv. Mater. Res.*, vol. 538, pp. 1650–1653, 2012.

[5] U. Hanoglu and B. Šarler, "Simulation of hot shape rolling of steel in continuous rolling mill by local radial basis function collocation method," *C. - Comput. Model. Eng. Sci.*, vol. 109, no. 5, pp. 447–479, 2015.

[6] U. Hanoglu and B. Šarler, "Multi-pass hot-rolling simulation using a meshless method," *Comput. Struct.*, vol. 194, pp. 1–14, 2018.

[7] U. Hanoglu and B. Šarler, "Hot rolling simulation system for steel based on advanced meshless solution," *Metals (Basel).*, vol. 9, no. 7, 2019, doi: 10.3390/met9070788.

[8] J. G. Cao, S. J. Liu, J. Zhang, P. Song, T. L. Yan, and Y. Z. Zhou, "ASR work roll shifting strategy for schedule-free rolling in hot wide strip mills," *J. Mater. Process. Technol.*, vol. 211, no. 11, pp. 1768–1775, 2011.

[9] S. Y. Kim and Y. T. Im, "Three-dimensional finite element analysis of non-isothermal shape rolling," *J. Mater. Process. Technol.*, vol. 127, pp. 57–63, 2002.

[10] X. Duan and T. Sheppard, "Three dimensional thermal mechanical coupled simulation during hot rolling of aluminium alloy 3003," *Int. J. Mech. Sci.*, vol. 44, pp. 2155–2172, 2002.

[11] L. M. Galantucci and L. Tricarico, "Thermo-mechanical simulation of a rolling process with an FEM approach," *J. Mater. Process. Technol.*, vol. 92–93, pp. 494–501, 1999.

[12] P. Montmitonnet, "Hot and cold strip rolling processes," *Comput. Methods Appl. Mech. Eng.*, vol. 195, no. 48–49, pp. 6604–6625, 2006.

[13] T. Kim, W. Lee, and S. Hwang, "An integrated FE process model for the prediction of strip profile in flat rolling," *Isij Int. - ISIJ INT*, vol. 43, pp. 1947–1956, Jan. 2003.

[14] Y. Li, J. Cao, G. Yang, D. Wen, Y. Zhou, and H. Ma, "ASR bending force mathematical model for the same width strip rolling campaigns in hot rolling," *steel Res. Int.*, vol. 86, Sep. 2014.

[15] H. Ding, K. Hirai, T. Homma, and S. Kamado, "Numerical simulation for microstructure evolution in AM50 Mg alloy during hot rolling," *Comput. Mater. Sci.*, vol. 47, pp. 919–925, 2010.

[16] X. Wang, F. Li, Q. Yang, and A. He, "FEM analysis for residual stress prediction in hot rolled steel strip during the run-out table cooling," *Appl. Math. Model.*, vol. 37, pp. 586–609, 2013.

[17] D. Benasciutti, E. Brusa, and G. Bazzaro, "Finite elements prediction of thermal stresses in work roll of hot rolling mills," *Procedia Eng.*, vol. 2, pp. 707–716, 2010.

[18] R. S. Nalawade, A. J. Puranik, G. Balachandran, K. N. Mahadik, and V. Balasubramanian, "Simulation of hot rolling deformation at intermediate passes and its industrial validity," *Int. J. Mech. Sci.*, vol. 77, pp. 8–16, 2013.

[19] G. Johnson and W. Cook, "A constitutive model and data for metals subjected to large strains, high strain rates and high temperatures," *7th Int. Symp. Ballist.*, vol. 21, pp. 541–547, 1983.

[20] F. J. Zerilli and R. W. Armstrong, "Dislocation-mechanics-based constitutive relations for material dynamics calculations," *J. Appl. Phys.*, vol. 61, pp. 1816–1825, 1987.

[21] X. Wang, K. Chandrashekhara, S. A. Rummel, S. Lekakh, D. C. Van Aken, and R. J. O'Malley, "Modeling of mass flow behavior of hot rolled low alloy steel based on combined Johnson-Cook and Zerilli-Armstrong model," *J. Mater. Sci.*, vol. 52, pp. 2800–2815, 2017.

[22] S. Shida, "Empirical formula of flow stress of carbon steels-resistance to deformation of carbon steels at elevated temperature," *J. Japan Soc. Technol. Plast.*, vol. 10, pp. 610–617, 1969.

[23] P. Montmitonnet, P. Gratacos, and R. Ducloux, "Application of anisotropic viscoplastic behaviour in 3D finite-element simulations of hot rolling," *J. Mater. Process. Technol.*, vol. 58, pp. 201–211, 1996.

[24] J. Chen, K. Chandrashekhara, C. Mahimkar, S. N. Lekakh, and V. L. Richards, "Study of void closure in hot radial forging process using 3D nonlinear finite element analysis," *Int. J. Adv. Manuf. Technol.*, vol. 62, pp. 1001–1011, 2012.

[25] D. Pustovoytov, A. Pesin, A. P. Zhilyaev, and G. I. Raab, "FEM simulation of influence of asymmetric cold rolling on through-thickness strain gradient in low-carbon steel sheets," *Defect Diffus. Forum*, vol. 385, pp. 455–460, 2018.

[26] P. O. Aiyedun, L. G. M. Sparling, and C. M. Sellars, "Temperature changes in hot flat rolling of steels at low strain rates and low reduction," *Proc. Inst. Mech. Eng.*, vol. 211 Part B, pp. 261–284, 1997.

[27] M. Saby, P. O. Bouchard, and M. Bernacki, "A geometry-dependent model for void closure in hot metal forming," *Finite Elem. Anal. Des.*, vol. 105, pp. 63–78, 2015.

[28] V. Nalawade, R. S., Patil, P.P., Balachandran, G., Balasubramanium, "Void closure in a large cross section bars hot rolled from a low alloy steel ingot casting," *Trans. Indian Inst. Met.*, vol. 69, pp. 1711–1721, 2016.

[29] F. Faini, A. Attanasio, and E. Ceretti, "Experimental and FE analysis of void closure in hot rolling of stainless steel," *J. Mater. Process. Technol.*, vol. 259, pp. 235–242, 2018.

[30] H. Gao, Z. Ai, H. Yu, H. Wu, and X. Liu, "Analysis of internal crack healing mechanism under rolling deformation," *PLoS One*, vol. 9, pp. g001–g006, 2014.

[31] D. Bai, E. Moe, C. Rawlinson, V. Clark, S. Hanssen, and Y. Wang, "Effect of pass schedule on deformation penetration in plate rolling," in *AISTech*, 2018, pp. 2287–2294.

[32] M. Chen, Y. C. Lin, G. Liu, M. Chen, and J. Zhong, "Prediction of static recrystallization in a multi-pass hot deformed low-alloy steel using artificial neural network," *J. Mater. Process. Technol.*, vol. 209, pp. 4611–4616, 2009.

[33] Y. Sun, W. D. Zeng, Y. Q. Zhao, Y. L. Qi, X. Ma, and Y. F. Han, "Development of constitutive relationship model of Ti600 alloy using artificial neural network," *Comput. Mater. Sci.*, vol. 48, pp. 686–691, 2010.

[34] X. Wang, S. Ganguly, K. Chandrashekhara, M. F. Buchely, S. N. Lekakh, D. C. Van Aken, and R. J. O'Malley, "Modeling and simulation of mass flow of steel plate/slab during hot rolling," in *International Conference on Recent Developments in Plate Steels*, 2018, pp. 63–71.

[35] Dassault Systemes, *Abaqus 6.16 Documentation*, 2016th ed. 2016.

[36] J. G. Lenard and L. Barbulovic-Nad, "The coefficient of friction during hot rolling of low carbon steel strips," *J. Tribol.*, vol. 124, pp. 840–845, 2002.

[37] M. J. Peet, H. S. Hassan, and H. K. D. H. Bhadeshia, "Prediction of thermal conductivity of steel," *Int. J. Heat Mass Transf.*, vol. 54, pp. 2602–2608, 2011.

[38] H. Hasan, M. Peet, J. Jalil, and H. Bhadeshia, "Heat transfer coefficients during quenching of steels," *Heat Mass Transf.*, vol. 47, pp. 315–321, 2011.

[39] M. Qin, J. Liu, and J. Li, "Establishment and application of the void closure prediction model of 316LN," *Metals (Basel).*, vol. 9, pp. 538–556, 2019.

[40] K. Chen, Y. Yang, G. Shao, and K. Liu, "Strain function analysis method for void closure in the forging process of the large-sized steel ingot," *Comput. Mater. Sci.*,vol. 51, no. 1, pp. 72–77, 2012.

[41] M. Kukuryk, "Experimental and FEM analysis of void closure in the hot cogging process of tool steel," *Metals (Basel).*, vol. 9, pp. 538–556, 2019.

[42] D. Xu, C. Ji, H. Zhao, D. Ju, and M. Zhu, "A new study on the growth behavior of austenite grains during heating processes," *Sci. Rep.*, vol. 7, pp. 3968 (1–13), 2017.

[43] Y. Madi, Y. Shinohara, and J. Besson, "Effect of prestrain on ductility and toughness in a high-strength line pipe steel," *Int. J. Fract.*, vol. 1, pp. 146–153, 2020.

II. MODELING AND SIMULATION OF MASS FLOW DURING HOT ROLLING LOW CARBON STEEL I-BEAM

S. Ganguly[1], X. Wang[1], K. Chandrashekhara[1], M. F. Buchely[2], S. Lekakh[2], and R. J. O'Malley[2]

1. Department of Mechanical and Aerospace Engineering
2. Department of Materials Science and Engineering
Missouri University of Science and Technology, Rolla, MO 65409

A. Kumar and V. Thapliyal

Nucor Yamato Steel, Blytheville, AR 72316

ABSTRACT

Continuously cast near net shape blanks have been widely used in industry owing to the benefit of producing items close to final shape. However, for complicated shaped blanks, such as I and H beams, using near net shape blanks is not enough to prevent unwanted mass flow and deformation during hot rolling. The strength of the rolled material, pre-existing defects, and hot rolling parameters all have a major influence on the final shape of the rolled beam. In this study, the shaping of a low carbon steel during the breakdown mill hot rolling process was investigated using finite element analysis. The geometry of the as cast beam blank, mill roll profiles and hot rolling pass schedule were modeled identically to that used during the production hot rolling operation. The results showed that the I-beam has more deformation in the flange than in the web for breakdown mill rolling. A small depression or waviness was found to develop along the beam flange during the simulation. A parametric study of the effect of the roll gap on mass flow and beam blank surface depressions was performed. It was observed that for a

larger roll gap, the surface depression increased in size. In contrast, the depression was found to decrease with a smaller rolling gap due to greater mass flow. These results agreed with the industrial produced I-beam. It was also predicted that the presence of a pre-existing surface defect on the beam blank flange has a significant influence on final size of the depression.

1. INTRODUCTION

Deformation and mass flow behavior of steel during hot rolling is a complex phenomenon and its analysis is important to improve final product quality. Viscoplastic deformation results in plastic strain and the corresponding strain energy contributes to microstructural development in the steel product. During hot rolling, the geometry of the as cast steel blank strongly influences the mass flow behavior. Compared to round billet hot rolling, near net shape beam blanks have more complex stress and strain distributions. It is hard to employ traditional analytical methods to investigate this highly nonlinear material deformation process during hot rolling. Numerical analysis has been used to improve the product design and optimization since the 1980s [1]. Finite element analysis (FEA) has an advantage over other numerical methods to simulate and analyze the hot rolling manufacturing process involving complicated geometries and non-linear boundary conditions. Using a calibrated constitutive model, FEA provides an effective and successful way to study mass flow behavior, optimize rolling designs, and enhance final steel quality and productivity.

It is important for the numerical analysis to be equipped with a robust material model to provide accurate results. Material models can be broadly categorized as

empirical and physical based models. The physical models are based on the physics of the deformation process and utilize variables that represent the physical state of the material. However, such models are much more complex to develop. Empirical models have a closed mathematical form and need very few tests to identify their coefficients. Empirical models are usually preferred over physical models due to their low computation and experimental costs. In order to describe the viscoplastic behavior of steel, a number of constitutive empirical models and physical models have been proposed in the recent decade as reviewed by Lin and Chen [2]. The Johnson-Cook (JC) model [3] is one of the most widely used empirical based phenomenological constitutive models and considers the effects of strain hardening, strain rate hardening, and temperature softening on flow stress. The Ludwig empirical model [4] is similar to the JC model with the limitation of the temperature range (maximum 100 °C). The empirical model developed by Shida [5] was also found to be effective at low strain rates (< 0.7 /s).

Physical constitutive models differ from phenomenological models as they are based on complex mathematical theories obtained from the kinetic models of the metallurgical processes to derive flow stress-based equations. Zerilli–Armstrong (ZA) model [6] is one of the widely used physical models based on dislocation mechanisms. The ZA model considers the coupled effect of temperature and strain rate and exhibits more flexibility than the JC model in predicting material properties. However, the coupled effect of temperature and strain rate in the ZA model is limited, and numerous modified versions have been proposed. Similar physical models have been independently considered by Bergstrom [7]. The model compared well with the JC model but was unable to predict the strain jumps. The simplified expression and easy implementation

contribute to the extensive use of the JC model. Furthermore, the JC model is effective for strain rates varying between 0.002 – 600 /s and hence ideal for modeling an exhaustive range of manufacturing operations over a wide temperature range.

Hot rolling has been investigated for many years by means of numerical simulation. The hot rolling process simulation involves large deformations, coupled thermomechanical analysis, non-linear boundary conditions and non-linear material behavior. Kim and Im [8] proposed a finite element model to simulate shape rolling for a non-uniform temperature distribution. Finite element method (FEM) has been used to study roll wear and flatness control by Cao et al [9]. Relationship between roll gap profile and bending force on strip profile was analyzed using FEM by Li et al. [10]. Yang et al. [11] investigated the blank size effect on strain and temperature distribution during hot rolling of titanium alloy ring using FEM. Nalawade et al. [12] investigated mass flow behavior of micro-alloyed 38MnVS6 steel during multi-pass hot rolling. Detailed strain distributions on a regular cross section showed that both tension and compression existed during hot rolling of the 38MnVS6 steel.

Structural shape rolling is widely used in industry to obtain final shapes such as I-beam, H-beam, U-beam channels and railroad rails. These types of beams have wide applications in bridges, architectural applications, railroads and the arts. As per the author's observations, studies regarding mass flow during hot rolling for such complicated shapes have been sparse. For complex shaped cast sections, the effect of a non-uniform temperature gradient is of greater importance when compared to round or square billets and slabs and needs to be taken into consideration. Thermal stresses usually develop due to the presence of non-uniform temperature gradients and influence final

product quality. Bulging and overfill along the flange [13] as well as edge waviness [14] are some common defects that are observed on rolling channel sections. The initial contact region for a beam blank is a cambered surface with non-uniform compressive forces. Takashima and Hiruta [13] conducted FEA of a U shaped channel and determined that the strain gradient between the flange and the web regions influenced the creation of bulge at the channel corners. Hence it was important to calibrate the roll gap accordingly to avoid the creation of deformities. Li et al. [15] studied nonlinear deformation during H-beam hot rolling using a finite element method and the proposed FEM was verified by comparing the simulated temperature with experimental data. In addition, for complicated as-cast and rolled shapes, the geometry of the free surface changes drastically and hence it is critical to develop a realistic finite element model to simulate the manufacturing process. Chenot et al. [16] studied the material flow for square to oval bar during hot rolling using a three dimensional finite element model. Liu et al. [17] made a detailed analysis of slab rolling by taking into consideration the change in width of the workpiece. Shin et al. [18] studied I-beam rolling using finite element simulations limited to cold rolling. The cross-sectional area changes significantly during rolling and this further influence rolling torque and mass flow. The study showed that in addition to the generation and loss of heat that affects the rolling torque [19], the specific geometrical factors need to be taken into consideration by adjusting the rolling parameters to improve product quality. However, literature on FEA that involves highly nonlinear geometries and elevated thermal conditions for three-dimensional I-beam hot rolling is limited.

Presence of metallic inclusions or shrinkage during the casting process may result in a pre-existing defect. The presence of existing as cast distortions on the profile of the

hot rolled beams also has a critical effect on its final shape. It has been found that the size of such defects have a direct correlation with the fatigue life of the rolled products [20]. Studies have shown that when the defects arising from rolling are critical they later lead to development of cracks [21]. Few studies have been conducted to verify the stress strain response of beams with distortions. Seo et al. [22] conducted fatigue analysis of rail beams with surface defects. The study found that residual stress distribution occurs due to the presence of indentation. This residual stress influenced the fatigue behavior of the material under contact stresses. Yu [23] used FEA to model the effect of existing cracks during slab rolling and observed that the friction and crack length were critical parameters that influenced the hot rolled slab profile.

In the current study, hot tensile tests were conducted to generate experimental data and develop an accurate JC material model for a low carbon steel. A three-dimensional nonlinear finite element model incorporating the developed material model was created to simulate the hot rolling of an I-Beam from the as-cast beam blank. It has been observed during the industrial rolling process that roll gap has a critical influence on the formation of deformities during hot rolling. The influence of roll gap on defect formation was studied. In addition, the effect of an existing deformity in the I-Beam on the final rolled shape was also analyzed.

2. MATERIALS AND METHODS

2.1. HOT TENSILE TESTS

A low carbon steel grade (0.075 wt.% C, 0.26 wt.% Si, 0.9 wt.% Mn and 0.016 wt.% Nb) was investigated in this study. Hot tensile tests were done using an MTS load

frame to perform thermomechanical testing at varying temperatures and strain rates to determine the material flow behavior. Cylindrical specimens of 15 mm height and 10 mm diameter were machined from an as-cast beam blank (Figure 1). The specimens were heated by an induction coil to 1300 °C at a heating rate of 260 °C/min , held for 3 minutes, and cooled to the desired test temperature. An additional hold of 2 minutes was included in the test schedule to minimize temperature gradients and establish a fully austenitic microstructure. After that the tensile test was performed at the selected temperatures and strain rates. Three temperatures (1000°C, 1100°C, and 1200°C) and four strain rates (0.01 s^{-1}, 1 s^{-1}, 5 s^{-1}, and 10 s^{-1}) were selected for hot tensile tests based on the actual hot rolling conditions. Each test parameter combination was replicated three times and a total of 48 specimens were tested.

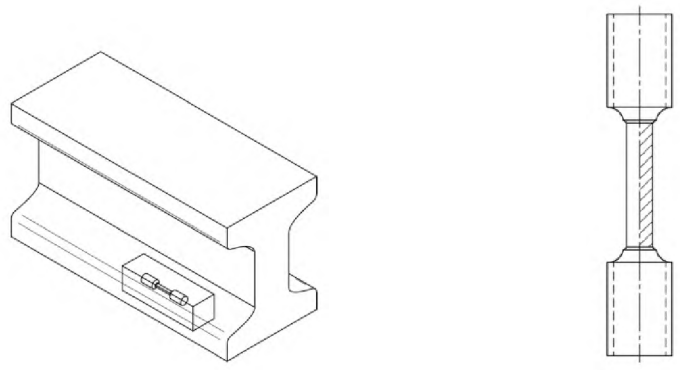

(a) (b)

Figure 1. Schematic view of testing samples utilized in the study: (a) initial as-cast beam blank, specimens were cut along the rolling direction and (b) final shape of tensile samples having gauge section (shaded) with 15 mm height and 10 mm diameter.

2.2. MATERIAL MODELING

The JC model is expressed as follows:

$$\sigma = (A + B\varepsilon^{n})(1 + C \ln \dot{\varepsilon}^{*})(1 - T^{*m}) \quad (1)$$

where: σ is equivalent stress, ε is equivalent plastic strain, $\dot{\varepsilon}^{*} = \dot{\varepsilon}/\dot{\varepsilon}_0$ is dimensionless strain rate, $\dot{\varepsilon}$ is strain rate, $\dot{\varepsilon}_0$ is reference strain rate, T is current temperature, and T^{*} is homologous temperature given by:

$$\mathrm{T}^{*} = \frac{T - T_r}{T_m - T_r} \quad (2)$$

where T_r is reference temperature and T_m is metal melting temperature, A is a yield stress at a user defined reference temperature and reference strain rate (1000°C and $1s^{-1}$), B and n are the strain hardening parameters, C is a strain rate hardening parameter, and m is a temperature softening parameter.

2.3. FINITE ELEMENT MODELING

A nonlinear three-dimensional finite element model was developed to study the beam blank hot rolling deformation process.

The matrix equation for dynamic analysis is given by equation 3.

$$[M^{e}]\{\ddot{\Delta}^{e}\} + [K^{e}]\{\Delta^{e}\} = \{F^{e}\} + \{F^{t}\} \quad (3)$$

where $[M^e]$ and $[K^e]$ are mass matrix and stiffness matrix respectively, $\{F^e\}$ is the mechanical loading vector, $\{F^t\}$ is the thermal loading, $[\ddot{\Delta}^e]$ and $[\Delta^e]$ are the acceleration and displacement vectors.The mechanical model was coupled to a thermal model using the following heat transfer formulation:

$$[C_T]\{\dot{\theta}\} + [K_T]\{\theta\} = \{Q\} \tag{4}$$

where $[C_T]$ is the heat capacitance matrix, $[K_T]$ is the conductivity matrix, $\{Q\}$ is total heat flow, Θ is the temperature. Q consists of the sum of internal heat generation by plastic deformation and heat flux across boundaries.

The explicit method in Abaqus [24] is used to solve the finite element formulation as it is more efficient to solve problems that include large deformation, complicated geometry and discontinuous contact. The explicit method obtains the solution by inverting the mass matrix and solving for the acceleration from the previous increment. Thereafter the kinematic state is advanced using the accelerations.

The equations of mechanical motion are integrated using the explicit central difference integration rule [25].

$$\{\ddot{U}\}_i = (M)^{-1}(\{F\}_i + \{F_T\}_i - \{I\}_i) \tag{5}$$

$$\{\dot{U}\}_{i+\frac{1}{2}} = \{\dot{U}\}_{i-\frac{1}{2}} + \frac{\Delta t_{i+1} + \Delta t_i}{2}\{\ddot{U}\}_i \tag{6}$$

$$\{U\}_{i+1} = \{U\}_i + \Delta t_{i+1}\{\dot{U}\}_{i+\frac{1}{2}} \tag{7}$$

where $\ddot{U}$ is the acceleration, $\dot{U}$ is the velocity, U is the displacement, subscript i refers to the increment number in an explicit dynamic step, and I is the internal force vector given by $\{I\}_i = [K]\{U\}_i$.

The beam blank breakdown mill hot rolling process of reheated continuous cast beam blanks was simulated. The initial flange and web widths of near net shape cast I-beam blank were measured as 0.412 m and 0.123 m respectively. Large deformations and significant mass flow were expected during the breakdown mill hot rolling process. There are three grooves in breakdown mill with multiple passes for reverse rolling. P1-P7 are in

the first groove, P8-P11 are in the second groove, and P12 and P13 are in the third groove. The schematic model of the breakdown mill roller profile is shown in Figure 2. A fixed roll gap was used in the simulation to deform the I-beam assuming no significant elastic deformation of the rollers.

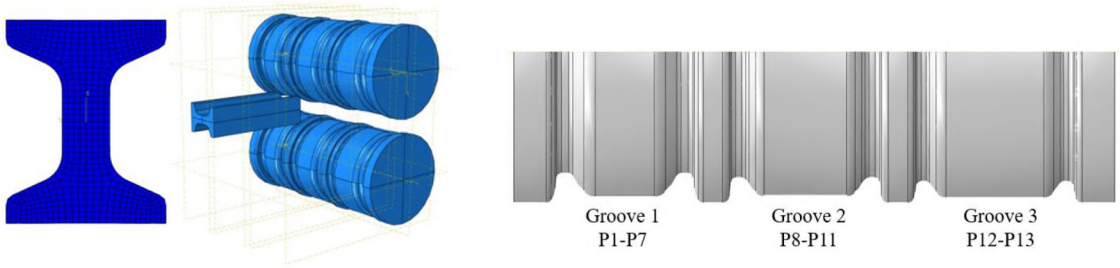

a) b) c)

Figure 2. Schematic of I-beam production: (a) near net shape cast blank, (b) breakdown mill, and (c) detail of the roller profile for Pass 1 to Pass 7 (Groove 1), Pass 8 to Pass P11 (Groove 2), and Pass 12 to Pass 13 (Groove 3).

The steel blank and roller geometries were modeled using ABAQUS software[24], as shown in Figure 3. Surface to surface hard contact was used to model the contact behavior between the steel bar and rollers. The friction behavior between contact pairs was defined by Coulomb's law of friction with a friction coefficient of 0.5 [26]. The I-beam was built as a three-dimensional deformable part using 8-node brick elements (C3D8RT) and rolls were modeled as rigid parts using 4-node rigid quadrilateral elements (R3D4) as shown in Figure 3.

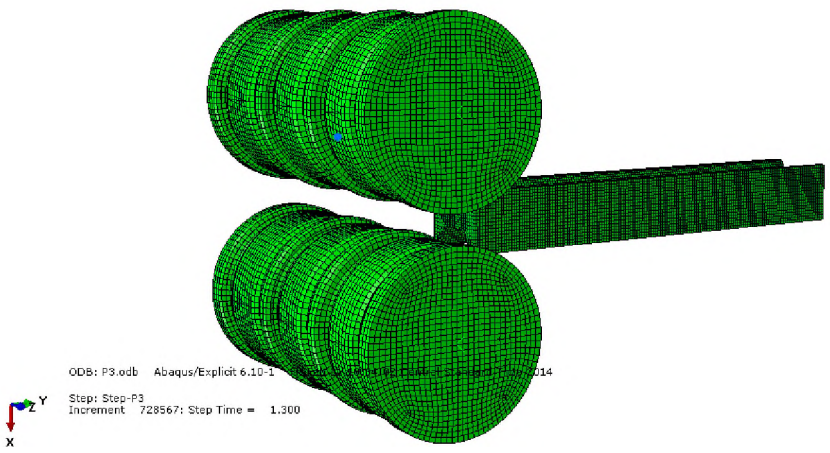

Figure 3. Mesh of I-beam hot rolling process

Since the I-beam has a large, highly complicated shape, using a very fine mesh results in high usage of computational space and time. Hence an appropriate mesh size was used for the I-beam. Similar mesh has also been used in prior hot rolling simulations [27][28]. The I-beam was meshed with brick elements having cross-section (15 mm X 15 mm), while a coarse mesh of quadrilateral elements having cross-section (300 mm X 300 mm) was enough for the rollers.

3. RESULTS AND DISCUSSION

3.1. TENSILE TEST AND MATERAL MODEL

The experimental results from the tensile tests are shown in Figure 4. Both engineering and true stress-strain curves are shown in these figures. The maximum true strain is observed to be within 0.4 in accordance with practical rolling conditions. However, the engineering stress-strain curves extend beyond 0.4 strain.

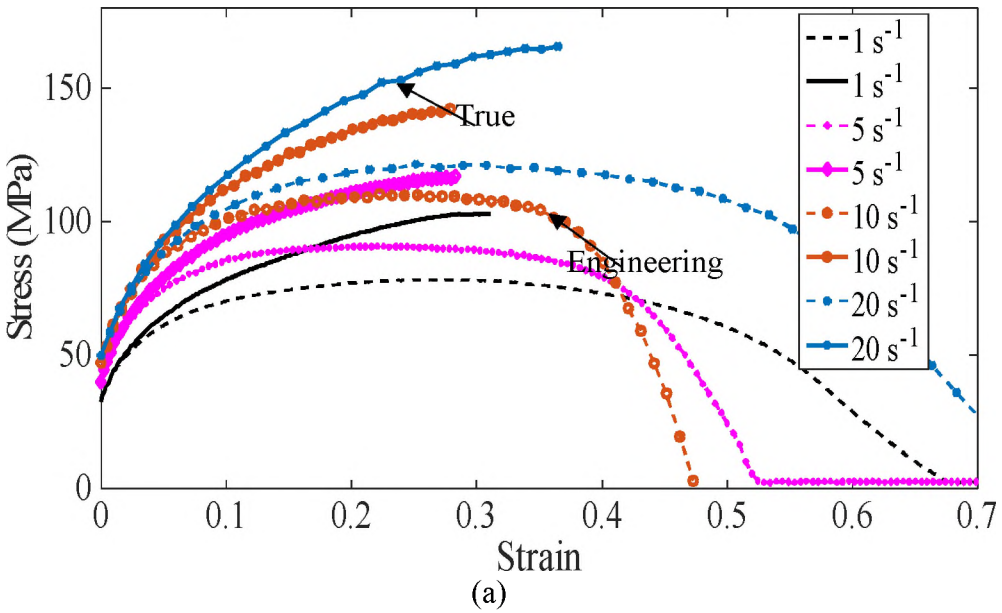

(a)

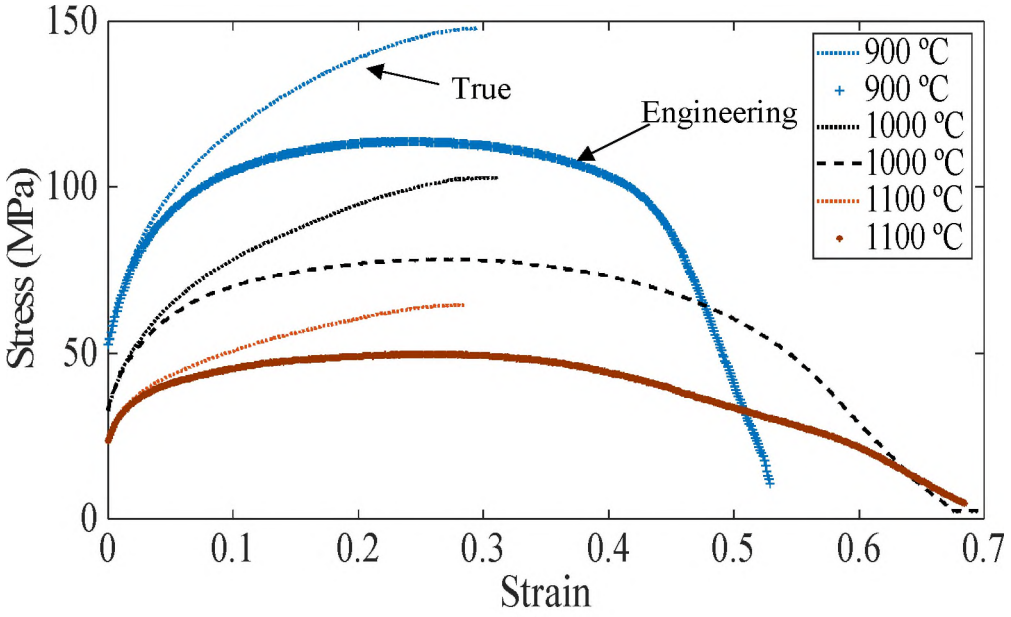

(b)

Figure 4. Experimental engineering and true stress-strain curves from hot tensile tests: (a) at different strain rates and constant 1000°C and (b) at different temperatures and constant strain rate of $1s^{-1}$.

Note that as temperature decreases (Figure 4b) and strain rate increases (Figure 4a), the flow stress increases as expected for this steel. Two different methods are frequently used to determine the JC parameters [29]. One approach uses curve fitting to determine the parameters individually. Another approach determines all five parameters simultaneously by an optimization method [30]. In the current study, initial parameters were determined by curve fitting optimization using nonlinear least-square method. JC model parameters built based on experimental stress-strain curves (Table 1) were implemented in the finite element model.

Table 1. Calibrated JC model parameters for the studied steel.

A	*B*	*C*	*n*	*m*
10.64	69.69	0.41	0.42	0.56

3.2. SIMULATION RESULTS OF BREAKDOWN MILL

During the first pass P1, the flange was deformed significantly along the area designated by red color in Figure 5. At the same time, there was no deformation along the web since the rolling gap is larger than the web thickness. During the second pass P2, there was greater contact between the flange and the rollers, resulting in deformation along the flange sides. Material flows from the flange sides into the center of the flange and then towards the web. The masss\ flow after each rolling pass was studied in detail. The effect of roll gap on the height of the depression was predicted after each roll pass. Hence a relationship between roll gap and depth of depression was obtained. Therefore, during the third pass P3, two peaks develop on the flange surface.

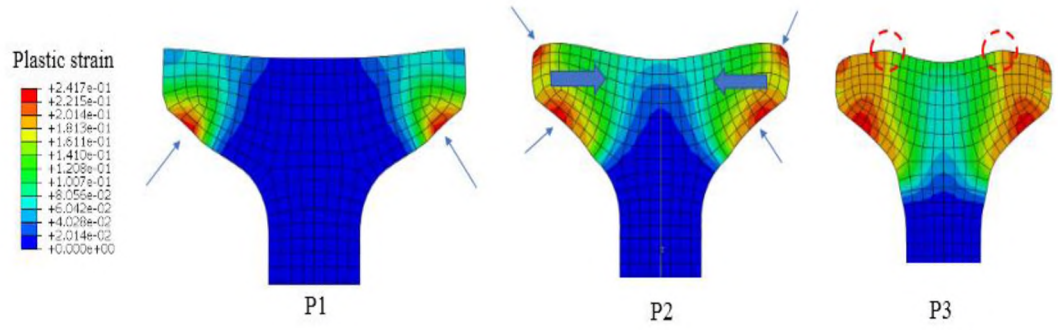

Figure 5. Deformation process and plastic strain of the beam blank from passes P1 to P3.

During the passes P4 to P7 (Figure 6), further deformation occurs along the thickness of the web and flange. The mass flow behavior from passes P4 to P7 is similar to pass P3 and the two peak regions increase in prominence on the surface of the flange. The distance between the two peaks decreases due to deformation.

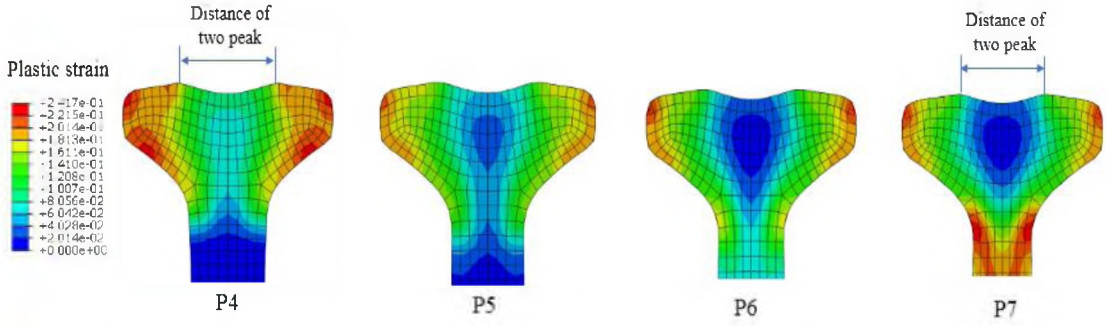

Figure 6. The deformation process form passes P4 to P7.

The I-beam was deformed using groove 2 from pass P8 to P11. Due to the change in rolling profile, the rolling gap for pass P8 was larger than the web thickness. The

material flows from the flange towards the web area during pass P8. As the rolling progresses, a further decrease in thickness of flange is observed. The deformations of I-beam during passes P8 - P11 was similar to that during pass P8 (Figure 7).

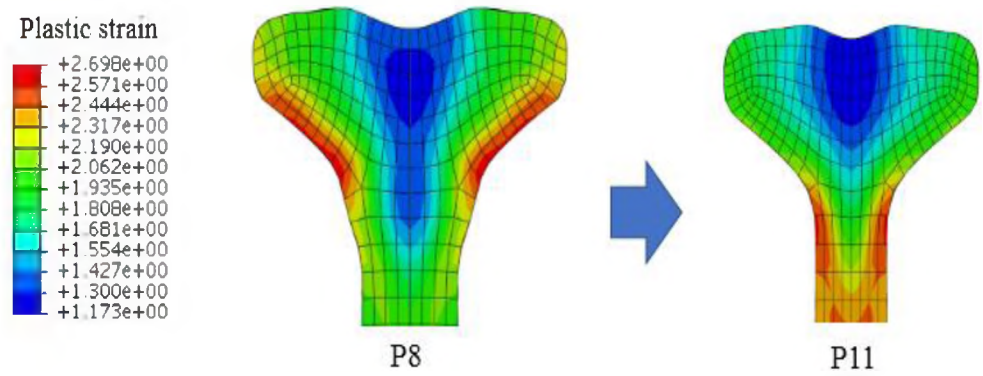

Figure 7. The I-beam shape and plastic strain for passes P8 and P11.

Finally, the I-beam was deformed using groove 3 during passes P12 and P13 using a very small pass reduction (not shown). Figure 8 shows the results of the hot rolling simulation after all 13 passes in the breakdown mill. During hot rolling, the web and the flange were deformed in the thickness direction and two peak regions were generated on the top surface of flange. The maximum stress is observed at the connection area between the flange and the web. After 13 passes, the flange and the web widths were reduced from 0.412 m to 0.182 m and from 0.123 m to 0.05 m, respectively. The maximum plastic strain and deformation were found in the center of web, while the center of the flange had minimal plastic strain due to material being able to flow freely towards the web region.

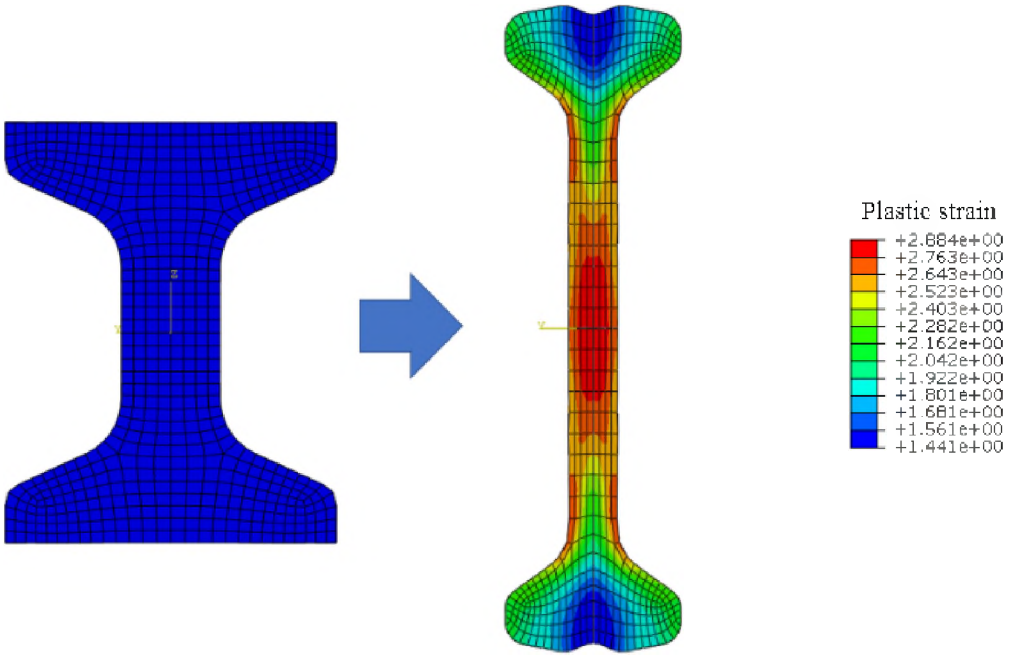

Figure 8. Simulated accumulated strain during hot rolling and changes in beam shape after 13 passes in the breakdown mill.

Experimental I-beam shapes after breakdown mill rolling at three different positions (head, middle, and tail) were compared to the final simulation results, as shown in Figure 9. The simulation results predicted a small depression on the flange surface along the head and tail regions, while the middle of I-beam showed a larger depression. The simulation correctly predicted the variation of I-beam cross-sectional shape along the longitudinal direction and compared well with the production hot rolled sample shapes.

3.3. EFFECT OF ROLLING GAP ON FINAL BEAM PROFILE

During hot rolling in the industrial setting, the roll gap generally varies within some amount from the designed roll gap due to rolling loads. Also, cast blanks have some degree of surface distortion related to solidification shrinkage.

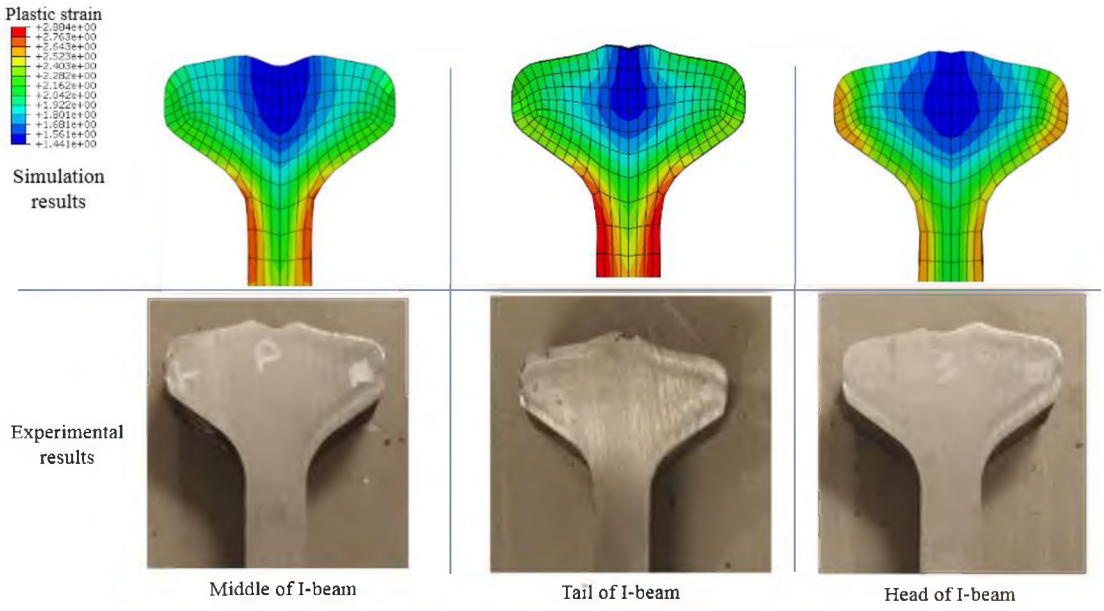

Figure 9. Comparison of I-beam shapes of simulation and experimental results.

The effect of rolling gap and as cast blank surface distortion on mass flow and surface geometry of hot rolled beam after breakdown mill were simulated and compared to industrial beams. Three different configurations, as designed, maximum and minimum gap profiles were investigated to perform a sensitivity analysis. The flange depression and peaks were measured for the maximum, minimum, and ideal (designed) roll gaps, as shown schematically in Fig 10 a. The simulated I-beam shapes for the three cases are shown in Fig 10 b. The gap between the peaks and the depressions for the simulated beam and the industrially rolled beam are enumerated in Table 2. It is evident that with a larger rolling gap, the predicted size of the depression on the surface of the flange is found to increase, while for smaller gaps the depression is reduced. A smaller roling gap is more conducive to disallow the mass flow of the material from the center of the flange towards the web and hence prevent increase in the depth of the depression.

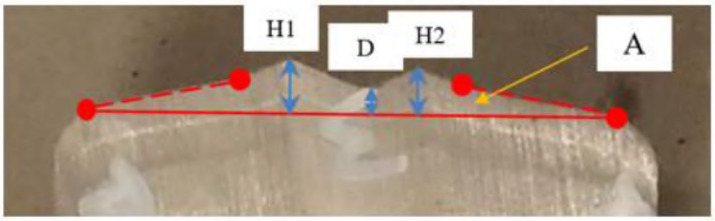

(a)

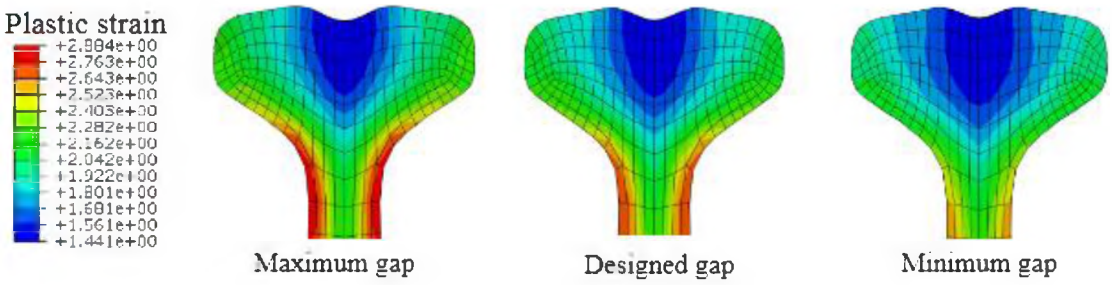

(b)

Figure 10. (a) Actual deformed shape of I-beam flange after rolling in industrial set up and (b) simulation results for maximum, designed and minimum gaps.

Table 2. Measurements of the flange depression after hot rolling (see Figure 10a for measuring. details in mm).

Parameter	*Experimental*	*Max. gap*	*Designed gap*	*Min. gap*
0.5(H1+H2)-D	7.45	10.25	8.37	7.23

3.4. EFFECT OF AS CAST BLANK DISTORTION ON FINAL BEAM PROFILE

Based on practical observations from industrial trials, a small surface as cast distortion was created in the I-beam model as shown in Figure 11. Such distortions develop due to solidification shrinkage and are often found along the flange surface of the beam blank. It is assumed that the presence of this surface dent is one of the most important factors that influences the mass flow behavior of the I-beam during hot rolling. Therefore, a surface dent similar to a realistic defect observed in industry was modeled

on the initial beam blank. The dent had a width of 3-inches and a depth of 0.25 inches in depth.

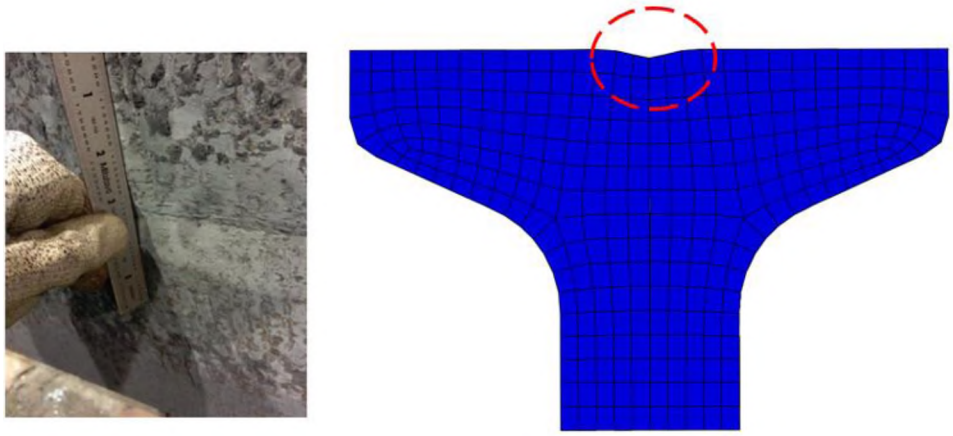

Figure 11. Flange surface distortion observed in as cast I beam (left) and used in model (right).

Full scale breakdown mill hot rolling simulations were conducted on the I-beam with this surface distortion. The simulation results showed that the distortion in the middle of flange surface has a significant influence on the deformed I-beam shape, as shown in Figure 12. The final shape of the rolled I-beam shows a much deeper depression on the flange surface in comparison to an I-beam without distortion. The detailed dimensions of the flange depression are enumerated in Table 3. The presence of an initial as cast distortion on the beam blank results in increasing the depth of the depression in hot rolled beam from 8.37 mm to 16.68 mm. Hence it is imperative to study the influence of as cast distortion on multi pass rolling and predict how the rolling parameters can be optimized to improve product quality.

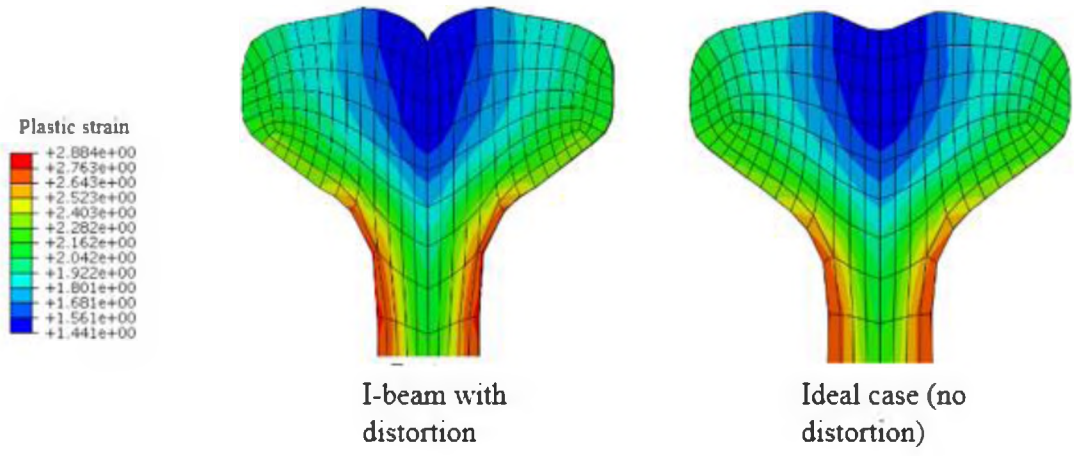

Figure 12. Comparison of accumulated plastic strain and simulated hot rolled I beam geometry for ideal shape of cast blank with cast blank having surface distortion.

Table 3. Effect of dent in the flange depression (mm) after hot rolling (see Figure 10a for measurement details).

Parameter	*With dent*	*Without dent*
0.5(H1+H2) - D	16.68	8.37

Hence the presence of an existing distortion on the beam blank results in an increase of almost 99% in the depth of depression in a hot rolled beam after breakdown mill. In addition, the combined effects of a surface distortion and roll gap setting were investigated. Discrete hot rolling simulations were conducted for an I-beam with a dent in combination with the designed roll gap (case 1) and a minimal roll gap (case 2) to investigate the mass flow behavior. Using a small rolling gap, greater material flowed towards the rolling gap resulting in a decrease in the depth of depression (Figure 13).

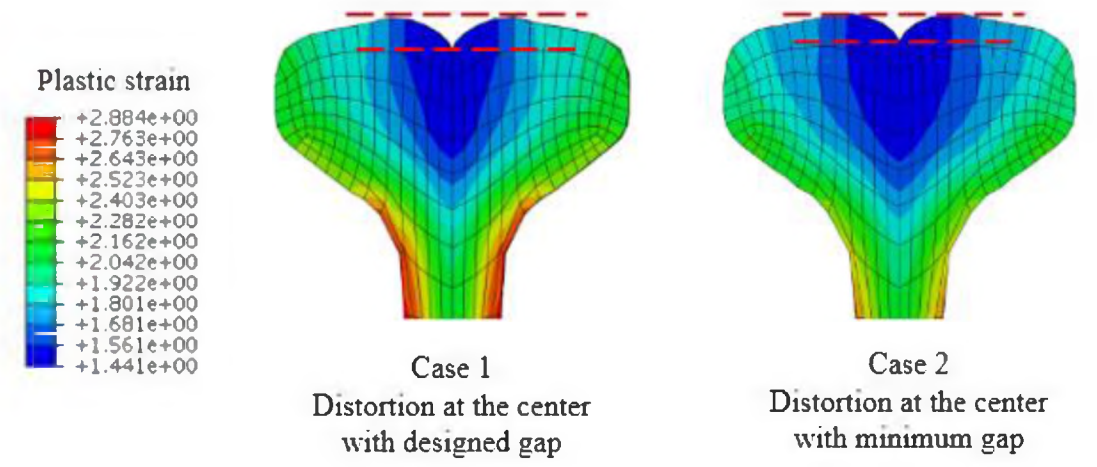

Figure 13. Simulation results of coupled effect of surface distortion and rolling gap on accumulated strain for designed gap and minimum gap.

It was noted that the depth of the depression decreased from 16.68 mm to 13.07 mm for case 2 by using a smaller roll gap as enumerated in Table 4.

Table 4. Coupled effect of dent and rolling gap in the flange depression (mm) after hot rolling (see Figure 10a for measuring details).

Parameter	***Case 1***	***Case 2***
0.5(H1+H2) - D	16.68	13.07

Thus, it can be predicted using the hot rolling simulations that the depression is reduced by using a smaller roll gap for the case of a beam blank with as cast flange distortion. Further, although the decrease in depth of depression is 13.6% for a normal I-beam, the decrease in depth is significantly higher (21.6%) in the case of a beam blank with a flange distortion.

4. CONCLUSION

In this study, the mass flow behavior and defect formation of a low carbon steel during hot rolling I-beam was investigated. High temperature tensile tests were performed to obtain the thermo-mechanical properties of steel at varying temperatures and strain rates. A Johnson-Cook model was developed using experimental results and was incorporated into a finite element model. A three-dimensional dynamic finite element model was built to study the I-beam hot rolling process. The influence of roll gap on defect formation and evolution of existing defects was predicted. The simulated shape of the hot rolled I-beam sample and the final size of the defect were compared with that observed during industrial plant rolling trials.

Based on simulation results, the I-beam was found to be deformed largely along the flange region during the initial passes P1 to P4. It is further observed that formation of a depression on the flange surface began from pass P4. On further rolling the thickness of the web and flange further reduced between passes P5 to P7. The rolling profile changed from groove 2 onwards (passes P8-P11) and the I-beam was considerably elongated. During rolling under groove 3, the size of the surface depression on the flange surface grew rapidly and was highly noticeable. Such waviness in the I-beam profile has been observed during industrial plant rolling as well. The effect of varying rolling gap on the flange profile was investigated using finite element simulation. The results showed that with a small rolling gap, more material flows towards the roll gap and the size of the formed flange depression is reduced.

The presence of metallic inclusions or occurrence of solidification shrinkage in the rolled material often leads to a condition similar to that of a pre-existing defect. A

surface distortion was introduced in the as-cast I-beam to represent a pre-existing defect. The effect of breakdown mill hot rolling on the I-beam profile having surface distortion was investigated. The simulation results showed that the central distortion on the as cast flange surface had a significant influence on the final shape of the I-beam. The presence of distortion on the as-cast shape can increase the depression and waviness at the flange center dramatically. Finally, it was predicted using simulations that the depth of the formed depression in the hot rolled beam with an existing dent was reduced considerably when a reduced rolling gap was used. This suggests that the roll gap is a very critical parameter that can be utilized to control the shape evolution in I-beams with an existing as cast surface irregularity.

ACKNOWLEDGEMENTS

This work was supported by the Peaslee Steel Manufacturing Research Center at Missouri University of Science and Technology.

REFERENCES

[1] G. Wang and Y. M. Rong, "Advances of physics-based precision modeling and simulation for manufacturing processes," *Adv. Manuf.*, vol. 1, pp. 75–81, 2013.

[2] Y. C. Lin and X. M. Chen, "A critical review of experimental results and constitutive descriptions for metals and alloys in hot working," *Mater. Des.*, vol. 32, pp. 1733–1759, 2011.

[3] G. R. Johnson and W. H. Cook, "A constitutive model and data for metals subjected to large strains, high strain rates and high temperatures," in *Proceedings of the 7th International Symposium on Ballistics*, pp. 541-547,1983.

[4] J. Van Slycken, P. Verleysen, J. Degrieck, L. Samek, and B. C. De Cooman, "High-strain-rate behavior of low-alloy multiphase aluminum- and silicon-based transformation-induced plasticity steels," *Metall. Mater. Trans. A Phys. Metall. Mater. Sci.*, vol. 37, pp. 1527–1539, 2006.

[5] S. Shida, "Empirical formula of flow stress of carbon steels-resistance to deformation of carbon steels at elevated temperature," *J. Japan Soc. Technol. Plast.*, vol. 10, pp. 610–617, 1969.

[6] F. J. Zerilli and R. W. Armstrong, "Dislocation-mechanics-based constitutive relations for material dynamics calculations," *J. Appl. Phys.*, vol. 61, pp. 1816–1825, 1987.

[7] K. Domkin, "Constitutive models based on dislocation density Formulation and implementation into finite element codes," Luleå University of Technology, 2005.

[8] S. Y. Kim and Y. T. Im, "Three-dimensional finite element analysis of non-isothermal shape rolling," *J. Mater. Process. Technol.*, vol. 127, pp. 57–63, 2002.

[9] J. G. Cao, S. J. Liu, J. Zhang, P. Song, T. L. Yan, and Y. Z. Zhou, "ASR work roll shifting strategy for schedule-free rolling in hot wide strip mills," *J. Mater. Process. Technol.*, vol. 211, pp. 1768–1775, 2011.

[10] Y. Li, J. Cao, G. Yang, D. Wen, Y. Zhou, and H. Ma, "ASR Bending Force Mathematical Model for the Same Width Strip Rolling Campaigns in Hot Rolling," *Steel Res. Int.*, vol. 86, Sep. 2014.

[11] H. Yang, M. Wang, L. G. Guo, and Z. C. Sun, "3D coupled thermo-mechanical FE modeling of blank size effects on the uniformity of strain and temperature distributions during hot rolling of titanium alloy large rings," *Comput. Mater. Sci.*, vol. 44, pp. 611–621, 2008.

[12] R. S. Nalawade, A. J. Puranik, G. Balachandran, K. N. Mahadik, and V. Balasubramanian, "Simulation of hot rolling deformation at intermediate passes and its industrial validity," *Int. J. Mech. Sci.*, vol. 77, pp. 8–16, 2013.

[13] Y. Takashima and T. Hiruta, "Characteristics of deformation behavior in channel universal rolling," *ISIJ Int.*, vol. 53, pp. 690–697, 2013.

[14] J. S. K. V. Zal, M. H. Naeini, A. R. Bahramian, "Experimental investigation on the roll forming of PVC /aluminum/glass fabric FMLs into channel section profiles," *Modares Mech. Eng.*, vol. 16, pp. 207–215, 2016.

[15] K. Li, P. Wang, G. Liu, P. Yuan, and Q. Zhang, "Development of simulation system for large H-beam hot rolling based on ABAQUS," *Int. J. Adv. Manuf. Technol.*, vol. 85, pp. 1649–1663, 2016.

[16] J. L. Chenot, P. Montmitonnet, A. Bern, and C. Bertrand-Corsini, "A method for determining free surfaces in steady state finite element computations," *Comput. Methods Appl. Mech. Eng.*, vol. 92, pp. 245–260, 1991.

[17] C. Liu, P. Hartley, C. E. N. Sturgess, and G. W. Rowe, "Finite-element modelling of deformation and spread in slab rolling," *Int. J. Mech. Sci.*, vol. 29, pp. 271–283, 1987.

[18] H.-W. Shin, D.-W. Kim, and N. Kim, "A study of the rolling of I-section beams," *Int. J. Mach. Tools Manuf.*, vol. 34, pp. 147–160, 1994.

[19] P. O. Aiyedun, L. G. M. Sparling, and C. M. Sellars, "Temperature changes in hot flat rolling of steels at low strain rates and low reduction," *Proc. Inst. Mech. Eng.*, vol. 211 Part B, pp. 261–284, 1997.

[20] T. Makino, Y. Neishi, D. Shiozawa, S. Kikuchi, S. Okada, K. Kajiwara and Y. Nakai , "Effect of defect length on rolling contact fatigue crack propagation in high strength steel," *Frat. ed Integrita Strutt.*, vol. 9, pp. 334–340, 2015.

[21] P. P. Sarkar, S. K. Dhua, S. K. Thakur, and S. Rath, "Analysis of the surface defects in a hot-rolled low-carbon C–Mn steel plate," *J. Fail. Anal. Prev.*, vol. 17, pp. 545–553, 2017.

[22] J. Seo, S. Kwon, and D. Lee, "Effects of surface defects on rolling contact fatigue of rail," *Procedia Eng.*, vol. 10, pp. 1274–1278, 2011.

[23] H. Yu, FE Analysis of Evolution of Defects during Rolling, *Finite Element Analysis*, InTech, 2010.

[24] *Abaqus 6.18, Theory Manual*. Hibbit, Karlsson & Sorenson Inc, 2018.

[25] J. Chen, K. Chandrashekhara, C. Mahimkar, S. N. Lekakh, and V. L. Richards, "Study of void closure in hot radial forging process using 3D nonlinear finite element analysis," *Int. J. Adv. Manuf. Technol.*, vol. 62, pp. 1001–1011, 2012.

[26] M. Awais, H. W. Lee, Y. T. Im, H. C. Kwon, S. M. Byon, and H. D. Park, "Plastic work approach for surface defect prediction in the hot bar rolling process," *J. Mater. Process. Technol.*, vol. 201, pp. 73–78, 2008.

[27] X. Wang, S. Ganguly, K. Chandrashekhara, M. F. Buchely, S. N. Lekakh, D. C. Van Aken, R. J. O'Malley, D. Bai, Y. Wang, "Modeling and Simulation of Mass Flow of Steel Plate - Slab during Hot Rolling," *Int. Conf. Recent Dev. Plate Steels*, pp. 63–71, 2018.

[28] S. Ganguly, X. Wang, D. B. K. Chandrashekhara, M. F. Buchely, S. Lekakh, R. J. O'Malley, and Y. Wang, "Modeling and simulation of void closure during Steckel Mill rolling for steel plate," *Steel Res. Int.*, doi: 10.1002/srin.202000293, pp.1-12, 2020.

[29] X. Wang, K. Chandrashekhara, S. A. Rummel, S. Lekakh, D. C. Van Aken, and R. J. O'Malley, "Modeling of mass flow behavior of hot rolled low alloy steel based on combined Johnson-Cook and Zerilli-Armstrong model," *J. Mater. Sci.*, vol. 52, pp. 2800–2815, 2017.

[30] N. Dusunceli, O. U. Colak, and C. Filiz, "Determination of material parameters of a viscoplastic model by genetic algorithm," *Mater. Des.*, vol. 31, pp. 1250–1255, 2010.

III. A MODIFIED JOHNSON-COOK MODEL INCORPORATING THE EFFECT OF GRAIN SIZE ON FLOW STRESS

S. Ganguly[1], M.F. Buchely[2], F. Okanmisope[1], K. Chandrashekhara[1], S. Lekakh[2], R. J. O'Malley[2]

[1]Department of Mechanical and Aerospace Engineering
[2]Department of Materials Science and Engineering
Missouri University of Science and Technology, Rolla, MO 65409

ABSTRACT

The mechanical properties of steel are influenced by grain size, which can change through mechanisms such as nucleation and growth at elevated temperatures. However, the classic Johnson-Cook model that is widely used in hot deformation simulations does not consider the effect of grain size on flow stress. In this study, the Johnson-Cook model was modified to incorporate the effects of austenite grain size on flow stress. A finite element model was employed to characterize the effects of grain size on the flow stress for different steel grades over a range of temperatures (900°C to 1300°C). Simulation results show good agreement with experimental observations.

1. INTRODUCTION

Finite element analysis is the most widely used numerical methodology for simulating complex manufacturing processes for metals, such as forming, rolling, machining, molding or forging. In order to develop an accurate finite element model, it is essential to accurately describe the material flow behavior using a constitutive model. The Johnson-Cook (JC) plasticity model has been widely used to describe the strain

hardening and temperature dependent behavior for metals undergoing large deformation [1]. The JC model is a phenomenological constitutive model that is derived by fitting experimental data using regression analysis or other curve fitting methods. The JC model assumes isotropic behavior and is reasonably accurate for most metallic alloys but is not very accurate in describing strain hardening behavior. In comparison, physics-based models utilize complex mathematical theories based on thermodynamics and kinetics to derive the flow stress-based equations. Other phenomenological models include the Arrhenius constitutive model [2] used for metals that takes in account the activation energy for deformation. . and the Durrenberger model [3], which predictes the flow stress as a function of a long range internal stress component and a thermally activated thermal stress component. The Zerrili-Armstrong model [4] relates the flow stress to the dislocation density. However, none of the models account for the effect of grain size on flow stress. Although grain size does not change significantly at room temperature for metals, it can change at elevated temperatures and the plastic deformation can have an effect on it [5].

In order, to model an accurate material behavior, it is essential to include the effect of grain size evolution as well. The classic Hall Petch equation [6] has shown that the coarsening of grains results in loss of material strength [7]. There have been some phenomenological models that have accounted for grain size. The KLH model [8] introduced the effect of grain size on yield stress. The recently proposed the Molinari–Ravichandran model simulates a flow stress as a function of the intrinsic resistance of the material, temperature, strain rate as well as grain size. However, most of these models

only incorporate the effect of grain size at room temperature. Hence these models are not suitable to be used to simulate manufacturing process at elevated temperatures.

In this work a modified version of the JC model was introduced that includes the effect of grain size evolution at high temperatures. The aim of the study was to determine the evolution of grain size in steel grades at elevated temperatures. In addition, the dependence of strength of the material from grain size was also obtained using experimental techniques. Finally, a new material model was developed based on the classical JC equation that modified to include the effect of grain size on flow stress.

2. EXPERIMENTAL PROCEDURE

2.1. JC STRENGTH MODEL

In this work, the isotropic thermomechanical behavior of steel was modeled using the Johnson-Cook (JC) strength model [1], which constitutive equation is given in Eq.1. An explanation of different JC parameters can be found in [9], [10]:

$$\sigma = (A + B\varepsilon^{n})(1 + C \ln \dot{\varepsilon}^{*})(1 - T^{*m}) \quad (1)$$

An MTS load frame was modified to performed hot tensile tests on AISI/SAE 15V38, ASTM A572, ASTM A690 and AISI/SAE 1018 grade steels. Details of this experiment were described in [11]. The stress-strain data was further processed to calibrate the material JC parameters. This calibration was done by global optimization methods using a Genetic Algorithm approach, as detailed explained in [12].

2.2. GRAIN GROWTH MODEL

The normal grain growth model relates the effect of temperature on grain size as given by the general grain growth law [13], as follows:

$$d^{n_G} = d_0^{n_G} + A_G \exp\left(-\frac{Q_G}{RT}\right) t \quad (2)$$

where: d and d_0 are the final and initial grain diameters, , A_G and n_G are material parameters, Q_G is the activation energy of grain growth, R is the gas constant, T is absolute temperature and t is the time.

The effect of temperature and time on grain size was measured using an experiment that involved heating a cylindrical steel sample above the austenization temperature, and then holding it for a time intervals ranging from 5 s to 600 s. Thereafter the sample was cooled below 750 ℃ for a short time to allow some ferrite to form along the austenite grain boundaries and then freeze the grain size by quenching in water, as shown in Figure 1a. After that, sample was cut and prepared 75ndependently75ally. The prior austenitic grain size was measured using an optical microscope for each temperature and time combination (Figure 1b), and then the experimental data was used to obtain the grain growth parameters in Eq.2.

2.3. MEASUREMENT OF FLOW STRESS

Another set of experiments were conducted to measure the effect of grain size on flow stress. In this test, cylindrical samples (0.5" diameter × 0.5" long) were subjected to compression using a MTS frame with induction heating. The sample was heated and soaked at 1200℃ for 60s using an induction coil. Then, the temperature was decreased to

the desired test temperature (1200ºC, 1100ºC or 1000ºC), and held for different times before compression testing.

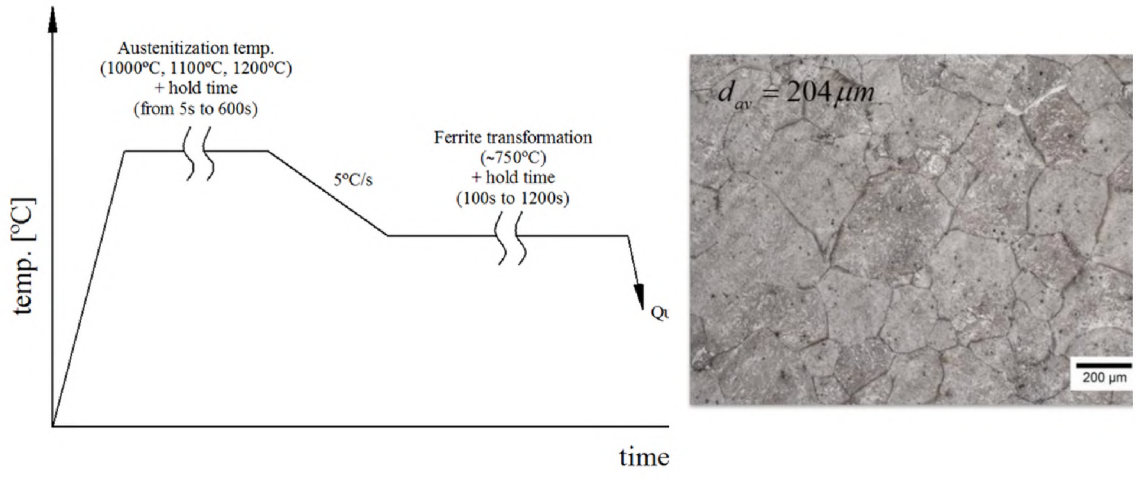

(a) (b)

Figure 1. (a) Steps during grain size measurement, and (b) metallographic observation of the prior austenitic grain size in A572 steel grade, after austenitization at 1100 ºC per 600 s.

Boron nitride compression plates were used to isolate the induction heated sample from the MTS system. Figure 2b shows an example of this test for the case of a holding times of 120 s. Compression test was performed at a constant 1 s^{-1} strain rate and 15% deformation (to avoid fracture of boron nitride plates).

After compression tests, the stress-strain data was used to evaluate the effect of the grain size on the flow stress, σ using the Eq3.

The effect of grain diameter on the flow stress can be expressed in the form of the following additional terms in the modified JC (JCM) model:

$$\sigma = (A + B\varepsilon^{n})(d/dref)^{-n_d}(1 + C\ln\dot{\varepsilon}^{*})(1 - \dot{T}^{\mathrm{m}}) \quad (3)$$

where: all parameters are the same of the previous JC model (Eq.1) while extra term (second bracket) was added to account for the effect of the grain size. In this model, d and d_{ref} are the actual and the reference grain sizes., In this study, the maximum experimentally measured grain size was used for d_{ref} and grain size exponent (n_d) was measured 77ndependently for each material.

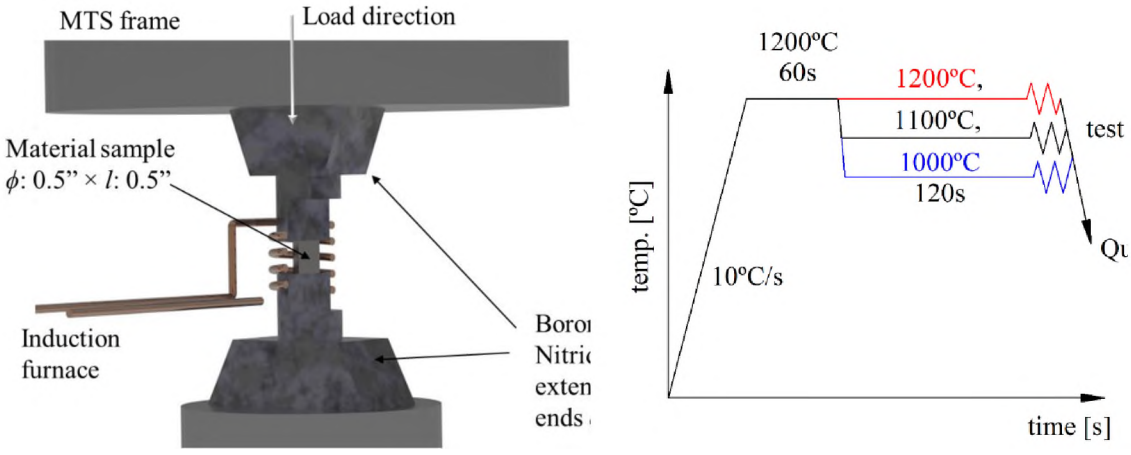

Figure 2. Compression test: (a) schematic view of the system, and (b) steps during flow stress measurement.

2.4. FINITE ELEMENT MODEL

The JCM model (Eq.3) was used to represent the material behavior for the various steel grades in the three-dimensional finite element model. The JC model is extremely effective in describing materials undergoing large plastic deformation at high temperatures. The JCM model used in this work is more accurate in that it accounts for

the change in grain size that affects the flow stress. This effect is highly pronounced at elevated temperatures where the grain growth is large.

Commercial code Abaqus 6.13 [14] was used to conduct the finite element simulation. A coupled thermal displacement analysis type in Abaqus explicit module was used to determine the finite element stiffness matrix. The JCM material model was coded in a user defined subroutine VUMAT [14] to update the flow stress varying with the strain. A rectangular shaped sample of size (100 mm × 100 mm × 400 mm) was created and meshed with three dimensional thermally coupled brick elements. The bottom surface of the sample was fixed while deformation was applied along the top surface as shown in Figure 3. The steel samples were compressed for 5% strain for 10 s and then the strain was held for 10 min at 1200 ℃. The grain size is expected to increase during this time. As the sample is held at constant deformation the stress should not vary unless the grain size changes. The flow stress and grain size were recorded with the progress of time during the simulation.

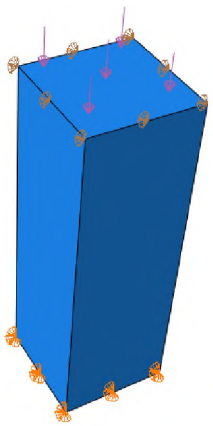

Figure 3. Boundary conditions applied to finite element model of rectangular sample used to simulate compression and relaxation.

3. RESULTS AND DISCUSSION

3.1. JC STRENGTH PARAMETERS

The Johnson-Cook (JC) material parameters were determined for the studied material and they are shown in Table 1. Notice that ε_{ref} was including as a material parameter, as discussed by Schwer [15].

Table 1. Calibrated Johnson-Cook parameters for studied steel grades.

Steel grade	*A* (MPa)	*B* (MPa)	*C*	*n*	*m*	$\dot{\varepsilon_{ref}}$
A690	14.4	107.49	0.2494	0.38	0.68	0.0399
A572	10.8	86.38	0.24	0.37	0.69	0.0163
1018	8.9	84.2	0.28	0.4	0.75	0.0291
15V38	16.94	45.91	0.62	0.55	0.64	0.0299

3.2. GRAIN SIZE EVOLUTION

Using the grain size data obtained for varying holding times, the grain diameter versus time relationships were determined for different steels studied at a temperature of 1100 ºC. Similar plots were also obtained using experiments conducted at 1000 ºC and 1200 ºC. The grain growth Eq. 2 was written in the following format:

$$\ln k = lnA_G - \left(\frac{Q_G}{RT}\right) \tag{4}$$

where: $k = (d^{n_G} - d_0^{n_G})/t$.

Hence, it is possible to obtain the range of values for constants A_G and n_G by plotting ln k versus $1/T$ as depicted in Figure 4. The intercept of the line along the ordinate axis provides the A_G parameter, while the slope of the line provides the Q_G

parameter. A large set of grain size for varying holding times was determined, thus enabling to obtain large number of k values at varying temperatures. A genetic algorithm was used to narrow down the results to realistic output. Using this process, the grain growth parameters were determined for the steel grades A690, A572, 1018 and 15V38, as shown in Table 2.

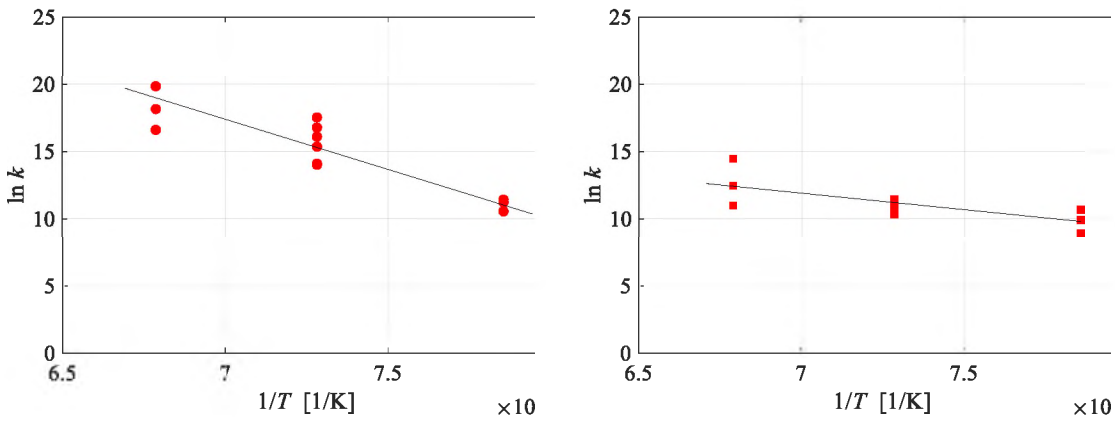

Figure 4. Grain growth parameter plot for (a) A572 steel and (b) A690 steel.

Table 2. Grain growth parameters for the studied steel grades.

Steel grade	n_G	Q_G **(J/mol)**	A_G
A690	4.092	645,200	1.34E30
A572	4.39	559,900	8.33E27
1018	2.58	169,400	6.91E9
15V38	5.006	956,900	1.09E44

3.3. FLOW STRESS EVALUATION

The compression tests carried out after holding the steel grades for times varying from 30 s to 300 s provided the stress-strain plots shown in Figure 5 for the different steels studied.

An average flow stress was calculated using the flow curves and further utilized to plot the average flow stress versus grain size, as shown in Figure 6. A line joining the data points allows us to determine the JCM parameter n_d using the slope.

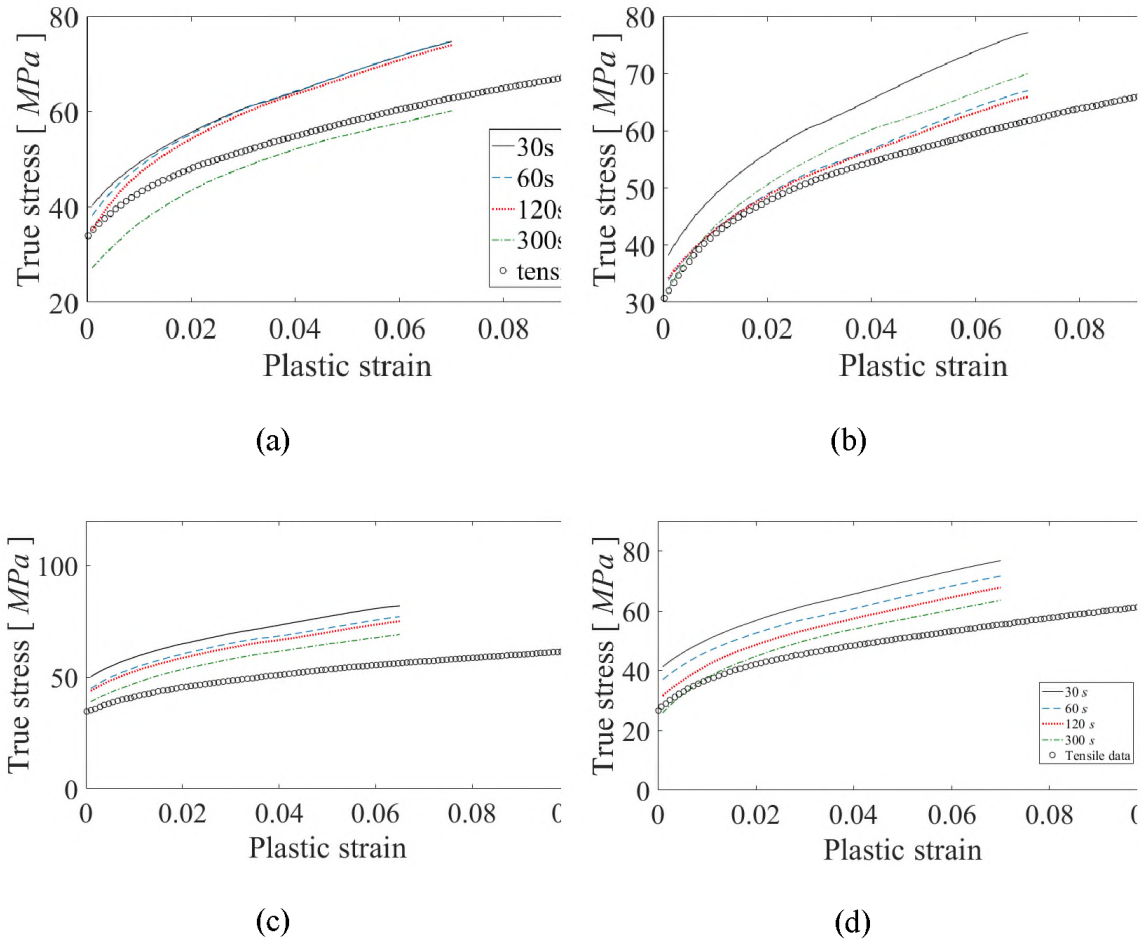

Figure 5. Stress strain curves after compression tests at 1100 °C and $1s^{-1}$: (a) A690, (b) A572, (c) 15V38, and (d) 1018 steel grades.

As mentioned before, the reference grain size d_{ref} was taken as the maximum grain size measured experimentally. In this manner the JCM parameters were determined using this experimental procedure, which are listed in Table 3. All the material parameters (Table 1, Table 2, and Table 3) were further utilized in developing the numerical material model for the steel grades.

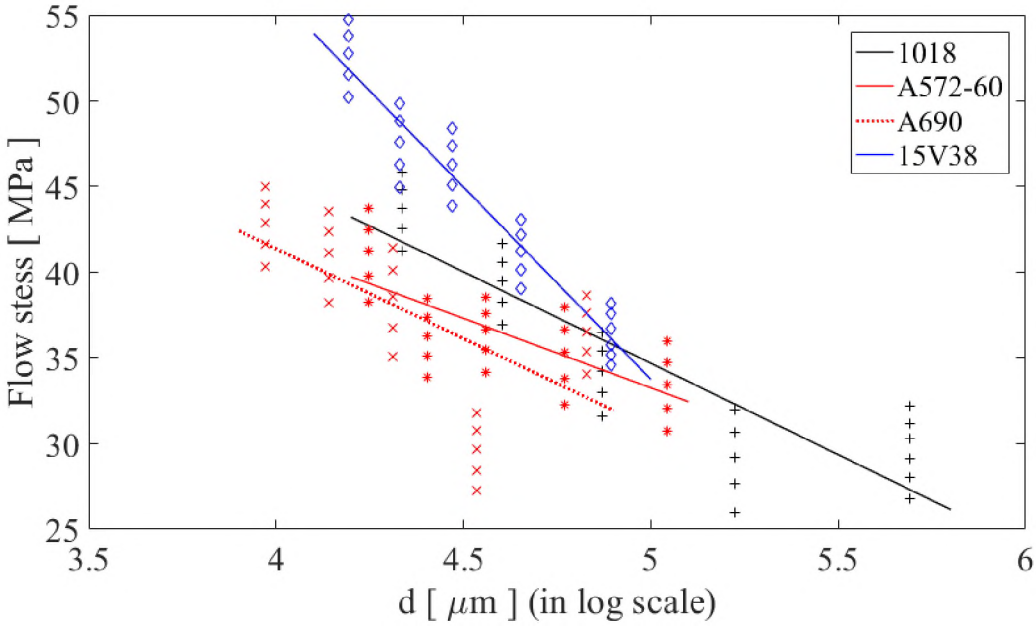

Figure 6. The maximum flow stress with varying grain size for the studied steel grades

Table 3. Modified JC model grain size parameter.

	1018	**A572**	**A690**	**15V38**
n_d	0.2391	0.1443	0.2430	0.4958
d_{ref} **[μm]**	501	322	125	133

3.4. NUMERICAL ANALYSIS

To start the simulations, the initial grain size of all steel grades was assumed to be 20 µm. The sample was then compressed up to 5% strain and thereafter left to relax. The loss in stress during the relaxation stage was recorded as the stress relaxation. It is observed from the simulations that the steel grade 1018 has largest grain growth whereas A690 steel grade has the lowest. 15V38 steel grade shows grain diameter increases 18.3 times, while A572 steel grade shows an increase of 14.5 times.

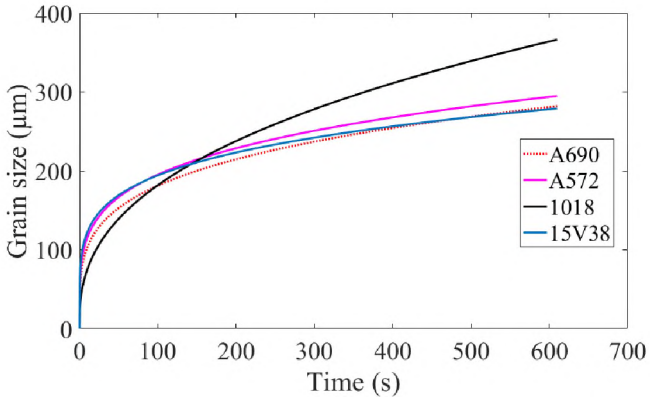

(a)

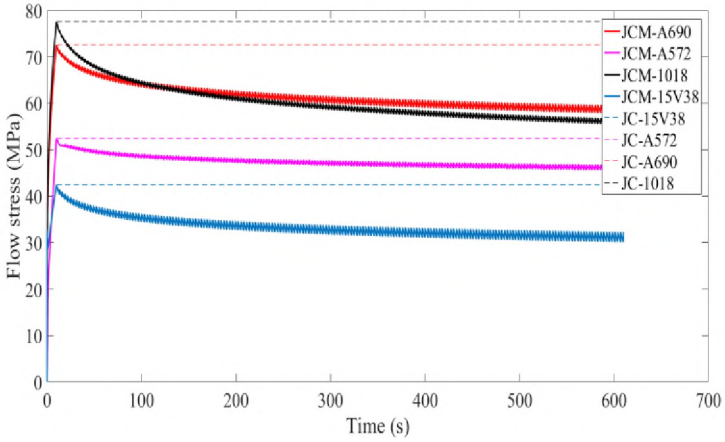

(b)

Figure 7. Comparison of varying steel grades: (a) evolution of grain size with time and (b) change in flow stress with time for modified JC model and classical JC model.

The numerical result agrees with the experimental data collection of grain size for the respective steel grades. Correspondingly it is also observed that considerably larger loss of flow stress is obtained for 1018 steel grade in comparison to the other steel grades. Figure 7 shows the drop in flow stress with time for steel grades A690, 1018, 15V38 and A572. Results have been compared with classical JC model. In the case of steel grade A690 the loss of flow stress is 18% while in the case of steel grade 1018 the loss is 27% (Table 4). Steel grades A 572 and 15V38 also show stress relaxation lower than steel grade 1018. Hence the new material model shows that the finer the grain size increases the strength of the material. The model effectively shows that as temperature driven grain coarsening results in stress relaxation and hence heating the material results in loss of residual stress as has been observed by prior studies as well. The material 15V38 shows the largest extent of stress relaxation.

Table 4. Comparison of stress relaxation for varying steel grades.

	Stress relaxation %
A690	18
A572	10.8
1018	27
15V38	24.2

4. CONCLUSIONS

In this study a modified version of the classical JC model has been introduced that accounts for the influence of grain size evolution on flow stress. This model is expected to be highly useful in simulating manufacturing processes at very high temperatures, such as forming, rolling etc. A novel experimental methodology has been used to study the evolution of grain size, as well as its effect on grain size at elevated temperatures in four different varieties of steel. The experimental study showed that all the steel grades showed significant grain size increase between temperatures of 1100 ºC and 1300 ºC. The study also showed a substantial decrease in flow stress with increasing grain size. The modified JC model was implemented using a user subroutine in commercial code Abaqus and compression test simulations were conducted to validate the effect of grain size on flow stress. The study showed that the modified JC model predicted the influence of grain size evolution on flow stress accurately. This model can be used in the future to simulate manufacturing processes involving the steel grades studied to obtain more realistic flow stress and mass flow influenced by grain size variations in comparison to the classical JC model.

ACKNOWLEDGEMENTS

This work was supported by the Peaslee Steel Manufacturing Research Center at Missouri University of Science and Technology.

REFERENCES

[1] G. R. Johnson and W. H. Cook, "A constitutive model and data for metals subjected to large strains, high strain rates and high temperatures," in *Proceedings of the 7th International Symposium on Ballistics*, 1983, pp. 541–547.

[2] Z. He, Z. Wang, and P. Lin, "A comparative study on arrhenius and Johnson–Cook constitutive models for high-temperature deformation of Ti2AlNb-based alloys," *Metals (Basel).*, vol. 9, no. 2, pp. 1–13, 2019.

[3] Y. C. Lin and X. M. Chen, "A critical review of experimental results and constitutive descriptions for metals and alloys in hot working," *Mater. Des.*, vol. 32, no. 4, pp. 1733–1759, 2011.

[4] R. W. Armstrong and F. J. Zerilli, "Dislocation mechanics based analysis of material dynamics behavior," *J. Phys.*, pp. 529–534, 1988.

[5] Z. Jiang, J. Zhao, H. Lu, D. Wei, K. Manabe, "Influences of temperature and grain size on the material deformability in microforming process," *Int. J. Mater. Form.*, vol. 10, no. 5, pp. 753–764, 2017.

[6] B. P. Kashyap and K. Tangri, "Hall-Petch relationship and substructural evolution in boron containing type 316L stainless steel," *Acta Mater.*, vol. 45, no. 6, pp. 2383–2395, 1997.

[7] R. Saunders, A. Achuthan, A. Iliopoulos, J. Michopoulos, and A. Bagchi, "Influence of Grain Size and Shape on Mechanical Properties of Metal Am Materials," Solid Free. Fabr. 2018 Proc. 29th Annu. Int. 1751 Solid Free. Fabr. Symp. – An Addit. Manuf. Conf. Rev. Pap., pp. 1751–1762, 2018.

[8] L. T. A. Khan, H.Zhang, "Mechanical response and modeling of fully compacted nanocrystalline iron and copper," Int. J. Plast., no. 16, pp. 1459–1476, 2000.

[9] A. S. Milani, W. Dabboussi, J. A. Nemes, and R. C. Abeyaratne, "An improved multi-objective identification of Johnson-Cook material parameters," Int. J. Impact Eng., vol. 36, no. 2, pp. 294–302, 2009.

[10] L. Gambirasio and E. Rizzi, "On the calibration strategies of the Johnson-Cook strength model: Discussion and applications to experimental data," Mater. Sci. Eng. A, vol. 610, pp. 370–413, 2014.

[11] M. F. Buchely, D. C. Van Aken, R. J. O'Malley, S. Lekakh, and K. Chandrashekhara, "Hot rolling effect upon the high temperature Johnson-Cook strength and failure models for a 15V38 grade steel," in Proceedings on the Materials Science and Technology meeting (MS&T17), 2017, pp. 1045–1053.

[12] M. F. Buchely, X. Wang, D. C. Van Aken, R. J. O'Malley, S. N. Lekakh, and K. Chandrashekhara, "The use of genetic algorithms to calibrate Johnson-Cook strength and failure parameters of AISI/SAE 1018 steel," J. Eng. Mater. Technol., vol. 141, no. 2, p. 12, 2019.

[13] E. Khzouz, "Grain Growth Kinetics in Steels," A Major Qualif. Proj. Rep. Submitt. to Fac. WORCESTER Polytech. Inst., pp. 5–6, 2011.

[14] Dassault Systemes, Abaqus 6.13 Documentation, 2013th ed. 2013.

[15] L. Schwer, "Optional strain-rateforms for the Johnson-Cook constitutive model and the role of the parameter Epsilon _ 0," in *Proceedings of the 6th European LS-DYNA Conference*, 2007.

IV. MODELING AND STATIC RECRYSTALLIZATION KINETICS OF HIGH STRENGTH STEEL DURING MULTI-PASS HOT ROLLING

S. Ganguly[1], A. Abdulaziz[1], S.K. Dasari[1], M.F. Buchely[2], K. Chandrashekhara[1], S. Lekakh[2], R. J. O'Malley[2]

[1]Department of Mechanical and Aerospace Engineering
[2]Department of Materials Science and Engineering
Missouri University of Science and Technology, Rolla, MO 65409

ABSTRACT

Static recrystallization is a microstructural change occurring when metals experience thermo-mechanical deformation that has a critical influence on its mechanical properties. Static softening occurs during static recrystallization and results in greater ductility in metals during hot rolling. In this study the extent of static recrystallization was measured using double hit tests performed on the Greeble machine and kinetics of static softening developed. Based on the experimental results the kinetics of static recrystallization was modeled. A finite element model of multi-pass rolling process was developed that calculated the fraction of recrystallization and static softening using explicit subroutines. Simulation results showed that the fraction of recrystallization was very much dependent on the extent of thickness reduction during rolling. Additionally, an increase in temperature greatly increased the degree of recrystallization and also the static softening.

1. INTRODUCTION

In metals undergoing deformation, the presence of dislocation density results in nucleation of new grains. This phenomenon is known as recrystallization and can be distinguished as dynamic and static. Recrystallization involves both grain nucleation due to subgrain coalescence and growth [1]. Dynamic recrystallization is the stage wherein its grain structure changes while the material undergoes deformation. While static recrystallization refers to the stage of grain refinement under high temperature after the deformation has occurred. Static recrystallization is a critical physical process that occurs in metallic materials at high temperature and deformation that influences microstructural changes as well as affects the properties. As a result of static recrystallization nucleation, new grains areinitiated within the material. Depending on the extent of static recrystallization, the entire or a portion of the material is replaced with new grains. The material experiences loss in residual stress and strain due to static softening during static recrystallization [2]. Consequently, the physical properties are highly affected due to the loss of residual strainThe driving force for static recrystallization is deformation. Various analytical models have been proposed to represent the recrystallization kinetics. Zurob [3] proposed a recrystallization model that considered the effect of precipitation in addition to nucleation and growth. Najafizadeh et al. [4] found that uptil a critical value strain influenced static recrystallization.

Multi-pass hot rolling process involves high deformation at elevated temperatures and hence is usually accompanied by static recrystallization during the rolling interpass. Usually for static recrystallization to occur, the strain showed exceed the critical strain wherein the stored energy is sufficient to initiate the process of nucleation and growth

[5]. The critical strain has been determined to be around 0.05 % – 0.1% for most metals [5]. Various factors such as rolling speed, rolling deformation, temperature, as well as interpass duration influence kinetics of static recrystallization. Static softening is expected to occur as a result of static recrystallization during rolling interpass. The influence of static recrystallization is expected to be much greater during hot strip rolling in comparison to dynamic recrystallization [6]. However, it is not easy to analytically determine the extent of static recrystallization during hot rolling for beams. Hodgson's model [7] predicted the recrystallization kinetics for hot strip rolling and also the effect on grain growth and strain. Jung et al. [8] modeled hot rolling with static softening and microstructural evolution. He et al. [9] simulated H beam rolling using a finite element model and static recrystallization. Although various models have been developed to study recrystallization kinetics, it is challenging to predict the effect on beams rolled in a hot mill. Finite element method remains the best way to study the evolution of recrystallization during hot rolling and influence of the various rolling parameters on static recrystallization.

In this work, a static recrystallization model was introduced influenced by strain, strain rate, and temperatures. A modified version of the traditional static recrystallization kinetics is suggested. The aim of the study was to determine the fraction of static recrystallization and strain recovery during multi-passhot rolling. The study determined that temperature and strain had critical effect on fraction of static recrystallization in comparison with rolling speed.

2. EXPERIMENTAL PROCEDURE

2.1. JC STRENGTH MODEL

In this work, the isotropic thermomechanical behavior of steel was modeled using the Johnson-Cook (JC) strength model [10], which constitutive equation is given in Equation 1.

$$\sigma = (A + B\varepsilon^{n})(1 + C \ln \dot{\varepsilon}^{*})(1 - T^{*m}) \quad (1)$$

where A, B, C, n, m are material parameter, ε is strain, $\dot{\varepsilon}$ is strain rate, and T is temperature. An MTS load frame was modified to perform hot tensile tests on US Steel AHSS (austenitic high strength steel). Details of this experiment were described in [11].

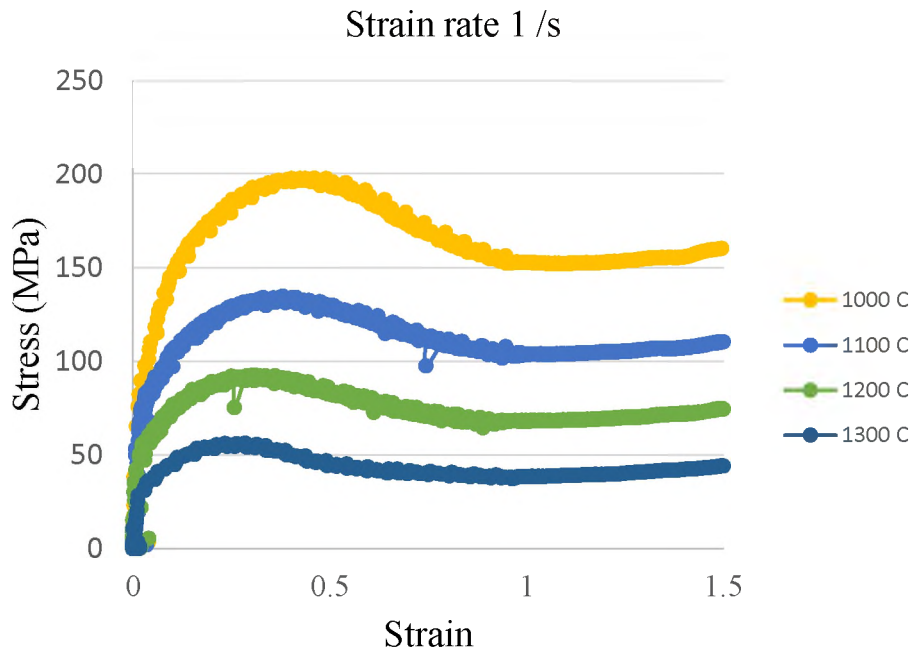

Figure 1. Experimental stress-strain curves for hot tensile tests for strain rate 1 and varying temperatures.

The stress-strain data (Figure 1) was further processed to calibrate the material JC parameters. This calibration was done by global optimization methods using a genetic algorithm approach, as detailed and explained in [12].

2.2. STATIC RECRYSTALLIZATION

The phenomenon of static recrystallization is dependent on strain, strain rate, and temperature experienced by the material under deformation. The half time for static recrystallization was determined by Sellars as [13]

$$t_{0.5} = A * d_0^S * \varepsilon^p * \dot{\varepsilon}^c * \exp\left(\frac{Q_s}{RT}\right) \quad (2)$$

where $t_{0.5}$ is the time required for the fraction of static softening reaches 50%, d_0 is the initial grain size, Q is activation energy for static recrystallization, R is the gas constant 8.314 J/(mol K), T is temperature, and A, S, p, and c are constants. The double hit compression experiment was performed to obtain the parameters influencing static recrystallization for AHSS (austenitic high strength steel) material. The specimen was heated up to an austenitization temperature of 1150 °C and held for around 5 min. Then the specimen was then cooled down to deformation temperatures of either 1000 °C or 1100 °C. Another hold time of around 5 min was applied at the deformation temperature before the first hit. Interpass delay time ranging from 1 – 100 s was held between the first and the second hit. Figure 2 shows the time frame of the performed double hit test. The hold time allows the material to undergo static recrystallization and soften. The degree of softening is measured to obtain the degree of static recrystallization.

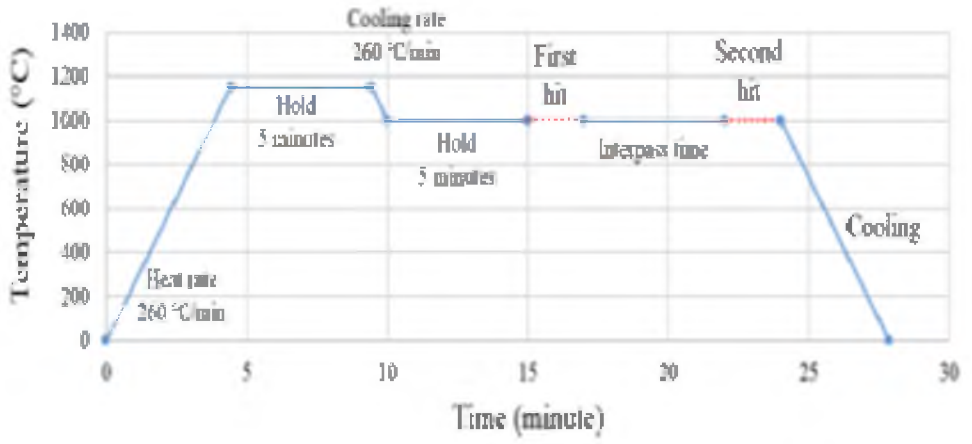

Figure 2. Steps during double hit test using the Gleeble machine.

2.3. DETERMINATION OF FRACTION OF RECRYSTALLIZATION

The softening behavior was investigated by analyzing the flow curves of the double hit test. First, the experimental stress and strain data were converted into their equivalent true values [14, 15]. For each deformation temperature, the stress-strain curves were obtained at pre-strain of 0.1 with strain rate varied as 1 s^{-1}, 5 s^{-1}, and 10 s^{-1}. The procedure was repeated for varying interpass delay times as 1 s, 5 s, 20 s, 50 s, and 100 s.

An offset method with an offset value of 0.2% was considered to obtain the yield stresses for the first and second compression hits as σ_0 and σ_r respectively. The maximum value of flow stress was determined as σ_m. Figure 3 shows the stress values obtained from a true stress-strain flow curve at different testing conditions. The value of fraction of static recrystallization (X_{srx}) was obtained using the following expression.

$$X_{srx} = \frac{\sigma_m - \sigma_r}{\sigma_m - \sigma_0} \tag{3}$$

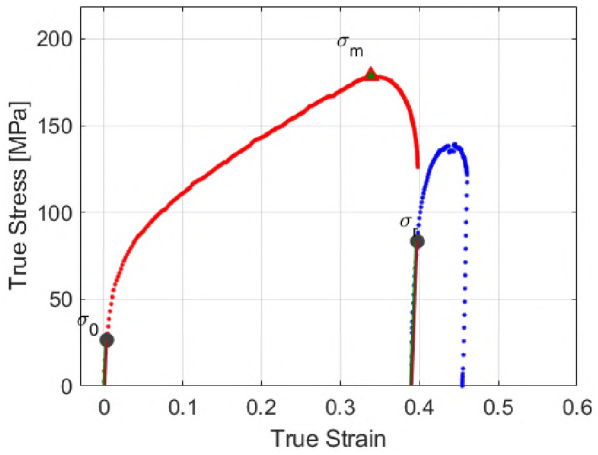

a)

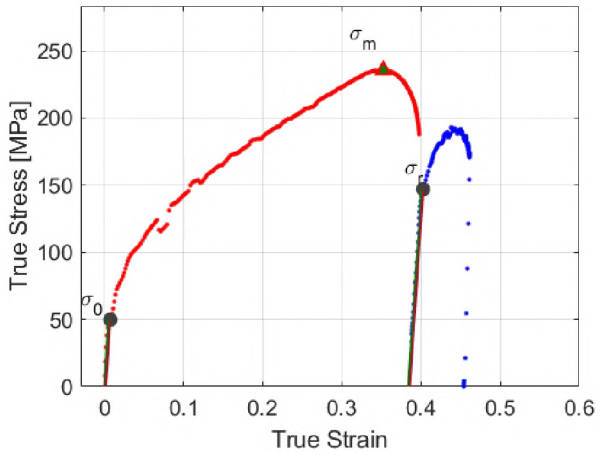

b)

Figure 3. Stress-strain curves obtained from double hit compression test at a strain rate of 5 /s, pre-strain of 0.4, and interpass time of 5s for temperatures of a) 1100 ºC and b) 1000 ºC.

2.4. MODELING THE KINETICS OF STATIC RECRYSTALLIZATION

A parametric study was conducted to investigate the effects of strain rate, pre-strain, temperature, and interpass delay time on the softening behavior. The values of X_{srx} were plotted against interpass times obtained for varying pre-strains, for a constant deformation temperature and strain rate varied as 1 s^{-1}, 5 s^{-1}, and 10 s^{-1}.

The following Figure 4 shows the effect of varying pre-strain on X_{srx} vs. time at 1100 ºC. While Figure 5 shows the effect of varying pre-strain on X_{srx} vs. time at 1000 ºC. A range of such data providing the change in degree of static recrystallization with time for varying temperature, strain and strain rate was obtained so that the half time or time taken to achieve 50% of recrystallization can be determined.

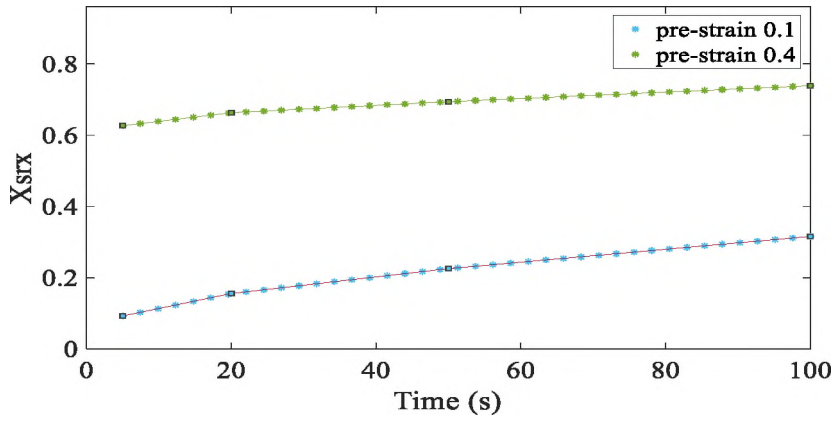

Figure 4. Experimentally obtained fraction of static recrystallization at 1100 °C and strain rate 5 /s

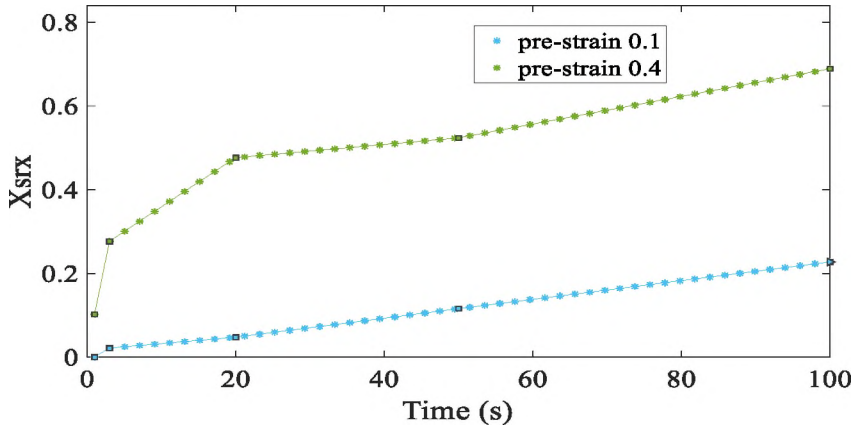

Figure 5. Experimentally obtained fraction of static recrystallization at 1000 °C and strain rate 5 /s

The expression used to define $t_{0.5}$ (Equation 1) can be written in a logarithmic form as

$$lnt_{0.5} = \ln A + s\ln d_0 + q\ln\varepsilon + c\ln\dot{\varepsilon} + \frac{Q}{RT} \quad (4)$$

Using the relationship between X_{srx} and time, values of $t_{0.5}$ under different conditions can be derived. Substituting the values of $t_{0.5}$ and pre-strain in Equation 3 the relationship between $t_{0.5}$ and ε can be obtained by power fitting and regression analysis. This is used to obtain the constant p as shown in Figure 6a.

Relationships between $t_{0.5}$ and strain rate (Figures 6b) is used to obtain the parameters for static recrystallization kinetics as c. The initial grain size is assumed to be 400 μm as obtained using optical microscopy of etched AHSS material. A range of half time values for static recrystallization was required to obtain relationship of half time with strain, strain rate and temperature. Curve fitting plots of half time for static recrystallization versus strain helped determine the parameter p. Similar curve fitting procedures were used to obtain parameter c and Q by plotting half time versus strain rate and temperature respectively. In this manner the static recrystallization kinetic parameters given by the Sellars equation were obtained.

The parameters defining the $t_{0.5}$ using Equation 1 were obtained and reported in Table 1.

Table 1. Static recrystallization kinetic parameters determined

	n	**k**	**p**	**c**	**Q** (J/mol)	**A**	**s**
AHSS	0.26	0.7	-0.47	-0.413	210000	3.6×10^{-4}	1

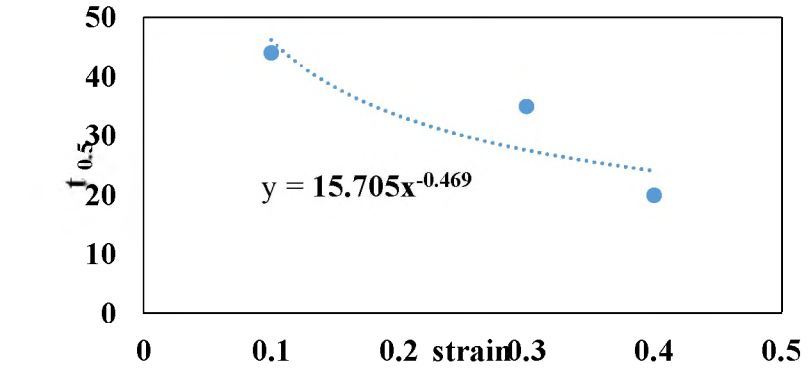

a)

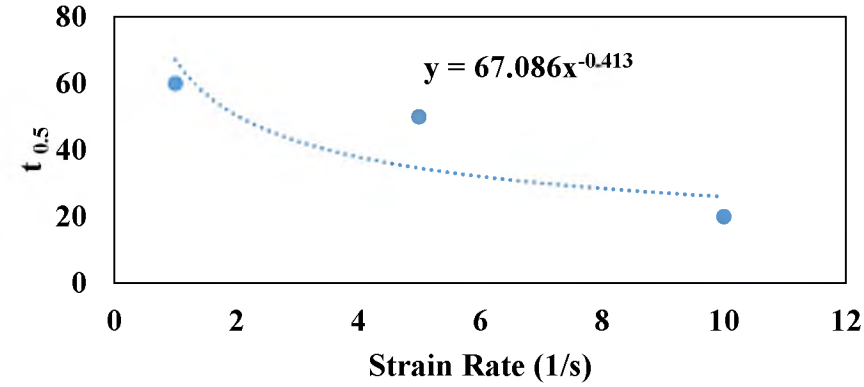

b)

Figure 6. Variation of half time with a) strain b) strain rate

Thereafter the Avrami equation was used to model the kinetics of static recrystallization. The Avrami equation relates X_{srx} to the half time of static recrystallization ($t_{0.5}$) as

$$X_{srx} = 1 - \exp\left(-k * \left(\frac{t}{t_{0.5}}\right)^{n}\right) \quad (5)$$

where k and n are material dependent parameters, t is time and $t_{0.5}$ is the half time for static recrystallization. Taking logarithm on both sides the following expression is obtained.

$$\ln(\ln(1/(1\text{-}X_{srx}))) = \ln(k) + n.\ln(t/t_{0.5}) \quad (6)$$

The parameters k and n are obtained by linear fitting and regression analysis of a large range of X_{srx} for varying pre-strains and interpass times. Based on the above relationship the parameters k and n were determined as 0.7 and 0.26 respectively. However, it is found that the parameters of static recrystallization kinetics determined using the traditional model is unable to describe the evolution of X_{srx} accurately when the temperatures changed. Hence the model was modified wherein the energy for static recrystallization (Q) was related with the temperature (T) as

$$Q = 442000 - 175T \tag{7}$$

Using this model, the evolution of X_{srx} with time is compared with the traditional model in Figure 7. The modified model was found to be more coincident with experimental values in comparison to the traditional model.

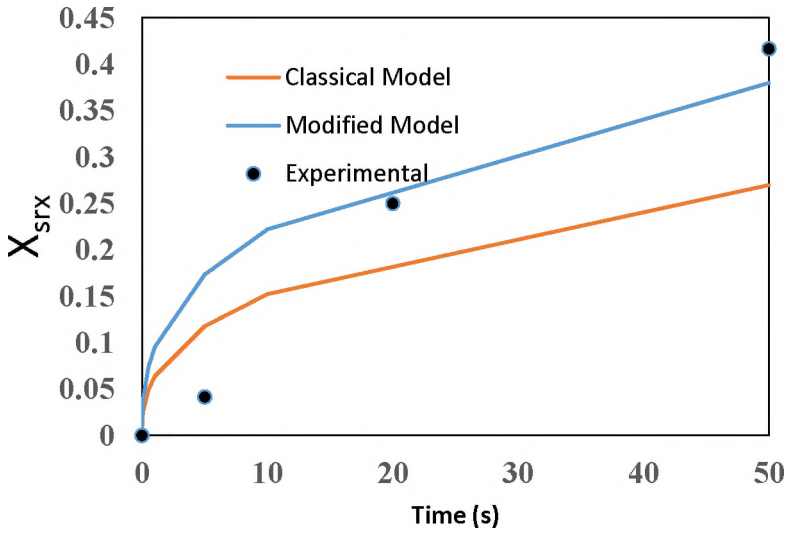

Figure 7. Comparison between the traditional and modified model for strain 0.1 at 1100 ° C and strain rate 5 /s

3. FINITE ELEMENT MODEL

The Johnson-Cook (JC) model (Equation 3) was used to represent the material behavior for the high stress austenitic steel grade in the three-dimensional finite element model. The JC material parameters were determined for the studied material and they are listed in Table 2. Notice that ε_{ref} was included as a material parameter, as discussed by Schwer [16].

Table 2. Calibrated Johnson-Cook parameters for studied steel grades.

Steel grade	***A* (MPa)**	***B* (MPa)**	***C***	***n***	***m***	$\dot{\varepsilon_{ref}}$
AHSS	40	333	0.07	0.3	0.68	1

Commercial code Abaqus 6.18 [17] was used to conduct the fin121ite element simulation. A coupled thermal displacement analysis type in Abaqus explicit module was used to determine the finite element stiffness matrix. The industrial hot rolling process consisted of consecutive edger (vertical) and roughing (horizontal) rollers. A similar hot rolling model was created for the simulation is shown in Figure 8. The horizontal rollers have a diameter of 1102.5 mm, while the edger rollers have a diameter of 742.5 mm. The rolled slab was created with an initial dimension of size (200 mm × 1m × 2 m) and meshed with three dimensional thermally coupled brick elements (C3D8RT). Whereas the rollers were meshed with 4 node rigid elements (R3D4). The user defined subroutine VUSDFLD [17] was used to determine the fraction of recrystallization X_{srx} based on the strain, strain rate, and temperature experienced by the slab during hot rolling. The static

softening was determined based on the X_{srx} that was assumed to be initiated after deformations were experienced due to hot rolling by a set of vertical and horizontal rollers.

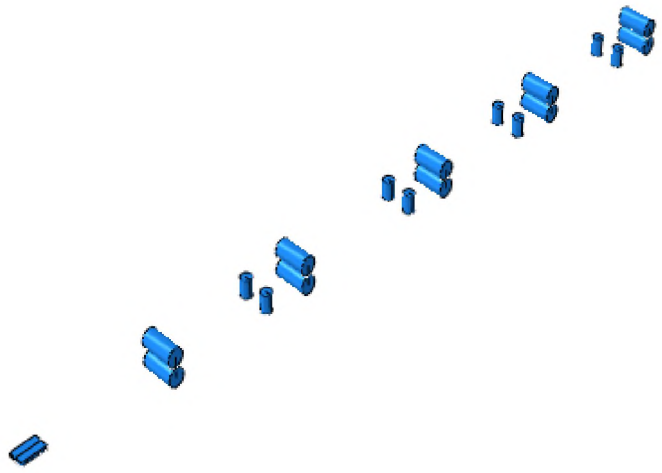

Figure 8. Finite element model of the rectangular slab and rollers used to simulate the hot rolling process.

For each time step during the interpass, the X_{srx} is updated by adding the increment of the fraction of static recrystallization as given by Equation 8.

$$dX_{\mathrm{srx}} = \left[-\exp\left(-k\left(\frac{t}{t_{0.5}}\right)^{n}\right).\left(-kn\left(\frac{t}{t_{0.5}}\right)^{n-1}\right).\frac{1}{t_{0.5}} \right] dt \tag{8}$$

Due to grain refinement, the residual strain is lost within the material. The extent of loss of strain depends on the extent of recrystallized grains and is defined by

$$\varepsilon_p = \varepsilon(1 - X_{srx}) \tag{9}$$

4. RESULTS AND DISCUSSION

Hot rolling simulations were conducted for three edger and horizontal strands using the same rolling parameters considered in industrial trials. The initial slab temperature was kept at 1000 °C and roller speed set to 1.11 m/s. The edger rollers and horizontal rollers are kept in proximity such that as soon as the slab passes through the edgers it reaches the adjacent horizontal roller. Static recrystallization is expected to be initiated after the slab transits the horizontal roller. The thickness reduction experienced during the first horizontal roller is 25%, for the second roller set is 13% and for the final roller set is 44.3%.

4.1. EVOLUTION OF STATIC RECRYSTALLIZATION AND SOFTENING

The evolution of static recrystallization and plastic softening during the first interpass was studied using the simulation results. Figure 9 shows the progression of the fraction of recrystallization after the first rolling pass. The degree of static recrystallization is observed to be 0.3 after 5 s and slowly increases to 0.6 in 25 s case. The degree of static recrystallization is slightly higher at the surface (0.34) than at the center(0.33) after 5 s. This gradient decreases as recrystallization progresses with time. At the end of the interpass, the degree of static recrystallization is almost uniformly and is about 0.6 along the thickness.

The extent to which the material undergoes static recrystallization, till that extent the material looses its stored strain energy and relaxes. This phenomenon is due to the formation of new grains that eat up the old grains. Hence it is highly critical to study the effect of rolling parameters as pass reduction, temperature and rolling speed on the extent

of recrystallization and hence in turn on the residual strain in the material. Overall, the final material properties are highly influenced by the rolling parameters that influence the extent of recrystallization and inturn effect the strain energy. The lower the strain energy in the material the greater the softening of the material and hence more the ductility.

The state of recrystallization of the slab at the end of each horizontal rolling pass showed that the rate of recrystallization is highly sensitive to the deformation. The greater the pass reduction the greater the strain the material experiences. Hence although high deformation results in large strains it also results in large strain removal and material softening. The fraction of static recrystallization is observed to be higher along the edges and the surfaces and slightly lower at the center. The surface and edges hence undergo greater strain softening and hence results in a strain gradient within the material.

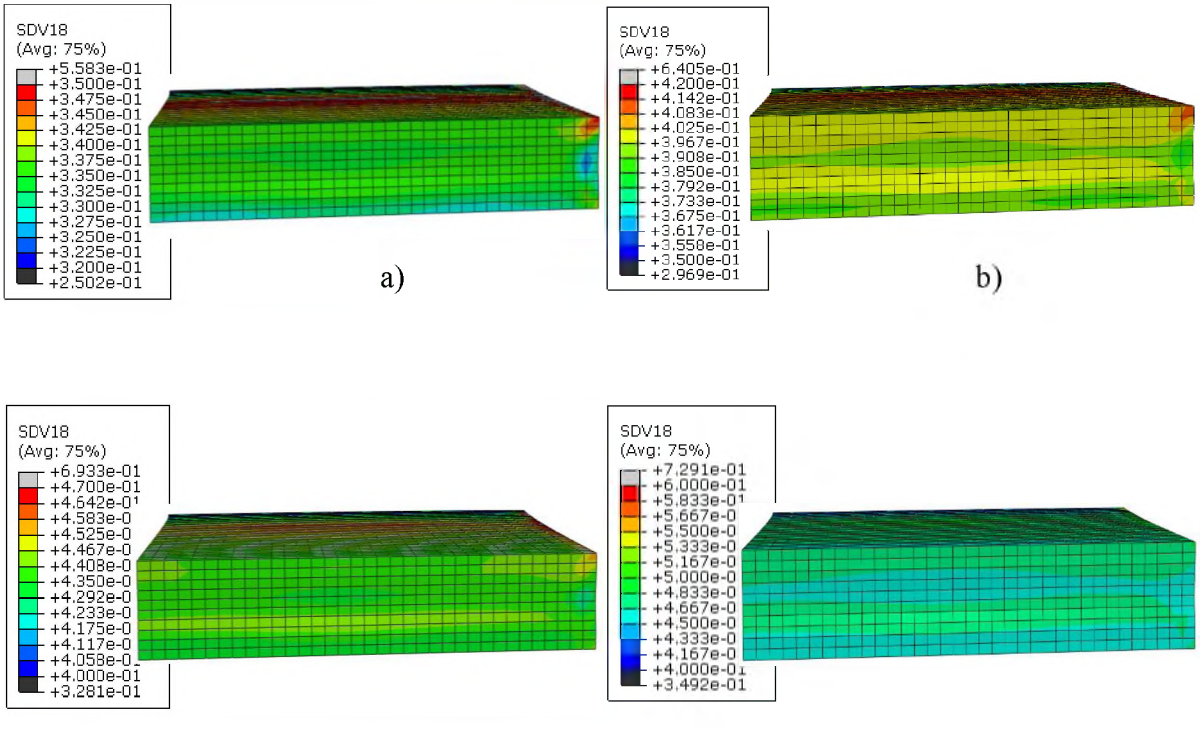

Figure 9. Fraction of static recrystallization after a) 10 s b) 15 s c) 20 s, and d) 25 s

The corresponding plastic strains after the same interim time duration are shown in Figure 10. The strain concentrations are observed along the edges of the slab. The strain is higher at the top and bottom surfaces and decreases towards the center region. This different decreases as recrystallization progresses with time.

4.2. EFFECT OF PASS REDUCTION ON STATIC RECRYSTALLIZATION

As the thickness reduction is highest for the third rolling pass (44.3%), the degree of static recrystallization X_{srx} is observed to be highest for the third set of rollers (0.78) and lowest for the second set (0.32). Figure 11 shows the increase/decrease in fraction of static recrystallization after each rolling pass.

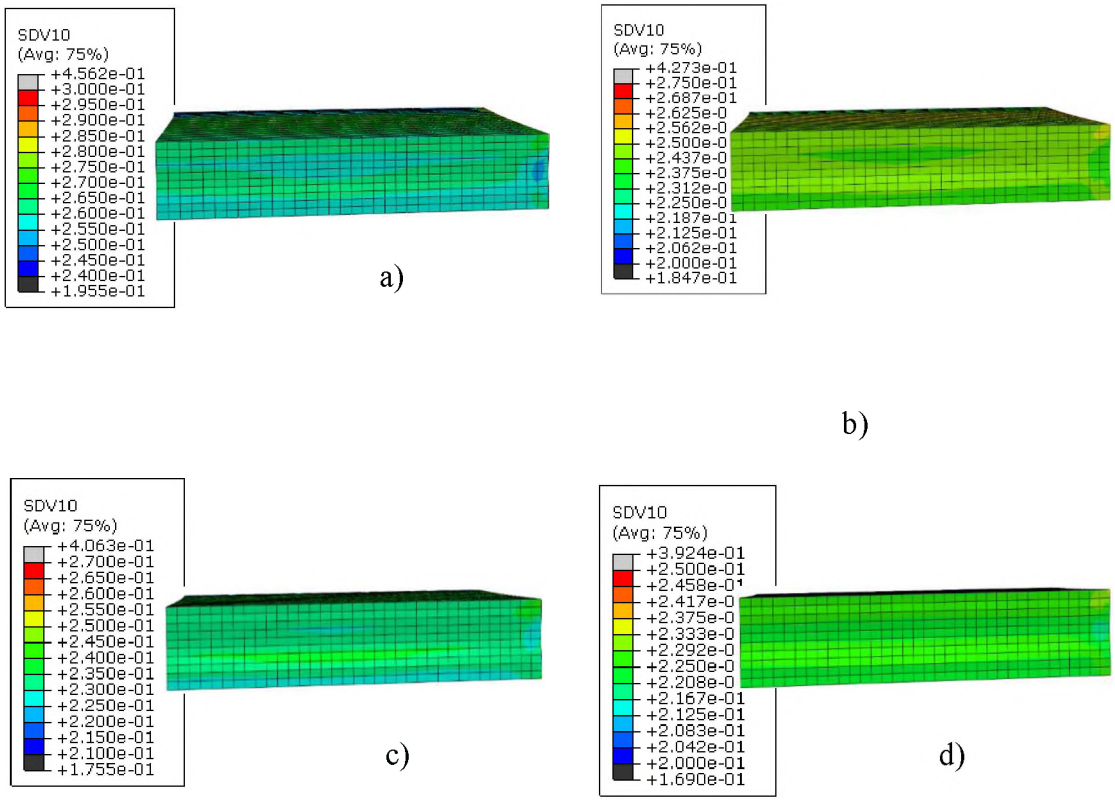

Figure 10. Plastic strain after a) 10 s b) 15 s c) 20 s and d) 25 s

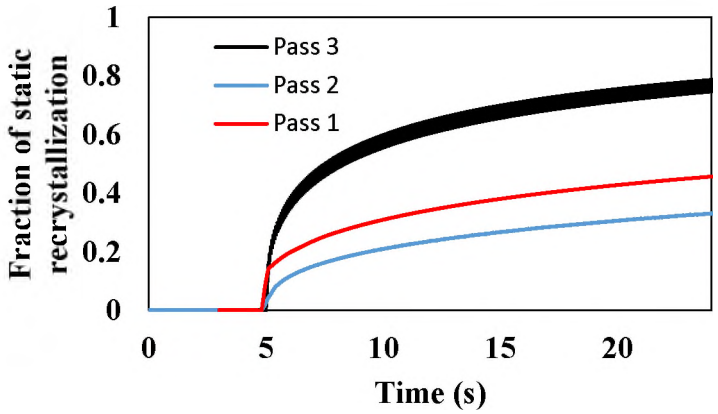

Figure 11. Variation of degree of static recrystallization during the first three rolling passes at 1000 °C

The residual strain at the slab surface at the end of each rolling pass is seen in Figure 12. The loss in residual strain is found to be 21.4%, 17.1%, and 29.2% for the first, second, and third passes respectively.

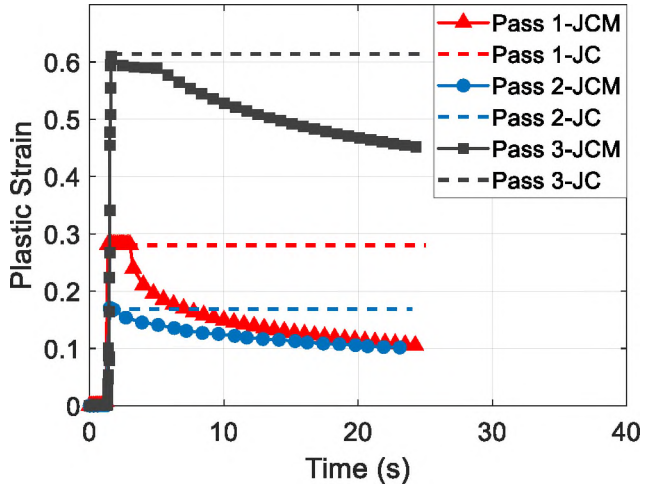

Figure 12. Static softening for different rolling passes for classical JC model and modified JC model

The state of recrystallization of the slab at the end of each horizontal rolling pass was studied. The fraction of static recrystallization is observed to be higher along the edges and the surfaces and slightly lower at the center. The fraction of static recrystallization is observed to be highest for pass 3 and lowest for pass 2 as observed in Figure 13.

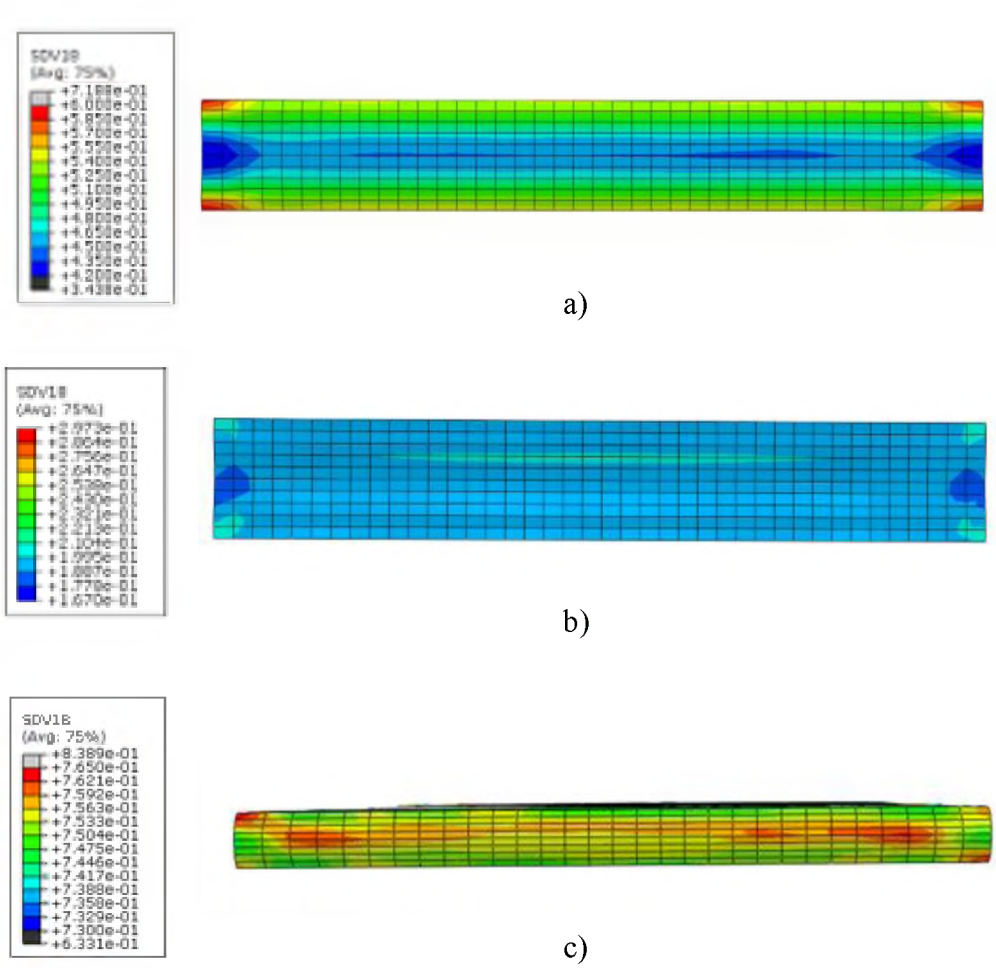

Figure 13. Simulation results for degree of recrystallization for a) pass 1, b) pass 2, and c) pass 3

It is evident from the study that pass 3 that has the highest pass reduction results in extremely high degree of recrystallization. While pass 2 that has the lowest pass reduction shows lowest degree of recrystallization. The material residual strain at the end of each interpass was compared (Figure 14). The strain is noted to be higher at the surface and comparatively less at the midplane. The strain is observed to be highest for the pass 3 rolling and lowest for pass 2.

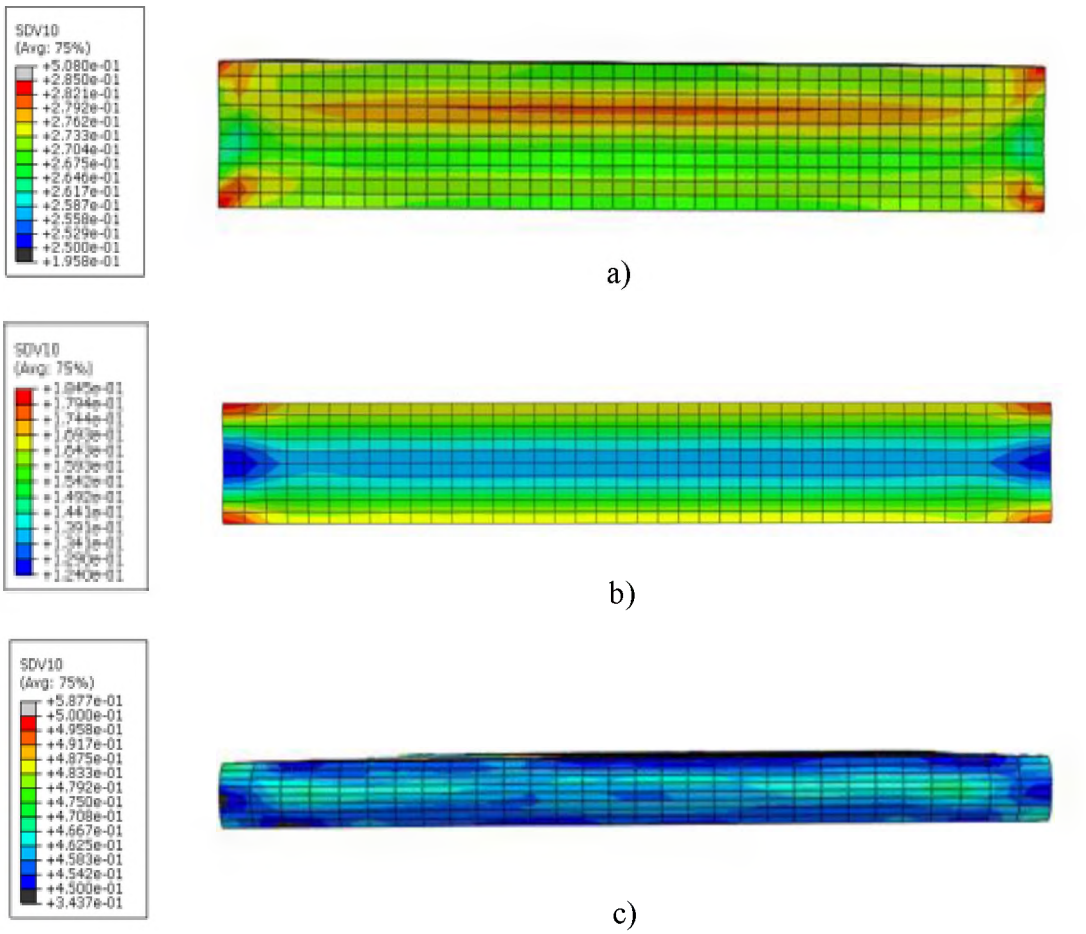

Figure 14. Simulation results for static softening during a) pass 1, b) pass 2, and c) pass 3.

On the other hand, the loss in strain across the thickness of the slab as the interpass time increased from 5 s to 25 s during the 1st pass is about 50% (Figure 16a) whereas the loss in strain across the thickness under the same conditions during the 3rd pass is about 25% (Figure 16b).

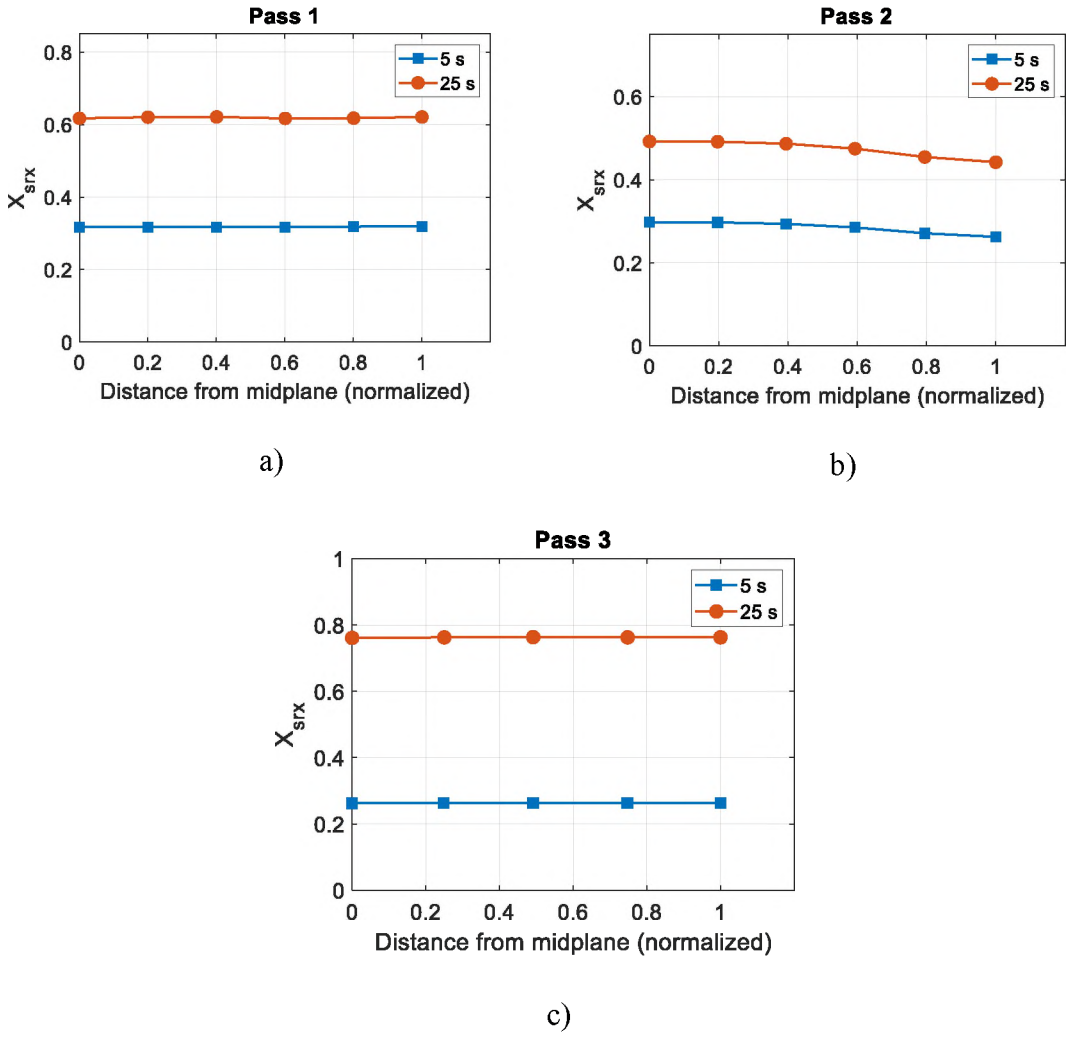

Figure 15. Increase in static recrystallization with time for a) pass 1, b) pass 2, and c) pass 3.

The fraction of static recrystallization is noted to be approximately 0.31 after 5 s and 0.61 after 25 s of interpass period after the first rolling pass. The corresponding plastic strain is observed to be 0.19 at the end of 5 s and decreases to 0.1 at the end of 25 s. The variation in both fraction of static recrystallization and plastic strain is found to be minimal along the thickness.

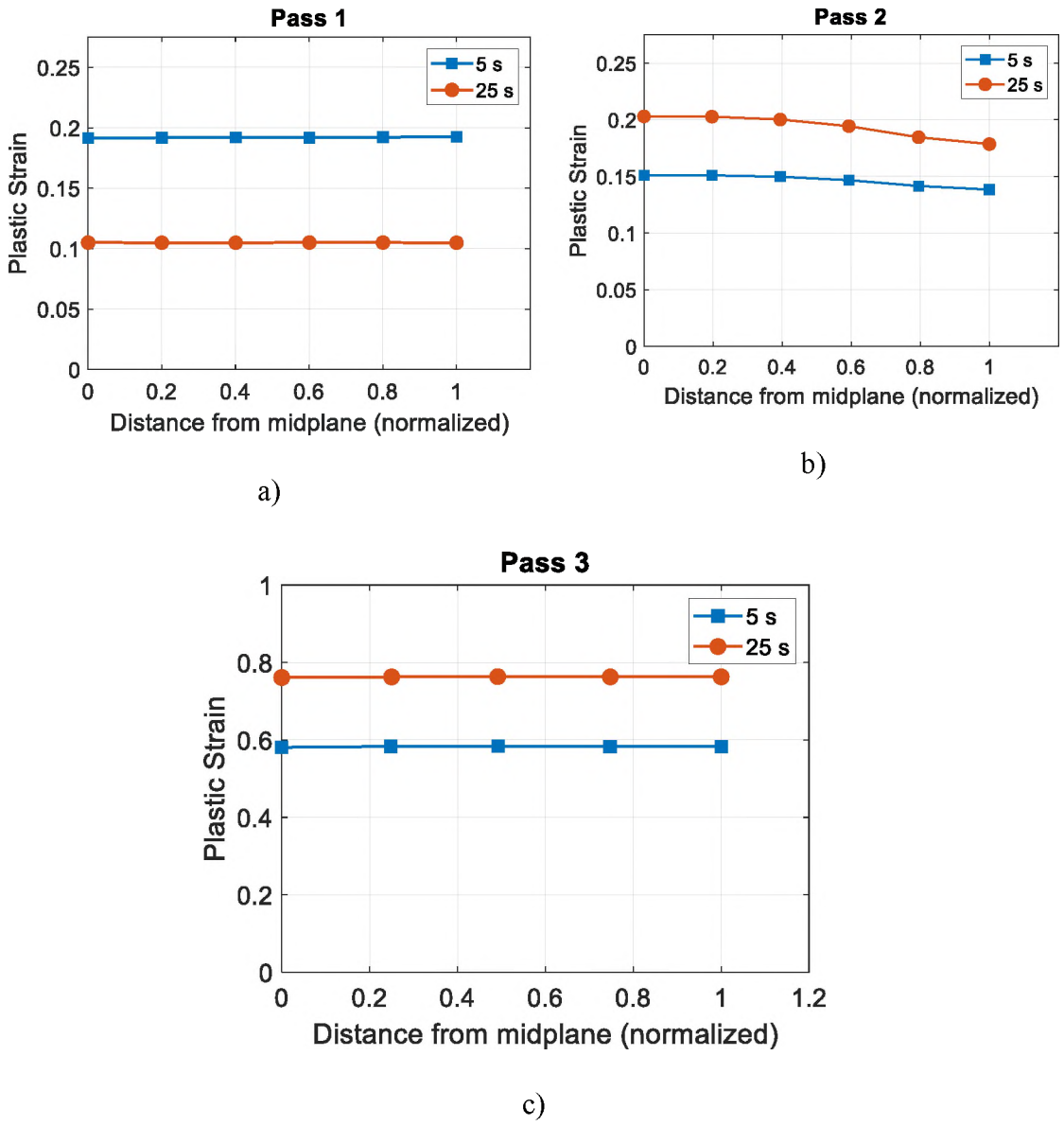

Figure 16. Increase in static softening with time for a) pass 1, b) pass 2, c) pass 3.

4.3. INFLUENCE OF TEMPERATURE ON RECRYSTALLIZATION

The first rolling pass was simulated for varying temperature profile of the rolled slab. The temperature has a critical influence on X_{srx} and varying the initial slab temperature can be used to reduce or increase the fraction of recrystallized grains. Simulations were conducted for three different temperatures 900 °C, 1000 °C and 1100 °C and an interpass time of 25 seconds. Almost fully recrystallized material was obtained for 1100 °C. While at 1000 °C, 47% and at 900 °C, 8.7% recrystallization was achieved (Figure 17).

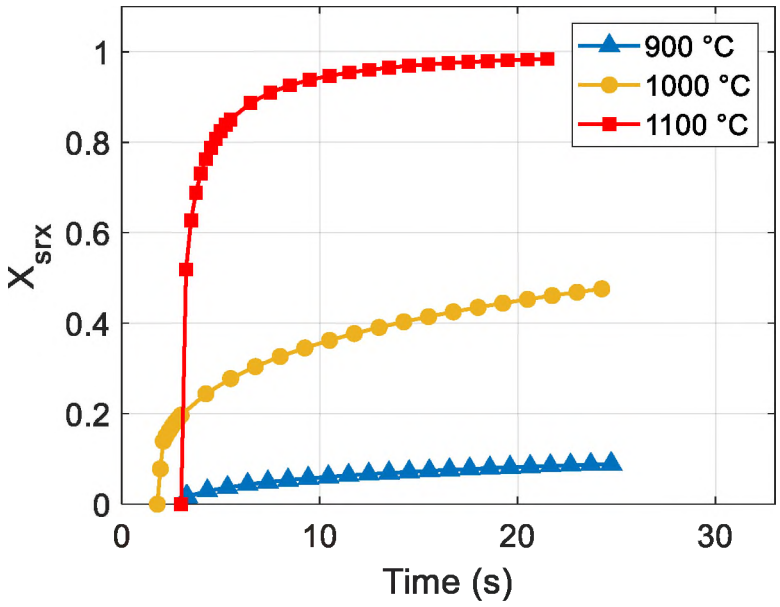

Figure 17. Variation of degree of static recrystallization during first rolling pass for different temperatures.

The extent of recrystallization at the end of the first rolling pass is shown in Figure 18 for the different temperatures. For temperature 900 °C, the fraction of static

recrystallization is observed to vary between 0.55 (at center) to 0.6 at the surface. The extent of recrystallization is observed to be highest when slab temperature maintained at 1100 °C wherein the fraction of recrystallization is observed to be 0.6 at the center and 0.65 at the surface.

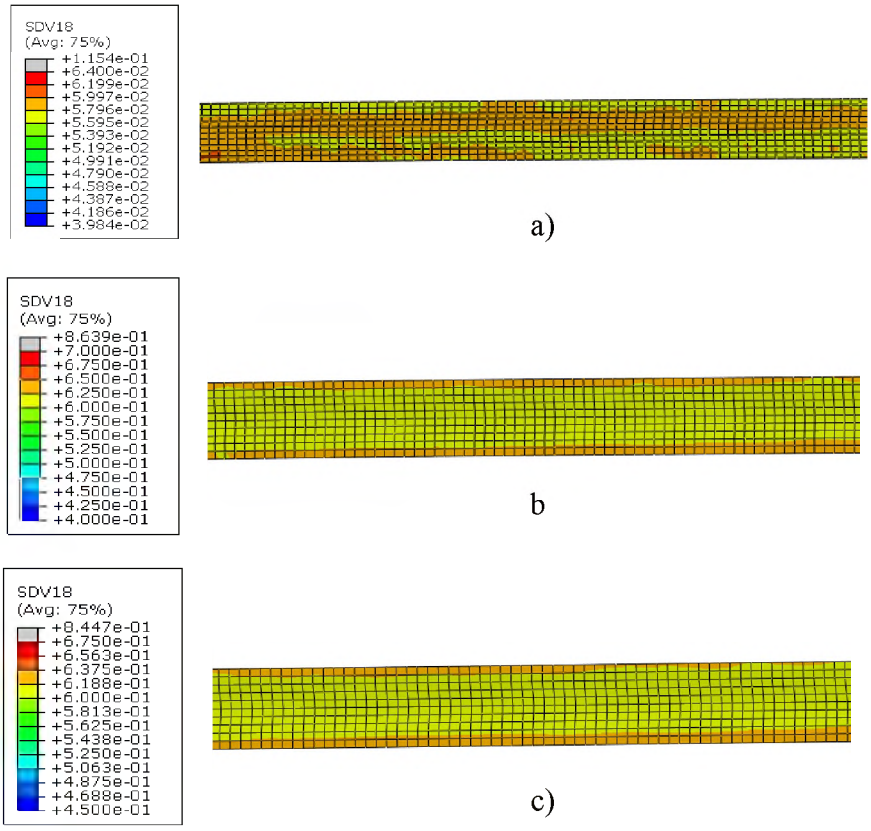

Figure 18. Simulation results for static recrystallization for a) 900 ℃, b) 1000 ℃, and c) 1100 ℃.

The corresponding loss of residual strain due to recrystallization is plotted in Figure 19. The loss in plastic strain is highest at 1100 °C (32%) and as the temperature of

slab decreases the strain relaxation is lower (7% at 900 °C). Hence, higher static softening and ductility is achieved at elevated temperatures.

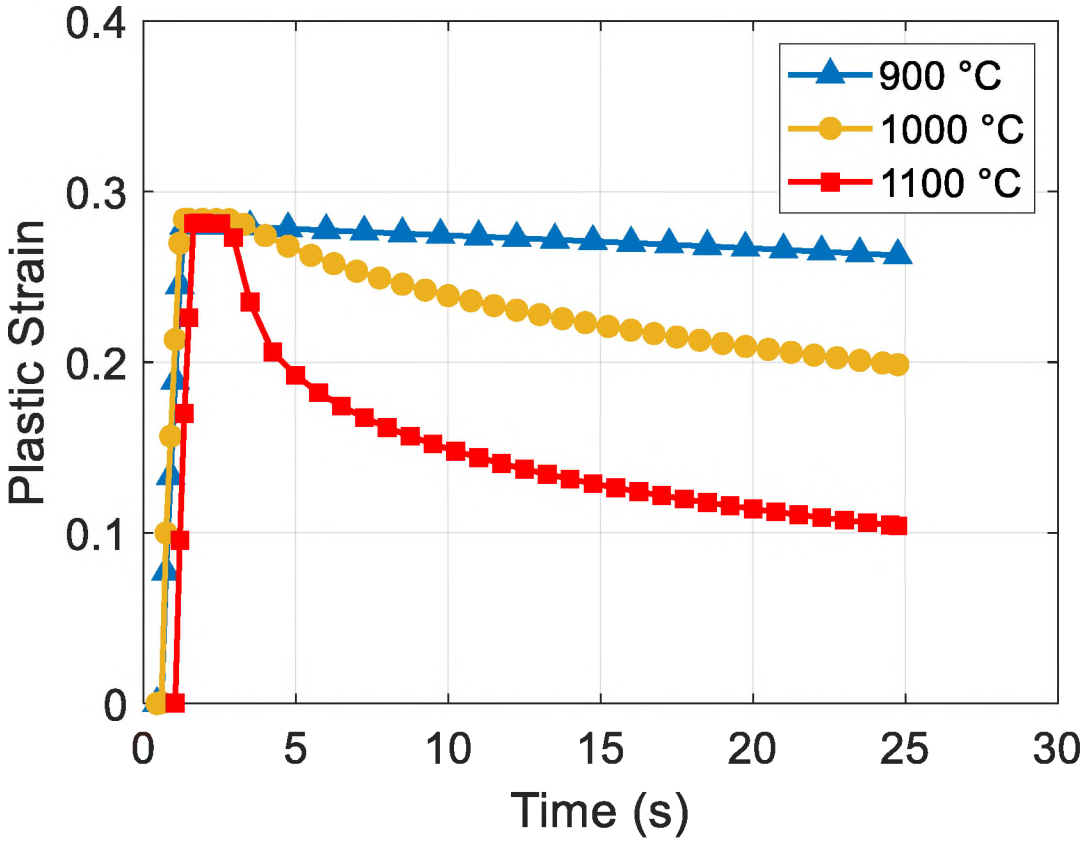

Figure 19. Static softening during the first rolling pass.

The plastic strain along the thickness of the rolled slab at the end of the first interpass for the simulations at varying temperature is shown in Figure 20. As the temperatures are higher along the surfaces the degree of static recrystallization is higher. Due to this the strain loss is lower along the center and higher along the surface for elevated temperatures.

4.4. INFLUENCE OF ROLLING SPEED ON RECRYSTALLIZATION

The speed of revolution of the rollers also influences the mass flow during hot rolling. The higher the speed of rolling the greater the strain rate in the rolled slab.

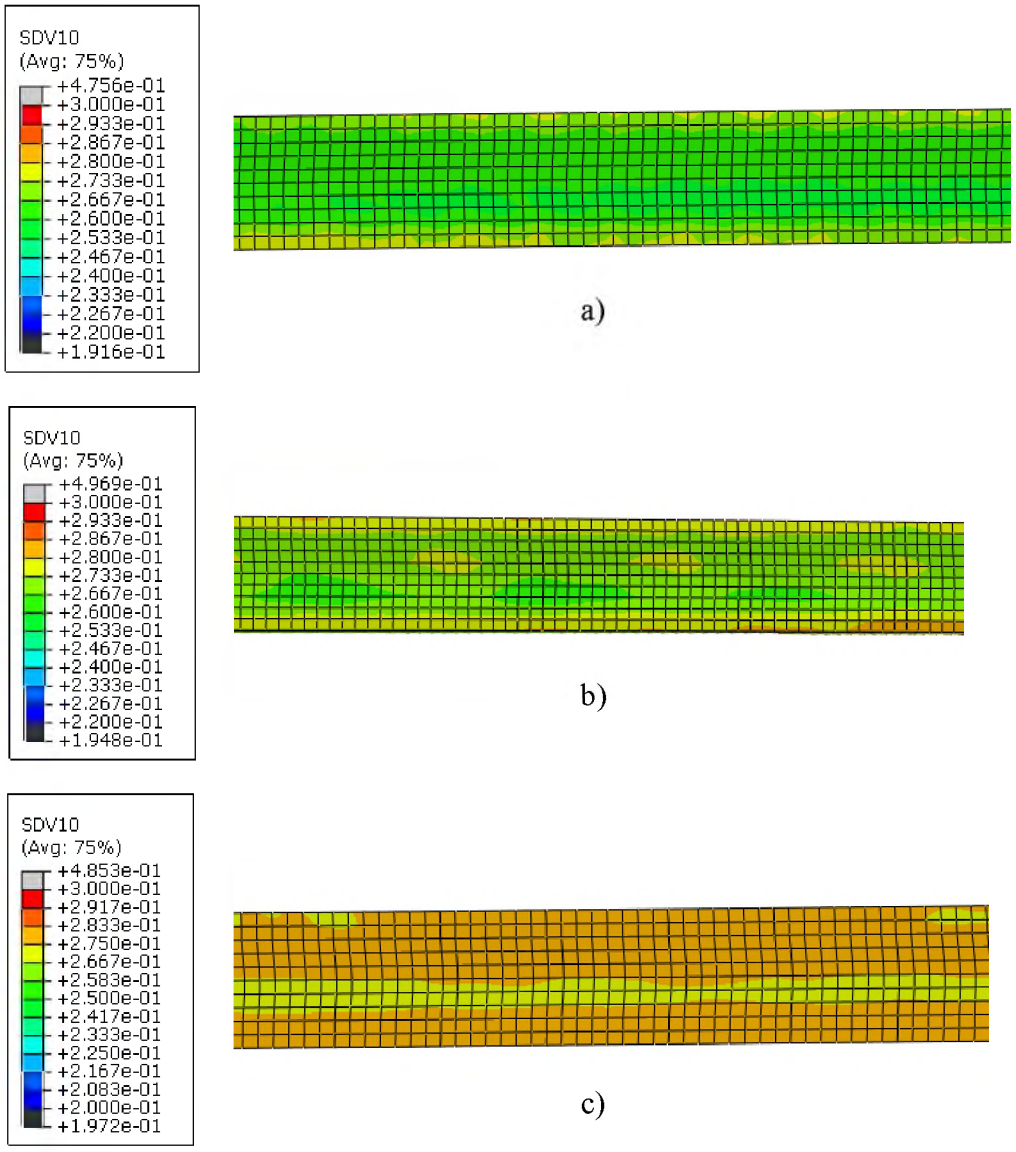

Figure 20. Simulation results of static softening at different temperatures a) 900 ºC, b) 1000 ºC, and c) 1100 ºC.

Hence, the speed of rolling is expected to influence the fraction of recrystallization X_{srx}. Hot rolling simulation for the first pass was conducted at 1000 °C for three different rolling speeds 2 m/s, 2.5 m/s, and 3 m/s respectively. As the rolling speed was increased from 2 m/s to 2.5 m/s, the fraction of static recrystallization was found to increase 5% (Figure 21). Further increase in rolling speed was found to marginally increase X_{srx}.

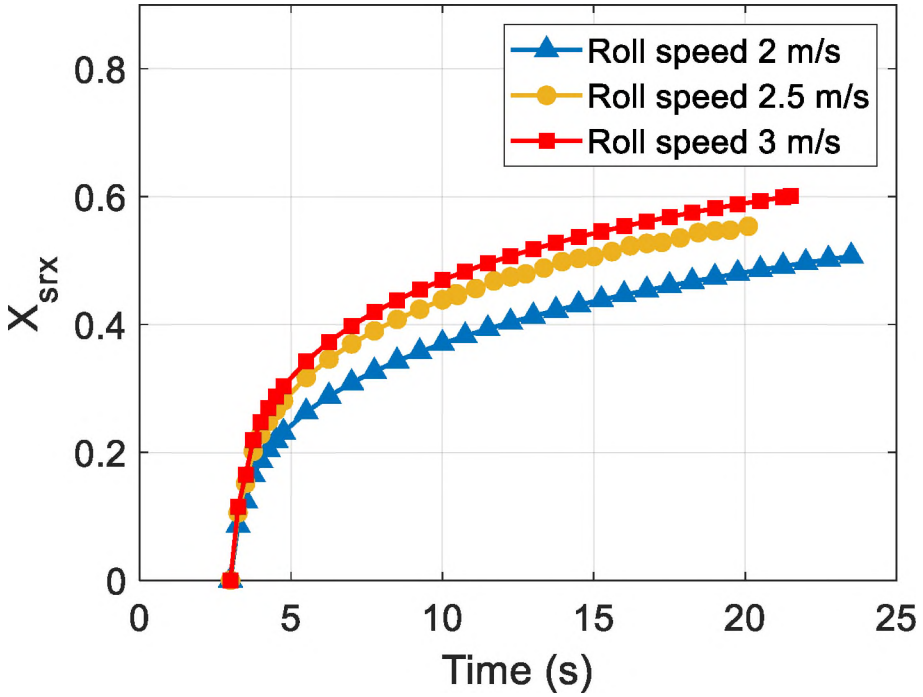

Figure 21. Variation of degree of static recrystallization for varying rolling speeds.

5. CONCLUSIONS

In this study, a new model to predict the degree of static recrystallization and static softening in high strength steel was developed. The classical JC model was used to model the plastic hardening of the material based on high temperature tensile tests at varying

strain rates. Static recrystallization kinetic parameters were determined by calibrating double hit compression test stress-strain curves. The evolution of fraction of static recrystallization and static softening was based on the strain, strain rate, and temperature during hot rolling. Hot rolling simulations were conducted representing the actual industrial runs and identical rolling parameters.

The rolling simulations predicted that the degree of static recrystallization and static softening was higher for third rolling pass wherein the extent of deformation was the highest. The static softening and recrystallization almost increases linearly with deformation.

The effect of increasing the temperature of the rolled slab was observed to result in a huge increase in the degree of static recrystallization. Almost full recrystallization was achieved at 1100 °C, while recrystallization was 47% at 1000 °C. At lower temperatures as 900 °C, the degree of recrystallization was minimal 8.7%. Correspondingly the extent of static softening was minimal at 900 °C, while as temperature increased, the softening was substantial. Finally, the effect of rolling speed was observed to marginally increase the degree of static recrystallization. The effect is more pronounced at lower rolling speeds, while at higher rolling speeds the difference in recrystallization is marginal.

ACKNOWLEDGEMENTS

This work was supported by the Peaslee Steel Manufacturing Research Center at Missouri University of Science and Technology.

REFERENCES

[1] P. R. Rios, F. Siciliano, H. R. Z. Sandim, R. L. Plaut, and A. F. Padilha, "Nucleation and growth during recrystallization," *Mater. Res.*, vol. 8, pp. 225–238, 2005.

[2] X. Wang *et al.*, "Experiment and simulation of static softening behavior of alloyed steel during round bar hot rolling," *J. Manuf. Process.*, vol. 52, pp. 281–288, 2019.

[3] H. S. Zurob, C. R. Hutchinson, Y. Brechet, and G. Purdy, "Modeling recrystallization of microalloyed austenite: Effect of coupling recovery, precipitation and recrystallization," *Acta Mater.*, vol. 50, no. 12, pp. 3077–3094, 2002.

[4] A. Najafizadeh, J. J. Jonas, G. R. Stewart, and E. I. Poliak, "The strain dependence of postdynamic recrystallization in 304 H stainless steel," *Metall. Mater. Trans. A Phys. Metall. Mater. Sci.*, vol. 37, no. 6, pp. 1899–1906, 2006.

[5] C. . Sellars, "Recrystallization of Metals during Hot Deformation," *Philos. Trans. R. Soc. London. Ser. A, Math. Phys. Sci.*, vol. 288, pp. 147–158, 1978.

[6] J. G. Lenard, *Primer on Flat Rolling*, 2nd ed. 2014.

[7] P. . Hodgson and R. . Gibbs, "and Microalloyed," *ISIJ Int.*, vol. 32, no. 12, pp. 329–338, 1992.

[8] K. Jung, H. W. Lee, and Y. T. Im, "A microstructure evolution model for numerical prediction of austenite grain size distribution," *Int. J. Mech. Sci.*, vol. 52, pp. 1136–1144, Sep. 2010.

[9] Q. He, J. Sun, J. Zhao, B. Yuan, and L. Xu, "Numerical Analysis of Multi-Pass H-Beam Hot Rolling Processing," *Appl. Mech. Mater.*, vol. 190–191, pp. 385–389, Jul. 2012.

[10] G. Johnson and W. Cook, "A constitutive model and data for metals subjected to large strains, high strain rates and high temperatures," *7th Int. Symp. Ballist.*, vol. 21, pp. 541–547, 1983.

[11] M. F. Buchely, D. C. Van Aken, R. J. O'Malley, S. Lekakh, and K. Chandrashekhara, "Hot rolling effect upon the high temperature Johnson-Cook strength and failure models for a 15V38 grade steel," in *Proceedings on the Materials Science and Technology meeting (MS&T17)*, pp. 1045–1053, 2017.

[12] M. F. Buchely, X. Wang, D. C. Van Aken, R. J. O'Malley, S. N. Lekakh, and K. Chandrashekhara, "The use of genetic algorithms to calibrate Johnson-Cook strength and failure parameters of AISI/SAE 1018 steel," *J. Eng. Mater. Technol.*, vol. 141, no. 2, p. 12, 2019.

[13] C. M. Sellars and J. A. Whiteman, "Recrystallization and grain growth in hot rolling," *Met. Sci.*, vol. 13, no. 3–4, pp. 187–194, Mar. 1979.

[14] I. Faridmehr, M. Hanim Osman, A. Bin Adnan, A. Farokhi Nejad, R. Hodjati, and M. Amin Azimi, "Correlation between Engineering Stress-Strain and True Stress-Strain Curve," *Am. J. Civ. Eng. Archit.*, vol. 2, no. 1, pp. 53–59, 2014.

[15] Y. Ling, "Uniaxial True Stress-Strain after Necking," AMP J. Technol., vol. 5, no. 1, pp. 37–48, 2004.

[16] L. Schwer, "Optional strain-rateforms for the Johnson-Cook constitutive model and the role of the parameter Epsilon _ 0," in *Proceedings of the 6th European LS-DYNA Conference*, 2007.

[17] Dassault Systemes, *Abaqus 6.18 Documentation*, 2018th ed. 2018.

SECTION

4. CONCLUSIONS

The first paper of this work deals with the healing of internal voids in rolled steel slab during reversible hot rolling process. Hot compression tests were conducted for the steel at varying temperatures and strain rates to obtain a range of stress-strain curves. Based on the stress-strain relationship of the steel and using a genetic algorithm the hardening behavior of the material was evaluated and Johnson-Cook parameters determined. Thereafter a three-dimensional finite element model was constructed for reversible hot rolling process for steel slab with existing cylindrical voids. The influence of rolling pass reduction, temperature, void location and recrystallization on void closure was predicted using simulations. Pass reduction was observed to increase the rate of void closure drastically, while increase in temperature and recrystallization increased the rate of void closure marginally.

In the second paper the kinetics of static recrystallization of steel during hot rolling was studied. Using the double hit compression test the fraction of static recrystallization was determined for a range of varying temperatures above the austenizing temperature of steel, pre-strains and strain rates. The parameters defining the half time for static recrystallization were calibrated as per the Sellars model. The kinetics of static recrystallization was modeled as per the Avrami equation and the effect on softening of steel determined. The model was implemented in a program and incorporated into a finite element model. Three dimensional FEA analysis of industrial hot rolling process was conducted to determine the influence of pass reduction,

temperature and rolling speed on extent of static recrystallization and static softening. The analysis showed that with increasing pass reduction the extent of static recrystallization increased as well as static softening. Temperature also had a critical influence, dramatically increasing static recrystallization. Rolling speed was found to have minimum effect on static recrystallization.

The effect of defect formation during hot rolling of I-beam was studied using FEA. Breakdown mill rolling of I-beam was investigated that had thirteen rolling passes. After the fourth rolling pass a small depression is observed to form along the middle of the flange. The depth of the depression is predicted to decrease if a smaller rolling gap is used. Further, influence of a pre-existing surface distortion on the shape of the depression after rolling was studied using simulation. It was found that the distortion increases the depth of the depression.

In the fourth paper a modified version of JC model was proposed that accounted for the influence of grain size on flow stress. Four different grades of steel were considered and experiments were conducted at elevated temperatures to measure the increase in grain size with time. This enabled to obtain the relationship between grain size with temperature and time for each of the steel grades. Experiments were also carried out to measure the change in strength of the steel at elevated temperatures for different grain size. A modified JC model was introduced that considered the material stress was sensitive to its grain size. Compression test simulations were carried out and the change in flow stress was determined for the different steel grades. The steel grades showed an increase in grain size with time. The grades that showed larger increase in grain size also showed considerably higher drop in flow stress.

BIBLIOGRAPHY

[1] J. H. Ryu, P. Lee, and H. G. Bhadeshia, "Model for Mechanical Properties of Hot-Rolled Steels," *Grad. Inst. Ferr. Technol.*, vol. Master, 2008,.

[2] M. F. Buchely, X. Wang, D. C. Van Aken, R. J. O'Malley, S. N. Lekakh, and K. Chandrashekhara, "The use of genetic algorithms to calibrate Johnson-Cook strength and failure parameters of AISI/SAE 1018 steel," *J. Eng. Mater. Technol.*, vol. 141, no. 2, p. 12, 2019.

[3] R. W. Armstrong and F. J. Zerilli, "Dislocation Mechanics Based Analysis of Material Dynamics Behavior," *Le J. Phys. Colloq.*, vol. 49, no. C3, pp. C3-529-C3-534, 1988.

[4] G. R. Johnson and W. H. Cook, "A constitutive model and data for metals subjected to large strains, high strain rates and high temperatures." , 7th International Symposium on Ballistics, vol 21, 541-547, 1983.

[5] S. Shida, "Empirical formula of flow stress of carbon steels-resistance to deformation of carbon steels at elevated temperature," *J. Japan Soc. Technol. Plast.*, vol. 10, pp. 610–617, 1969.

[6] J. Van Slycken, P. Verleysen, J. Degrieck, L. Samek, and B. C. De Cooman, "High-strain-rate behavior of low-alloy multiphase aluminum- and silicon-based transformation-induced plasticity steels," *Metall. Mater. Trans. A Phys. Metall. Mater. Sci.*, vol. 37, no. 5, pp. 1527–1539, 2006.

[7] C. . Sellars, "Recrystallization of Metals during Hot Deformation," *Philos. Trans. R. Soc. London. Ser. A, Math. Phys. Sci.*, vol. 288, pp. 147–158, 1978.

[8] J. G. Lenard, *Primer on Flat Rolling*, 2nd ed. 2014.

[9] X. Wang *et al.*, "Experiment and simulation of static softening behavior of alloyed steel during round bar hot rolling," *J. Manuf. Process.*, vol. 52, pp. 281–288, 2019.

[10] J. J. Jonas, X. Quelennec, L. Jiang, and É. Martin, "The Avrami kinetics of dynamic recrystallization," *Acta Mater.*, vol. 57, no. 9, pp. 2748–2756, 2009.

[11] K. Jung, H. W. Lee, and Y. T. Im, "A microstructure evolution model for numerical prediction of austenite grain size distribution," *Int. J. Mech. Sci.*, vol. 52, pp. 1136–1144, Sep. 2010.

[12] C. M. Sellars and J. A. Whiteman, "Recrystallization and grain growth in hot rolling," *Met. Sci.*, vol. 13, no. 3–4, pp. 187–194, Mar. 1979.

[13] B. P. Kashyap and K. Tangri, "Hall-Petch relationship and substructural evolution in boron containing type 316L stainless steel," *Acta Mater.*, vol. 45, no. 6, pp. 2383–2395, 1997.

[14] Y. Takashima and T. Hiruta, "Characteristics of deformation behavior in channel universal rolling," *ISIJ Int.*, vol. 53, no. 4, pp. 690–697, 2013.

[15] P. O. Aiyedun, L. G. M. Sparling, and C. M. Sellars, "Temperature changes in hot flat rolling of steels at low strain rates and low reduction," *Proc. Inst. Mech. Eng.*, vol. 211 Part B, pp. 261–284, 1997.

[16] J. Seo, S. Kwon, and D. Lee, "Effects of surface defects on rolling contact fatigue of rail," *Procedia Eng.*, vol. 10, pp. 1274–1278, 2011.

[17] Dassault Systemes, *Abaqus 6.18 Documentation*, 2018.

VITA

Shouvik Ganguly grew up in Pune, India. In 2000, he received his B.S in Metallurgical Engineering from Visvesvaraya National Institute of Technology, India. Thereafter he worked as a research assistant in IIT Mumbai, India. In May 2005, he received his M.S degree in Mechanical Engineering from Tuskegee University Alabama, USA.

In December 2005, he joined Geometric Software Solution Ltd and worked as a software engineer responsible for finite element software Patran customization. Later he also worked for Siemens Ltd from June 2010 to August 2014 as a computational engineer for computer aided design.

In August 2016, he started his Ph.D. in Mechanical Engineering at Missouri University of Science & Technology (Missouri S&T) in Rolla, Missouri, USA. During his Ph.D., he worked as a research assistant at Missouri S&T for hot rolling simulation and optimization studies. His research was in collaboration with multivarious steel making companies as Nucor, Gerdau and US Steel.

He received his Doctor of Philosophy in Mechanical Engineering from Missouri University of Science & Technology in May 2021.